REDOX-RESPONSIVE BIODEGRADABLE POLYMERIC MATERIALS FOR BIOMEDICAL APPLICATIONS

by

Filiz Çalık

B.S., Chemistry, Ondokuz Mayıs University, 2000

M.S., Chemistry, Boğaziçi University, 2014

Submitted to the Institute for Graduate Studies in
Science and Engineering in partial fulfillment of
the requirements for the degree of
Doctor of Philosophy

Graduate Program in Chemistry

Boğaziçi University

2022

REDOX-RESPONSIVE BIODEGRADABLE POLYMERIC MATERIALS FOR BIOMEDICAL APPLICATIONS

DATE OF APPROVAL: 08.06.2022

ACKNOWLEDGEMENTS

First, I would like to thank to my thesis supervisors Prof. Rana Sanyal and Prof. Amitav Sanyal. I always admired their patience, mentoring, and positive discipline strategies, all of which helped me to enhance my scientific skills and get to where I am now.

I would like to extend my thanks to my thesis juries Prof. İlknur Doğan, Prof. Sevgi Güngör, Assoc. Prof. Oktay Demircan and Assist. Prof. Özgül Gök for their constructive reviews on the final manuscript of the thesis.

I would like to thank to all my fellow labmates of the Sanyal group who we studied together throughout my graduate program. I would like to extend my thanks to all the members of the faculty in the Chemistry Department.

I would like to thank to Aysun Değirmenci for her patience in running all the cell studies in my thesis.

I would to thank to Bogazici University Research Funds (Project No. 17B05D3) for financial support.

I would like to acknowledge Dr. Ufuk Sebüktekin Fellowship, which I received to support my graduate studies.

Aslan, I am aware that I had to spent the first years of your childhood by studying very hard which I had to substitute with your playtime but I am sure that you will be proud of me in the future.

Finally, I would like to thank my family and friends for their personal support throughout my studies.

Dedicated to my dear family

ABSTRACT

REDOX-RESPONSIVE BIODEGRADABLE POLYMERIC MATERIALS FOR BIOMEDICAL APPLICATIONS

In recent years, biodegradable and stimuli-responsive polymeric materials have gained importance in cancer research and biomedical applications. Such materials can be used as implants in the body and a nano-sized drug delivery system. Within the scope of this thesis, three different stimulus-sensitive biodegradable polymer dendron conjugate systems were prepared, and micellar nanostructures were obtained with these structures. The hydrophobic drug was physically loaded into the micelle structures in the first three projects. In the first and second projects, a targeting group was used to increase the efficiency of the drug delivery system. These micellar carriers make the hydrophobic drug water-soluble in body fluid and use both passive and active targeting pathways to ensure that the drug is collected in tumor tissues. The size of micellar structures was appropriate in all three projects when examined in terms of their suitability for delivery based on the enhanced permeability and retention (EPR) effect. The first two projects used cyclic RGDfK as the targeting group. It was observed that the drugs incorporated into the micellar nanostructures with the targeting group accumulated more effectively in the breast cancer cells. Doxorubicin was used as a chemotherapy agent. The last study synthesized cryogels containing varying amounts of a thiol-reactive monomer. Facile and reversible functionalization of cryogels were demonstrated through the attachment of a fluorescent dye (Bodipy-SH) and bioactive ligands such as biotin-thiol and mannose-thiol to recognize Streptavidin and Concanavalin-A, respectively. The proteins bound to the cryogels were amenable to release through treatment with a thiol-containing reducing agent such as dithiothreitol (DTT). Overall, the novel thiol-reactive macroporous cryogel structures will be a fascinating platform for various biomedical applications where a catch and release approach of analytes is necessary.

ÖZET

REDOX'A DUYARLI BİYOBOZUNUR POLİMERİK MALZEMELERİN BİYOMEDİKAL UYGULAMALAR

Son yıllarda biyobozunur ve uyaranlara duyarlı polimerik malzemeler kanser araştırmalarında ve biyomedikal uygulamalarda önem kazanmıştır. Bu tür malzemeler vücutta implant olarak ve nano boyutlu bir ilaç taşıma sistemi olarak kullanılabilir. Bu tez kapsamında, uyarıcıya duyarlı üç farklı biyobozunur polimer dendron konjugat sistemi hazırlanmış ve bu yapılarla misel nanoyapılar elde edilmiştir. İlk üç projede hidrofobik ilaç fiziksel olarak misel yapılarına yüklenmiştir. Birinci ve ikinci projelerde, ilaç dağıtım sisteminin etkinliğini artırmak için bir hedefleme grubu kullanıldı. Bu misel taşıyıcılar, hidrofobik ilacı vücut sıvısında suda çözünür hale getirir ve ilacın tümör dokularında toplanmasını sağlamak için hem pasif hem de aktif hedefleme yollarını kullanır. Artmış geçirgenlik ve alıkonma (EPR) etkisine dayalı olarak teslime uygunlukları incelendiğinde, misel yapılarının boyutu her üç projede de uygundur. İlk iki proje, hedefleme grubu olarak döngüsel RGDfK'yi kullandı. Hedefleme grubu ile misel nanoyapılarına dahil edilen ilaçların meme kanseri hücrelerinde daha etkin bir şekilde biriktiği gözlemlendi. Kemoterapi ajanı olarak doksorubisin kullanıldı. Son çalışma, değişen miktarlarda tiyol reaktif monomer içeren kriyojelleri sentezledi. Kriyojellerin kolay ve tersine çevrilebilir işlevselleştirilmesi, sırasıyla Streptavidin ve Concanavalin-A'yı tanımak için bir floresan boya (Bodipy-SH) ve biyotin-tiyol ve mannoz-tiyol gibi biyoaktif ligandların eklenmesiyle gösterildi. Kriyojellere bağlanan proteinler, ditiyotreitol (DTT) gibi tiyol içeren bir indirgeyici madde ile işleme tabi tutularak salıverilmeye müsaitti. Genel olarak, yeni tiyol reaktif makro gözenekli kriyojel yapıları, analitleri yakalama ve bırakma yaklaşımının gerekli olduğu çeşitli biyomedikal uygulamalar için büyüleyici bir platform olacaktır.

TABLE OF CONTENTS

ACKNOWLEDGEMENTS iii
ABSTRACT v
ÖZET vi
TABLE OF CONTENTS vii
LIST OF FIGURES xi
LIST OF TABLES xx
LIST OF ACRONYMS/ABBREVIATIONS xxi
1. INTRODUCTION 1
1.1. Biomedical Applications of Polymeric Materials 1
1.2. Stimuli-Responsive Biomaterials in Drug Delivery System 2
1.2.1. pH Responsive Polymeric Materials for DDS 4
1.2.2. Redox Responsive Polymeric Materials for DDS 6
1.3. Stimuli-responsive Polymers in Drug Delivery Systems for Cancer 10
1.3.1. Passive and Active Targeting in Cancer Therapy 11
1.3.2. Polymeric Nanocarriers in Cancer Treatment 14
1.3.3. Polymer Dendron Conjugates as Drug Delivery Systems 15
1.4. Cryogels as an Emerging Scaffold for Biomedical Applications 19
2. RESEARCH OVERVIEW 24
3. DENDRON-POLYMER CONJUGATE BASED CROSSLINKED MICELLES: A ROBUST AND VERSATILE NANOSYSTEM FOR TARGETED DELIVERY 26
3.1. Introduction 26
3.2. Experimental Section 28
3.2.1. Materials 28
3.2.2. Instrumentation 29
3.2.3. Synthesis of cRGDfK Containing Polymer-Dendron Conjugate (PDC-R) 29
3.2.4. Micelle Formation from Polymer-Dendron Conjugate and Related Measurements 30
3.2.5. Core Crosslinking Experiments. 30
3.2.6. Stability Experiments 31

3.2.7. Encapsulation and *in vitro* release of DOX 31
3.2.8. *In vitro* Cytotoxicity. 32
3.2.9. Cellular Internalization 32
3.3. Results and Discussion 33
3.3.1. Synthesis of Targeting Group Containing Polymer-Dendron Conjugate 33
3.3.2. Determination of Critical Micelle Concentration (CMC) 36
3.3.3. Preparation and Characterization of Crosslinked Micelles 36
3.3.4. Drug Loading into NCL and CL Micelles and Release 39
3.3.5. *In vitro* Cytotoxicity and Cellular Internalization 40
3.4. Conclusions 42
4. REDOX-RESPONSIVE DENDRON-POLYMER CONJUGATES: VERSATILE BUILDING BLOCKS FOR FABRICATION OF STIMULI-RESPONSIVE TARGETED DELIVERY SYSTEMS 44
4.1. Introduction 44
4.2. Experimental Section 46
4.2.1. Materials 46
4.2.2. Instrumentation 46
4.2.3. Synthesis of 3rd Generation Polyester Dendron (DG3) 47
4.2.4. Synthesis of 4th Generation Polyester Dendron (DG4) 47
4.2.5. Conjugation of Linear PEG Dendron (PEGDG4, PEGDG3 and HOOC-PEGDG4) 48
4.2.6. Synthesis of cRGDfK Containing Linear Peg Dendron Conjugate 48
4.2.7. Micelle Formation from Polymer-Dendron Conjugate and Related Measurements 48
4.2.8. Stability Experiments 49
4.2.9. Release of NR from PEGDG4 in Response to Two Stimuli 49
4.2.10. Encapsulation and *in vitro* Release of DOX 50
4.2.11. Procedure of GSH-mediated Cytotoxicity 50
4.2.12. Procedure for Internalization and Flow Cytometry 51
4.3. Results and Discussion 52
4.3.1. Synthesis of Redox-responsive Polymer-Dendron Conjugates 52
4.3.2. Determination of Critical Micelle Concentration (CMC) 56

4.3.3. Preparation and Characterization of RGD containing Micelles 58
4.3.4. Drug Release Studies and *in vitro* Studies. 61
4.3.5. *In vitro* Cytotoxicity and Cellular Internalization. 63
4.4. Conclusion 66
5. MICELLAR TYPE NANOCARRIER FOR DRUG DELIVERY SYSTEMS FROM DENDRONIZED POLYMERS 68
5.1. Introduction 68
5.2. Experimental Section 70
5.2.1. Materials 70
5.2.2. Instrumentation 70
5.2.3. Synthesis of Thiol group Containing Polyester Dendron 71
5.2.4. Synthesis of p(PEGMEMA)-b-p(PDSM) Block Copolymer 71
5.2.5. Synthesis of Dendronized Polymer (DP) 72
5.2.6. Obtaining Micellar Nanoparticles from Dendronized Polymers 72
5.2.7. Stability Experiments 73
5.2.8. Encapsulation and *in vitro* release of DOX 73
5.2.9. Cellular Internalization 74
5.2.10. *In vitro* Cytotoxicity 74
5.3. Results and Discussion 75
5.3.1. Synthesis and Characterization of Dendronized Polymer 75
5.3.2. Synthesis and Characterization Copolymer 78
5.3.3. Synthesis of Dendronized Polymer 80
5.3.4. Preparation and Characterization of Micelles. 82
5.3.5. Drug Loading and Release into Micelles Obtained from Dendronized Polymers 86
5.3.6. Cellular Internalization and *in vitro* Cytotoxicity 88
5.4. Conclusion 90
6. 'CATCH AND RELEASE' CRYOGELS: FABRICATION, FUNCTIONALIZATION AND REVERSIBLE PROTEIN IMMOBILIZATION 92
6.1. Introduction 92
6.2. Experimental Section 94
6.2.1. Materials 94
6.2.2. Instrumentation 94

6.2.3. Synthesis of 2-(pyridin-2-yldisulfanyl)ethanaminium (PDS-NH_2)..... 95
6.2.4. Synthesis of PEG-Based 2-(acryloyloxy)ethyl methacrylate..... 95
6.2.5. Synthesis of PEG-Based Pyridyl-Disulfide Group Containing Methacrylate (PDS-PEG-MA) Monomer 96
6.2.6. Fabrication of PDS-PEG-MA Functionalized Cryogels 96
6.2.7. Fabrication of Control Cryogel 96
6.2.8. Water up taking of Cryogels 97
6.2.9. Pyridothione Release Studies 97
6.2.10. Scanning Electron Microscopy (SEM) 97
6.2.11. Direct immobilization of BODIPY-SH..... 98
6.2.12. Catch and Release of Streptavidin onto the Biotinylated..... 98
6.2.13. Immobilization ConA from Lectins Mixture. 98
6.2.14. Cellular Attachment on Cryogel 99
6.3. Results and Discussion..... 99
6.3.1. Fabrication, Characterization, and Functionalization of Pyridyl Disulfide Containing Cryogels..... 99
6.3.2. Direct immobilization of BODIPY-SH..... 103
6.3.3. Catch and Release of Streptavidin onto the Biotinylated Cryogels .. 104
6.3.4. Immobilization ConA from Lectin mixture. 105
6.3.5. Cytotoxicity and RGD-based Cell Attachment..... 106
6.4. Conclusion..... 108
7. CONCLUSION 109
REFERENCES 111
APPENDIX A: ADDITIONAL DATA..... 111
APPENDIX B: PERMISSIONS FOR FIGURES 142

LIST OF FIGURES

Figure 1.1. Examples of common polymeric materials for biomedical applications.. 1

Figure 1.2. Intrinsic/extrinsic stimuli and stimuli-responsive nanocarriers (NCs). Reprinted from [29]. 4

Figure 1.3. pH changes at the cellular and organism levels. Reprinted from [32]. 5

Figure 1.4. (a) Chemical structure of disulfide-bridged block copolymer and schematic illustration of redox-responsive nanoparticles for overcoming cancer cell multidrug resistance (b). Reprinted from [54]. 7

Figure 1.5. Examples of functional materials fabricated using pyridyl-disulfide containing polymers. Reprinted from [55]. 8

Figure 1.6. Fabrication of redox-responsive NGs using the pyridyl-disulfide thiol exchange reaction. Reprinted from [56]. 9

Figure 1.7. Pyridyl-disulfide group containing hydrogel coating for selective attachment and release of target proteins and cells. Reprinted from [57]. 10

Figure 1.8. Representation of the mechanism for active and passive tumor targeting. Reprinted from [64]. 11

Figure 1.9. The design and synthesis strategy for the ligand-linked DACHPt/m is depicted in this diagram. Reprinted from [76]. 14

Figure 1.10. Timeline of FDA Approval of Therapeutic Nano and Microparticles. Reprinted from [83]. 15

Figure 1.11. Schematic structural illustration of a dendron. Reprinted from [89].....16

Figure 1.12. Various dendron-polymer conjugates utilized for fabrication of nanosized drug delivery systems. Reprinted from [90].....17

Figure 1.13. Micelles can be passively and actively targeted in the tumor environment. Reprinted from [97].....19

Figure 1.14. Schematic illustration of cryogelation technique. 20

Figure 1.15. *In vitro* doxorubicin release profiles of cryogels and bulk gels in acetate buffer pH = 5.4. Reprinted from [102].....21

Figure 1.16. Schematic illustration of impact of linker length and porosity on the extent of biomolecule conjugation onto gel substrates. Reprinted from [103]. 22

Figure 3.1. Illustration of fabrication of drug loaded core-crosslinked targeted micelles.....28

Figure 3.2. ^{1}H NMR spectrum of polymer-dendron conjugate 34

Figure 3.3. Synthesis of cRGDfK containing polymer dendron conjugate (PDC-R).....35

Figure 3.4. ^{1}H NMR spectrum of polymer-dendron conjugate PDC-R containing peptide. 35

Figure 3.5. Pyrene excitation spectra of PDC-R based micelles. Left inset: I_{338}/I_{334} vs log concentration graph to calculate CMC value. 36

Figure 3.6. Synthesis of core crosslinked micelles CL-R from copolymer PDC-R. 37

Figure 3.7. (a-d) Size distributions of drug loaded and empty crosslinked (CL-R) vs non-crosslinked (NCL-R) micelles from PDC-R, (e) comparative Z-average diameter of micelles as determined by DLS at 37 oC, and (f) TEM micrographs of drug loaded NCL-R and CL-R micelles.....38

Figure 3.8. Stability of a) Crosslinked (CL-R) and b) Non-crosslinked (NCL-R) micelles from PDC-R against dilution as probed using DLS. 39

Figure 3.9. *In vitro* release of DOX at pH 7.4 and 5.4 from NCL-R and CL-R micelles. 40

Figure 3.10. Viabilities of MDA-MB-231 incubated with polymer (PDC-R), DOX loaded non-targeted micelle (CL-C) and DOX loaded targeted micelle (CL-R), and free drug after 48h treatment as (a) dot plot and (b) as histogram. 41

Figure 3.11. Fluorescence microscopy images of MDA-MB-231 cells treated with free DOX and DOX loaded non-targeted (CL-C) and targeted (CL-R) micelles. Cell nuclei were stained with DAPI (blue). Scale bar = 50 μm. 42

Figure 4.1. General scheme of cleavage of disulfide bond reductive environment. 45

Figure 4.2. ^{1}H NMR spectrum of generation 4 dendron. 52

Figure 4.3. Representative synthesis of PEG-SS-DEN4. 53

Figure 4.4. ^{1}H NMR spectrum of (PEGDG4). 54

Figure 4.5. Synthesis of cRGDfK containing redox-responsive polymer dendron conjugate (R-PEGDG4). 55

Figure 4.6. ^{1}H NMR spectrum of polymer-dendron conjugate 56

Figure 4.7. Pyrene excitation spectra of non-targeted producing PEGDG3, PEGDG4 and 20% RGD containing micelles R-PEGDG4. Insets: I_{338}/I_{334} vs log concentration graph to calculate CMC value. 57

Figure 4.8. The diameters of (a) empty (b) DOX loaded (c) DOX loaded (2 days later) micelles assembled from a mixture of R-PEGDG4 dendron-polymer conjugate.....58

Figure 4.9. The diameters of (a) empty (b) DOX loaded (c) DOX loaded (2 days later) micelles assembled from a mixture of PEGDG3 dendron-polymer conjugates. 59

Figure 4.10. TEM micrographs of drug-loaded micelles fabricated using (a) R-PEG-DG4 and (b) PEGDG3 dendron-polymer conjugates.....59

Figure 4.11. Stability under dilution in aqueous environment.....60

Figure 4.12. Change in the fluorescence intensity of NR-loaded micelles after incubation with and without 5/10 mm GSH at pH = 7.4 and 5.4. 61

Figure 4.13. *In vitro* release of DOX at pH 7.4 and 5.4, with and without 10 mM GSH from micelles. 62

Figure 4.14. Viabilities of MDA-MB-231 cells incubated with polymer free DOX, DOX loaded targeted micelle R-PEGDG4 with or without GSH and free drug after 48h treatment as (a) dot plot and (b) as histogram. 64

Figure 4.15. Fluorescence microscopy images (scale bar = 50 μm).....65

Figure 4.16. Flow cytometry histograms, of MDA-MB-231 cells treated with free DOX and DOX targeted micelles with and without GSH. 66

Figure 5.1. Illustration of fabrication of dendronized polymer-based nanoaggregate.....69

Figure 5.2. Synthesis of 1st, 2nd and 3rd generation polyester dendrimers. 76

Figure 5.3. Synthesis of 1st, 3rd and 2nd generation thiol-containing polyester dendrons. 77

Figure 5.4. ^{1}H NMR thiol group containing 1st and 2nd generation polyester dendron. 78

Figure 5.5. Synthetic route of PDSM bearing random copolymer 78

Figure 5.6. ^{1}H NMR Spectrum of Pyridyl Disulfide Ethyl Methacrylate (PDSM) monomer. 79

Figure 5.7. ^{1}H NMR spectra of random copolymer. 79

Figure 5.8. Synthesis of dendronized polymer using 1st, 2nd and 3rd generation polyester dendron. 80

Figure 5.9. ^{1}H NMR spectra of dendronized copolymers P-SS-G1, P-SS-G2, and P-SS-G3. 81

Figure 5.10. SEC traces of parent polymer and dendronized polymers. 82

Figure 5.11. I_{338}/I_{334} vs. log [mg/mL] graph to calculate CMC value. 83

Figure 5.12. Effective size diameters of empty and DOX loaded P-SS-G3 micelles. 84

Figure 5.13. TEM micrographs of a) P-SS-G3 b) P-SS-G2 dendronized copolymer based micellar nanosized aggregates. 84

Figure 5.14. Stability of micelles from P-SS-G3, P-SS-G2 and P-SS-G1 against dilution as probed using DLS. 85

Figure 5.15. Stability of micelles from P-SS-G3, P-SS-G2 (a-c) before (c-d) after DTT treatment. 86

Figure 5.16. SEC traces of parent polymer and P-SS-G3 before and after DDT treatment. 86

Figure 5.17. *In vitro* release of DOX at pH 7.4 and 5.4 with and without GSH for a) P-SS-G2 and b) P-SS-G3 dendronized copolymers. 88

Figure 5.18. Fluorescence microscopy images showing the comparison of internalization of Nile Red and Nile Red-loaded micellar aggregate by MDA-MB-231 human breast cancer cells. Scale bar is 100 μm. 89

Figure 5.19. Viabilities of MDA-MB-231 cells treated with DOX loaded P-SS-G3 under normal and redox environments. 90

Figure 6.1. (a) Synthesis pathway and (b)1H NMR spectrum of PDS-PEG-MA. 100

Figure 6.2. Synthesis PDS-PEG-MA monomer and fabrication of PDS-PEG-MA containing cryogels. 101

Figure 6.3. (a) Pyridothione release profiles from cryogels, and (b) photographs of the top views of dry, and wet cryogels. 101

Figure 6.4. Scanning electron micrographs of cryogels synthesized using (a) 10% (b) 20% (c) 30% PDS (scale bar is 50 μm), and (d) graphical representation of the equilibrium swelling values of cryogels. 103

Figure 6.5. (a.b,c,d) Fluorescence microscopy images of the BODIPY-SH immobilized cryogels. (e) The cryogels' relative fluorescence intensities after being functionalized with BODIPY-SH. 104

Figure 6.6. (a,b,c,d) TRITCstreptavidin immobilized cryogels fluorescence microscopy pictures, and (e) Fluorescence intensity intensities of cryogels upon protein attachment 105

Figure 6.7. Fluorescence microscopy images of ConA and TRITC-PNA immobilized cryogels (a) before washing (b) after washing. 106

Figure 6.8. Images of cells trapped on the RGD-attached cryogel layer captured with fluorescence microscopy. After detachment, merged fluorescence microscopy pictures indicate viable (green) cells. 107

Figure A.1. ^{1}H NMR spectrum (in $CDCl_3$) of polymer-dendron conjugate (PDC-C).....133

Figure A.2. SEC traces of polymer-dendron conjugate (PDC), copolymer and dendron 133

Figure A.3. Pyrene excitation spectrum of PDC-C micelles. Left inset: I_{338}/I_{334} vs log concentration graph to calculate CMC value. 134

Figure A.4. Size stability of crosslinked (CL-R) micelles from PDC-R in 10% FBS.....134

Figure A.5. Fluorescence microscopy images of MDA-MB-231 cells treated with free DOX and DOX loaded micelles. Cell nuclei were stained with DAPI (blue). Merged images were generated by overlapping DAPI channel (blue) with DOX channel (red) (Scale bar 50 μm).....135

Figure A.6. ^{13}C NMR spectrum of 4 generation polyester dendron.....135

Figure A.7. UV-Vis spectrum of pyridine-2-thione released from pyridyl sulfide-thiol exchange reaction during PEG-SS-DEN4 conjugation.....136

Figure A.8. ^{13}C NMR spectrum of 4 generation polyester dendron.....136

Figure A.9. GPC traces of dendronG4, PEG and PEG-SS-DEN4. 137

Figure A.10. ^{1}H NMR spectrum of redox-responsive (HOOC-PEGDG4).....137

Figure A.11. GPC traces of Dendron G4, PEG and R-PEG-SS-DEN4.....138

Figure A.12. Fluorescence microscopy images of MDA-MB-231 cells treated with free DOX and DOX loaded micelles.....138

Figure A.13. ^{1}H NMR spectrum of redox-responsive dendrimer SS(G1X)$_2$.....139

Figure A.14. ^{1}H NMR spectrum of redox-responsive dendrimer SS(G2X)$_2$.....139

Figure A.15. ^{1}H NMR spectrum of redox-responsive dendrimer SS(G3X)$_2$.....139

Figure A.16. ^{13}C NMR spectrum of PEG-based pyridyl-disulfide group containing methacrylate (PDS-PEG-MA).....140

Figure A.17. Scanning electron micrographs of control cryogels synthesized without reactive monomer.....140

Figure A.18. Water uptake profile of cryogels.....141

Figure A.19. Fluorescence micrographs of TRITC−streptavidin immobilized cryogels after DTT treatment.....141

Figure B.1. Copyright license of Figure 1.2.....142

Figure B.2. Copyright license of Figure 1.3.....143

Figure B.3. Copyright license of Figure 1.4.....144

Figure B.4. Copyright license of Figure 1.5.....144

Figure B.5. Copyright license of Figure 1.6.....145

Figure B.6. Copyright license of Figure 1.7.....146

Figure B.7. Copyright license of Figure 1.8. 147

Figure B.8. Copyright license of Table 1.1. 148

Figure B.9. Copyright license of Figure 1.9. 149

Figure B.10. Copyright license of Figure 1.10. 150

Figure B.11. Copyright license of Figure 1.11. 150

Figure B.12. Copyright license of Figure 1.12. 151

Figure B.13. Copyright license of Figure 1.13. 152

Figure B.14. Copyright license of Figure 1.15. 153

Figure B.15. Copyright license of Figure 1.16. 154

Figure B.16. Copyright license of Chapter 3. 155

LIST OF TABLES

Table 1.1. Commonly utilized targeting moiety examples. Reprinted from [66]. 13

Table 6.1. Conformation of cryogels with changing quantities of pyridyl disulfide monomer.....102

LIST OF ACRONYMS/ABBREVIATIONS

ACN	Acetonitrile
AIBN	2,2′-Azobis(2-methylpropionitrile)
ATRP	Atom Transfer Radical Polymerization
AUC	Area Under the Curve
CCK-8	Cell Counting Kit-8
$CDCl_3$	Deuterated Chloroform
CH_2Cl_2	Dichloromethane
cRGDfK	Cyclic Arginine-Gylcine-Aspartic acid-Phenyl alanine-Lysine
CMC	Critical Micelle Concentration
ConA	Concanavalin A
CTA	Chain Transfer Agent
CuAAC	Copper Catalyzed Azide-Alkyne Cycloaddition Reaction
DAPI	4',6-Diamidino-2-Phenylindole
DCC	*N,N'*-Dicyclohexylcarbodiimide
DDS	Drug Delivery System
DLS	Dynamic Light Scattering
DMAP	4-(Dimethylamino)pyridine
DMAc	Dimethylacetamide
DMF	Dimethylformamide
DMPA	2,2-Dimethoxy-2-phenylacetophenone
DOX	Doxorubicin
DTT	Dithiothreitol
ECM	Extracellular Matrix
EPR	Enhanced Permeability and Retention
EDCI	1-Ethyl-3-(3-Dimethylaminopropyl) Carbodiimide
EtOAc	Ethyl Acetate
FBS	Fetal Bovine Serum
FDA	Food and Drug Administration
FT-IR	Fourier Transform Infrared
GPC	Gel Permeation Chromatography

GSH	Glutathione
HEPES	4-(2-hydroxyethyl)-1-piperazineethanesulfonic Acid
J	Coupling Constant
kDa	Kilo Dalton
LC-MS	Liquid Chromatography–Mass Spectrometry
MALDI-TOF	Matrix-assisted laser desorption/ionization-Time of Flight
MDR	Multidrug-Resistant
MeOH	Methanol
MHz	Mega Hertz
mRNA	Messenger RNA
MTD	Maximum Tolerated Dose
MWCO	Molecular Weight Cut-Off
NMR	Nuclear Magnetic Resonance
NMP	Nitroxide Mediated Polymerization
PAMAM	Poly(amidoamine)
PBS	Phosphate Buffer Saline
PCL	Poly(ε-caprolactone)
PDI	Polydispersity index
PEG	Poly(ethylene glycol)
PEGDEMA	Poly(ethylene glycol) Dimethacrylate
RAFT	Reversible Addition- fragmentation Chain Transfer
SEM	Scanning Electron Microscopy
TEA	Triethylamine
TEM	Transmission Electron Microscopy
THF	Tetrahydrofuran
UV	Ultraviolet

1. INTRODUCTION

1.1. Biomedical Applications of Polymeric Materials

Polymeric materials have developed as an indispensable component of various biomedical devices that find applications in areas ranging from diagnostic to transport. Polymeric materials are highly desirable since they can be imparted with several functional attributes based on their chemical composition and physical properties, apart from their low-cost and easy availability. Some examples of widely encountered polymeric materials are micelles, nanoparticles, nanofibers, nanogels, cryogels, hydrogels, micropatterns, and polymeric aggregates in Figure 1.1 [1−6].

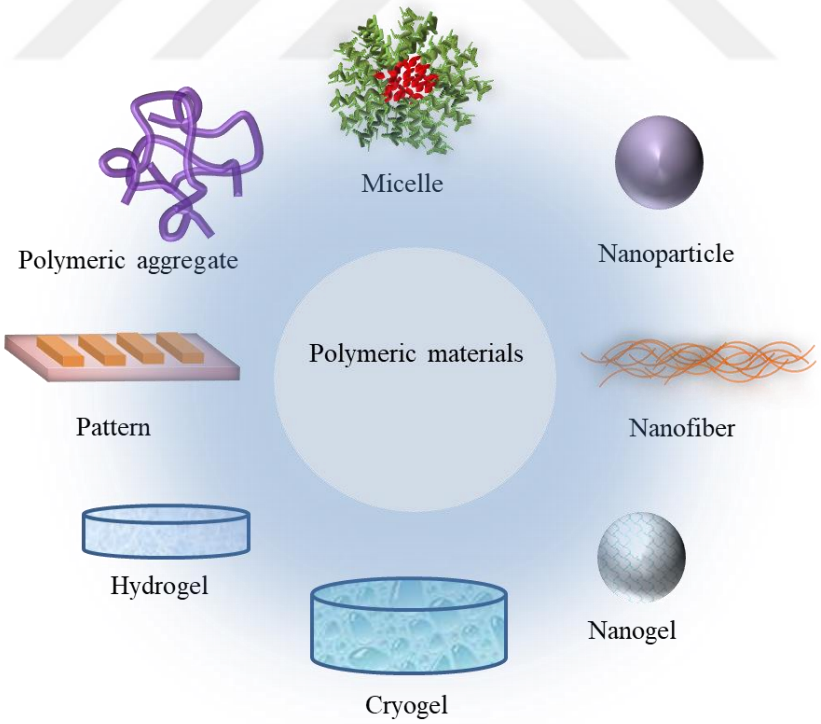

Figure 1.1. Examples of common polymeric materials for biomedical applications.

Over the past decades, polymers' role in biomedical devices has changed considerably. For example, the fundamental purpose of the first-generation polymers used for the implantable device was to ensure biological inertness and structural compatibility [7]. The changing perspective of has led to the development of new types of coating materials that, apart from providing inertness, interact with biological material/environment at a molecular level and are biocompatible [8, 9]. Synthetic polymeric materials appear close to natural tissues compared to their inorganic counterparts, such as metals and ceramics [10, 11]. Due to applications impacting human life quality, such as drug-based therapies, genetic therapies, diagnostic bioimaging, tissue engineering, regenerative medicine, and medical device implants, research in polymeric materials is actively pursued [12]. In particular, polymer-based drug delivery systems appear to provide solutions to many challenges in this area, such as temporal and spatial control over delivery. Needless to say, the ability to preferentially target the disease site will have ramifications in diagnostics and cures.

Along with drug delivery, polymeric materials play an important role in several other areas. Many areas such as diagnostic platforms, bio-separation, and growth of artificial tissues are addressed using smart polymeric structures [13–15]. These soft materials possess the ability to mimic the biological systems. Hydrogels, in particular, are polymeric scaffolds of high interest since these 3D-constructs swell in water, and can be designed to be stimuli-responsive. These materials can be designed to permanently immobilize proteins for biological assays, as well as for protein isolation and subsequent release using the catch-and-release strategy [16]. Changes in pH, temperature, or redox environment can cause hydrogels to undergo physical changes such as expansion/contraction or chemical changes such as bond cleavage [17–20].

1.2. Stimuli-Responsive Biomaterials in Drug Delivery System

Significant progress has been made in creating controlled biomaterials for specific applications throughout the past several decades [21−23]. Our ability to comprehend, design, and orchestrate materials that interface with biological frameworks in a predictable and regulated manner has advanced significantly in recent years. Because of advancements in organic and polymer synthesis, monomer accessibility, and improved handling techniques,

scientists have progressed beyond their reliance on commercial forerunners to make specific materials with application-specific characteristics. This shift has enabled the area of stimuli-responsive biomaterials to advance from static to dynamic materials that respond to specific inputs on demand. Materials into which stimuli-responsive behavior has been incorporated range from nanoparticles, hydrogels [24], cryogels [19], and polymeric structures. Even in nano, micro, or macroscopic materials, the biodegradability of polymeric materials is critical in biomedical applications. When implanted systems reach the end of their useful life, they require removal from the tissue [25]. Ideally, the polymer-based implants must biodegrade so that the patient does not have to undergo surgery, unless the implanted component is a long-term requirement. The choice of polymeric materials is crucial so that the lifetime of the implant is tunable. Furthermore, the nature of the degraded components should be such that they are amenable to elimination from the body without causing harm. Advances in the design and synthesis of synthetic polymeric materials are enabling specific tailoring of materials based on the particular demands of the application

On the other hand, stimuli-responsive biodegradable polymers have long been used in drug delivery systems such as nanocarriers [27, 28]. Conventional chemotherapy, radiotherapy, and surgery are common cancer treatments with limited efficacy against advanced tumors. During the last few decades, stimuli-responsive nanoparticles (SRN) have been extensively studied as effective drug delivery vehicles in tumor immunotherapy [28]. Nanoparticles responsive to endogenous (pH, enzyme, ROS, hypoxia, redox) and exogenous (radiation, electromagnetic, thermal) stimuli have been employed to increase the effectiveness of drug delivery in Figure 1.2 [29].

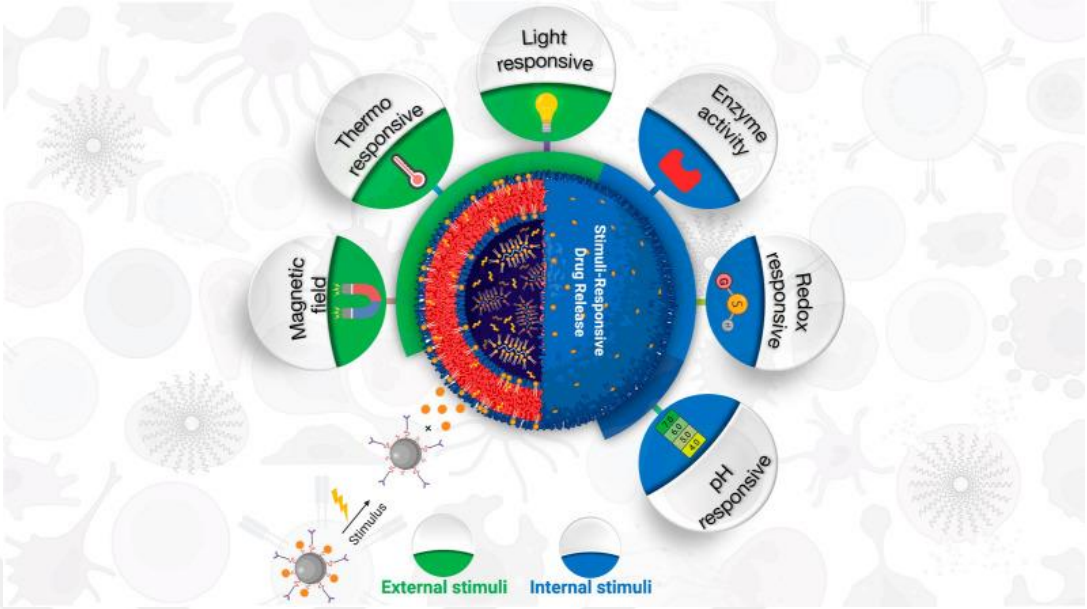

Figure 1.2. Intrinsic/extrinsic stimuli and stimuli-responsive nanocarriers (NCs). Reprinted from [29].

In this thesis, we will focus on polymeric DDS, which are sensitive to pH and environmental redox changes. Both of these are endogenous stimuli, and thus can be effectively utilized to design delivery agents which will predominantly release the therapeutic cargo upon reaching the disease site. It is well established that tumor and cancer cells have lower pH than normal tissues. The thiol-containing tripeptide glutathione (GSH) expression is upregulated in several types of cancers. Over the past several decades, polymer-based nanostructures responsive to either or both of these stimuli have been fabricated, but minimal work has been reported with dendritic structures, which is one of the main focus of this thesis. The sections below briefly highlight some examples of pH and redox-sensitive polymer-based DDSs.

1.2.1. pH-Responsive Polymeric Materials for Drug Delivery Systems

The pH value varies throughout organs, tissues, and cellular compartments, making it an appropriate stimulus for regulated medication release. Because they can administer medications regulated at a specified site and time, pH-responsive drug delivery systems have gained increasing interest as "smart" drug-delivery systems for addressing the drawbacks of

standard drug formulations [31, 32]. Utilization of acid-sensitive structures in the DDS to be prepared will often provide easy release of the transported drug in the targeted area in Figure 1.3.

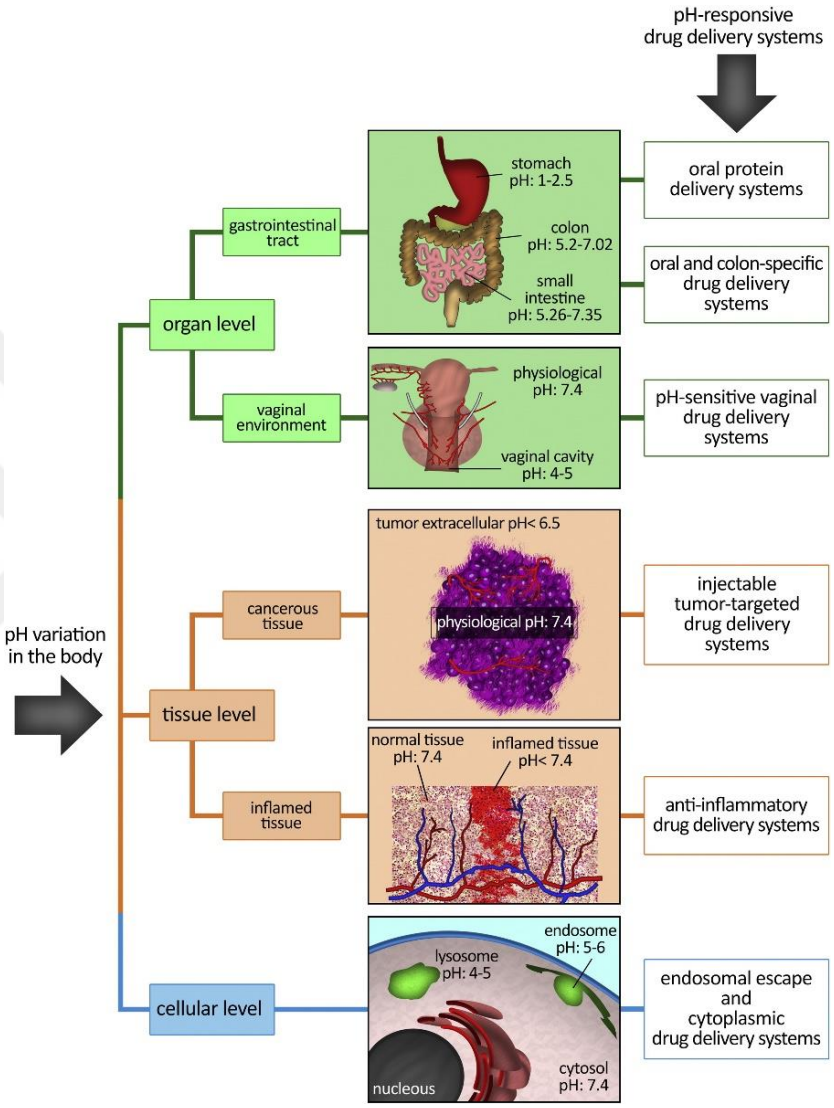

Figure 1.3. pH changes at the cellular and organism levels. Reprinted from [32].

In recent years, many pH-sensitive drug delivery systems have been used. Micelles [34–36], dendrimers [37–39], nanogels [39], and hydrogels [40] are among the most common structures used as pH-sensitive DDS. Acid labile linkers on polymeric materials are generally employed in drug delivery systems to impart pH sensitivity. Since the pH of healthy tissue is 7.4, acid-labile linkers enable drug release predominantly in tissues/cells, where the pH is lower than in healthy cells. pH-sensitive DDS are gaining popularity because

they can be engineered to release active drugs at a precise time based on the disease's pathophysiology, resulting in better patient treatment efficacy and compliance. Asthma [41], peptic ulcer, cardiovascular disorders [43–45], cancer, and hypertension [45] are some of the circumstances where pH-sensitive DDS show potential.

As a typical example, Hruby and coworkers developed and characterized a new polymeric micellar pH-sensitive method for doxorubicin drug delivery. The authors used a copolymer composed of a biocompatible hydrophilic poly(ethylene oxide) (PEO) block and a hydrophobic block containing doxorubicin covalently attached to the carrier by a pH-sensitive hydrazone bond. The drug release kinetics in aqueous buffers at pH 5.0 (near to endosome pH) and 7.4 were investigated (pH of blood plasma). At pH 5.0, the drug was released significantly faster than at pH 7.4. Static (SLS) and dynamic light scattering were used to investigate the changes in the particle at pH 5.0 and 7.4, which differentially degraded under these different environments [46].

1.2.2. Redox Responsive Polymeric Materials for DDS

Changes in redox conditions could provide an effective stimulus in biological systems that rely on the considerably different redox states in the circulation/extracellular fluids and intracellular compartments. Various redox-responsive polymeric systems have been created by incorporating redox-responsive linkages [48, 49]. Disulfide linkage with redox-responsive polymers has spurred interest in several therapeutic applications, from drug delivery vehicles to diagnostic interfaces. The cleavage of the disulfide linkage in the presence of an endogenous reducing agent (GSH), which is present in higher concentrations in diseased tissues, has promoted the integration of this specific linkage into several therapeutic platforms. GSH is a thiol-containing tripeptide that breaks down disulfide bonds in biological systems. In animal cells, glutathione/glutathione disulfide has been shown to be one of the most prevalent redox pairs [50, 51]. These redox pairs determine the anti-oxidative capability of cells. While GSH concentrations in the cytosol reach 2–10 mM, they decline to roughly 2–20 µmolar outside the cell [51]. Furthermore, *in vivo* research revealed that the tumors have a GSH concentration at least 4-fold higher than normal tissue. Researchers have designed several polymeric-based drug delivery systems that can utilize

this difference in the redox environment between normal and cancerous tissues to release the drug at the disease site. Thiol-disulfide exchange events with redox-active molecules like glutathione can cleave the disulfide bonds in the DDS to release the active ingredient [53–55].

Drugs may be conjugated to a polymeric drug carrier through disulfide bonds to achieve redox-triggered drug release. For example, Wang and coworkers reported redox-responsive micellar nanostructures to combat multidrug-resistant cancer in Figure 1.4. A disulfide-containing redox-responsive diblock copolymer was utilized. MCF7 breast cancer cell line and MCF7-ADR multidrug-resistant cancer cell line were employed. Multidrug resistance (MDR) is a crucial barrier to cancer treatment success. One of the most well-known and significant plasma membrane proteins is the P-glycoprotein, which can effluxion numerous anti-cancer medicines (e.g., doxorubicin and paclitaxel) out of MDR tumor cells due to its overexpression in the plasma membrane [54].

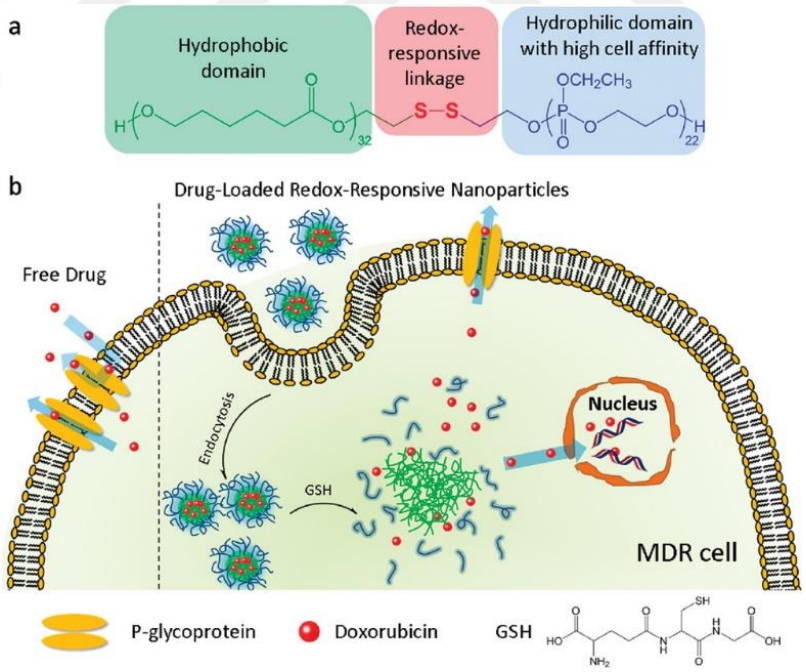

Figure 1.4. (a) Chemical structure of disulfide-bridged PCL-SS-PEEP block copolymer and schematic illustration of redox-responsive nanoparticles for overcoming cancer cell multidrug resistance (b). Reprinted from [54].

The thiol-disulfide exchange reaction has been extensively utilized as a tool to fabricate disulfide-containing polymeric materials. An activated disulfide moiety, namely, pyridyl disulfide (PDS) is employed to obtain disulfide-containing constructs with high efficiency and selectivity [55] . The PDS-thiol exchange chemistry has been used to obtain various redox-responsive polymeric materials ranging from soluble polymers, surface coatings, and crosslinked materials such as nanogels and hydrogels in Figure 1.5.

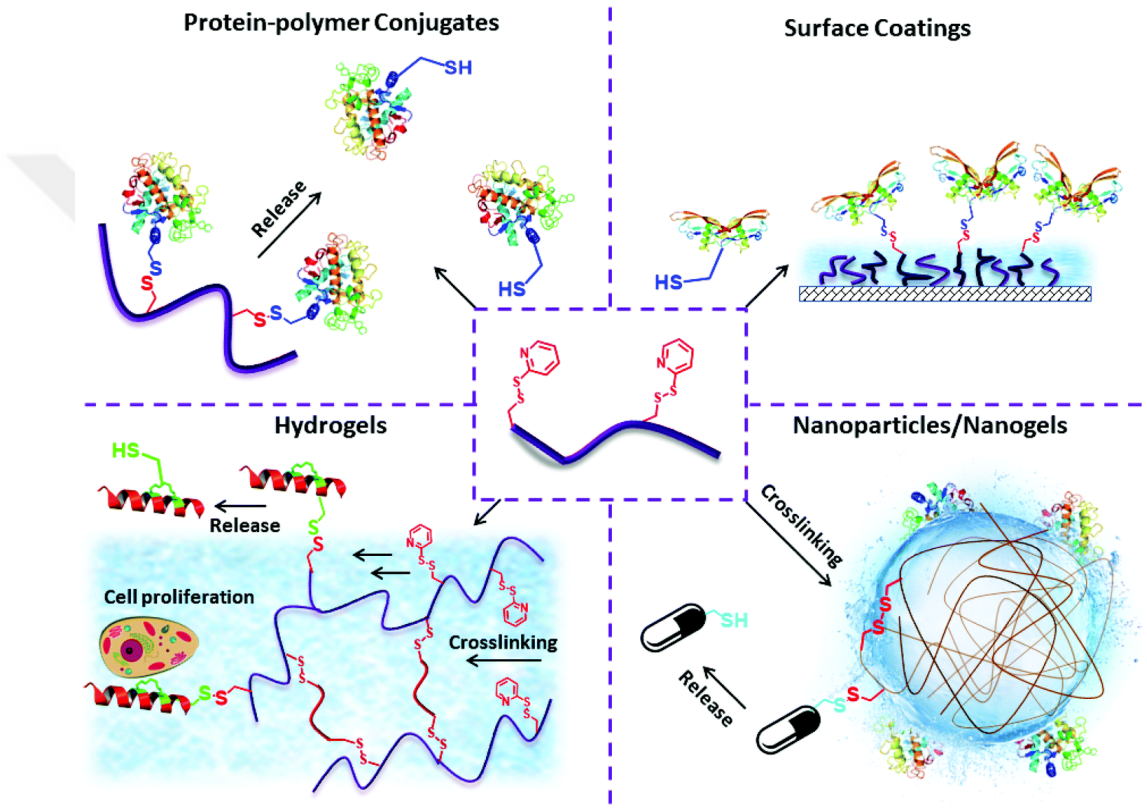

Figure 1.5. Examples of functional materials fabricated using pyridyl-disulfide containing polymers. Reprinted from [55].

The PDS-thiol exchange reaction has been exploited to engineer redox-responsive nanogels. The Thayumanavan and coworkers have made seminal contributions in this area. Over the past several years, they have constructed redox-responsive nanogels to deliver therapeutic molecules and biomolecules. For example, in one of their reports, copolymers containing the PDS-based monomer and PEG-based methacrylate were assembled as nanostructures by heating them above their lower critical solubilization temperature. Subsequent crosslinking of these self-assembled nanosized aggregates through inter-chain

cross-linking by partial hydrolysis of the PDS groups using DTT led to stable redox-responsive aggregates in Figure 1.6 [56].

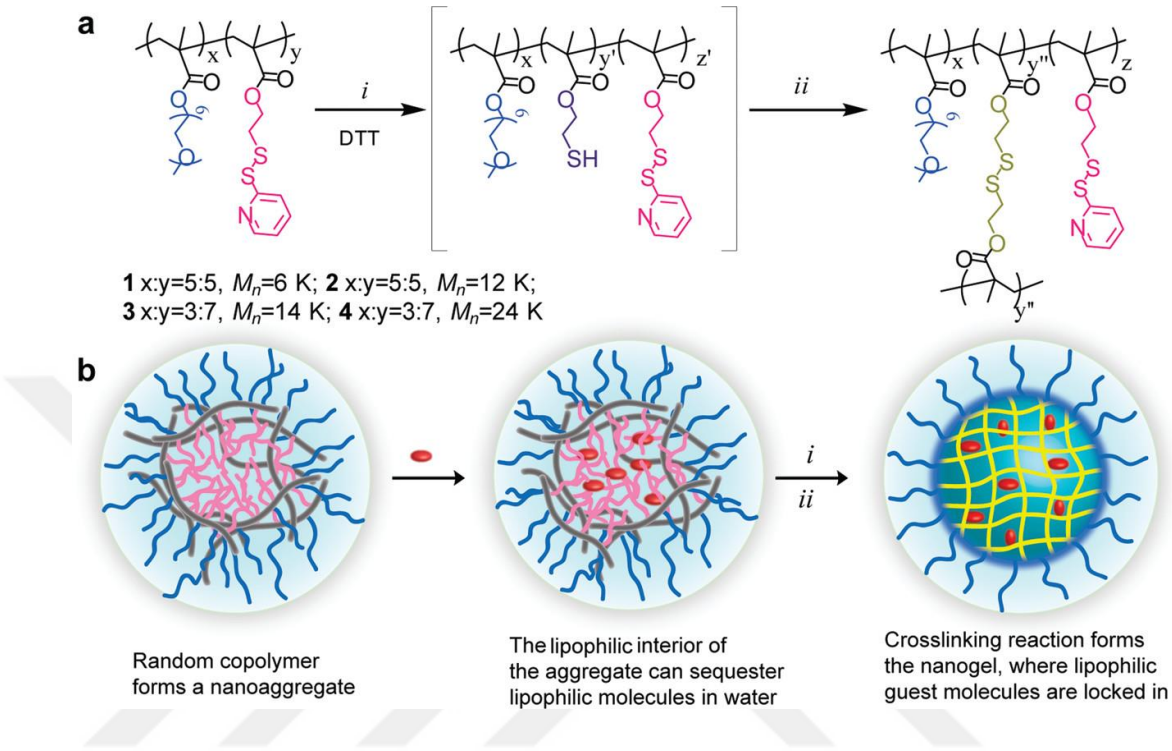

Figure 1.6. Fabrication of redox-responsive nanogels using the pyridyl-disulfide thiol exchange reaction. Reprinted from [56].

Incorporating the PDS group on polymeric interfaces such as coatings and crosslinked scaffolds is beneficial because it enables adding functional molecules to these materials through a reversible linkage [57]. In this regard, Sanyal and coworkers have reported the fabrication of hydrogels containing the PDS group in Figure 1.7. The PDS groups on the hydrogel could be modified with bioactive ligands and cell-adhesive peptides. Importantly, proteins and cells immobilized onto the hydrogels could be harvested by treatment with a thiol-containing reducing agent such as dithiothreitol (DTT).

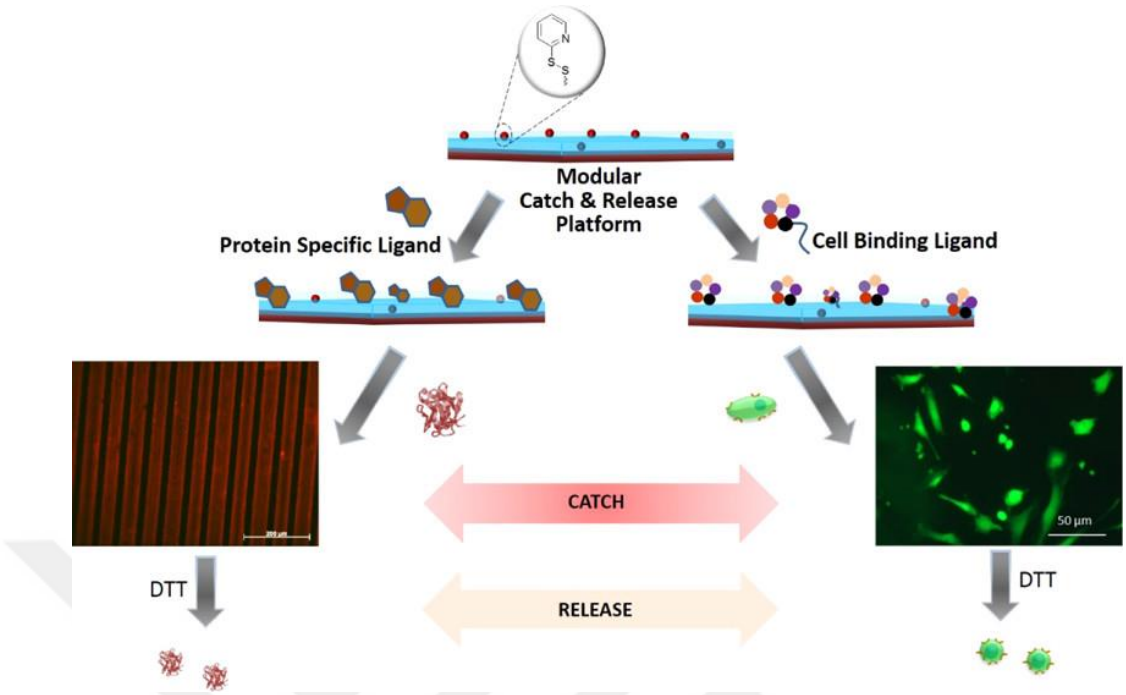

Figure 1.7. Pyridyl-disulfide group containing hydrogel coating for selective attachment and release of target proteins and cells. Reprinted from [57].

1.3. Stimuli-responsive Polymers in Drug Delivery Systems for Cancer

Cancer is one of the most severe health issues facing humanity. It is a dangerous and chronic condition that causes fear and disorientation by producing powerlessness and uncertainty [58]. Normal cells go through a predictable cycle of growth, division, and death [59]. On the other hand, cancer cells do not follow this cycle. They don't die; instead, they replicate and generate other aberrant cells [60]. These cells can infect organs like the breast, liver, lungs, and pancreas. They may also spread to other areas of your body via your blood and lymph system. Today, however, breakthroughs in cancer diagnosis and therapy have raised patient survival rates. Chemotherapeutics are used to treat cancer in the majority of cases, in addition to radiation therapy and surgery [61]. Chemotherapy is a drug treatment that uses powerful chemicals to kill fast-growing cells in your body. Many different chemotherapy drugs are available. Chemotherapy drugs can be used alone or in combination to treat various cancers. Though chemotherapy is an effective way to treat many types of cancer, chemotherapy treatment also carries a risk of side effects. Some chemotherapy side

effects are mild and treatable, while others can cause serious complications. While this sort of therapy has shown to be effective in some cancers, it has not been as effective in other cancers. Furthermore, it is harmful to healthy tissue.

1.3.1. Passive and Active Targeting in Cancer Therapy

Researchers develop medicines by learning how tumor cells differ from healthy cells. Because of their architectural and pathological abnormalities from healthy tissue, solid tumors have a different enhanced permeability and retention (EPR) effect [62]. Macromolecular medicines may selectively collect and stay in solid tumor tissues, but they might not distribute widely in healthy tissue [63].

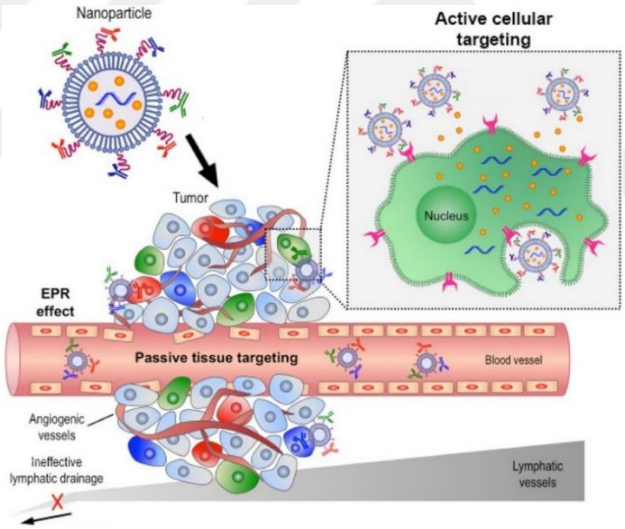

Figure 1.8. Representation of the mechanism for active and passive tumor targeting. Reprinted from [64].

Most solid tumors have a higher vascular density than normal tissues and organs, indicating angiogenesis, which is one of the most crucial properties of tumors to maintain their rapid growth [65]. Vascular angiogenesis could be seen even when tumor nodules were less than 0.2 mm [67, 68]. In addition, tumors frequently have uneven or variable blood flow. Many solid tumors have a defective structure. There are large spaces between endothelial cells and no smooth muscle layers. Thus, large molecules escape from the blood vessels to

the tumor area and accumulate there selectively in Figure 1.8. In addition, impaired lymphatic function is always present in tissues for the recovery of macromolecules in tumor tissues. As a result, once macromolecules accumulate in tumor tissues, they are not cleared from the tumor tissues and stay there for a long time.

Particle size of the drug delivery system is important in passive targeting. Organs select foreign particles like a sieve and deliver them to the desired area [69–71]. As the particle size decreases, the probability of the drug to penetrate the organs and the body increases. Cabral and coworkers investigated whether a series of micellar nanomedicines with diameters smaller than 100 nm and carrying the powerful tumoricidal drug 1,2-diaminocyclohexane-platinum(II) (DACHPt) (the parent complex of oxaliplatin) might accumulate and penetrate weakly permeable pancreatic tumors [70]. They discovered that long-circulating polymeric micelles' anti-tumor efficacy depends on micelle size and tumor penetration. Sub-100 nm micellar nanomedicines demonstrated no size-dependent limits on extravasation and penetration in hyper vascular tumors with a highly permeable structure. Nanomedicines smaller than 50 nm, on the other hand, can penetrate minimally permeable hypovascular tumors [71]. Moreover, utilizing a transforming growth factor signaling inhibitor to increase the permeability of hypo vascular tumors increased the formation and distribution of micelles with size bigger than 70 nm, suggesting a viable technique to enhance the effectiveness of larger nanomedicines [72].

Active targeting is achieved by conjugating bioactive molecules that will specifically attach to cell-specific receptors on the surface of the cells to be treated [73]. In the targeted smart drug delivery system, the component on the surface of the delivery system first recognizes the target, binds, and delivers the drug to the desired area to show the therapeutic effect [74]. Nanomedicine can be functionalized with targeting ligands to provide active tumor targeting. These ligands help cells recognize and bind to each other. The ligands on the nanoparticles bind to the receptors on the surface of the cancer cells to induce receptor-mediated endocytosis occurs [75]. Once internalized by the cells, the nanoparticles successfully release the cargo they carry. Table 1.1 shows some examples of commonly used targeting ligands.

Table 1.1. Commonly utilized targeting moiety examples. Reprinted from [75].

Class	Ligand	Targets	Advantages	Limitations	Clinical approve
Antibodies	a-Herceptin Rituxan b-CD19	-HER2 -CD20 -CD19 antigen	High affinity and strong binding; already in clinical trials; therapeutic potential	High production cost; pharmacokinetics; 'binding site barrier effect'; potential immunogenicity	a-Approved as antimetastatic breast cancer (i.e. trastuzumab). b-Approved as HIV Medicines.
Peptides	a-RGD b-NGR	-avb3 integrins, -Aminopeptidase N	High affinity	Reduced circulation half-life	a-[^{18}F] Galacto-RGD is approved as RGD PET tracer in human. b-NGR-hTNF/DOX as vascular targeting agent is in phase 1b.
Proteins	a-Transferrin LHRH	-Transferrin receptor -LHRH receptor	Already in clinical trials	High production cost	a-SGT-53, a scFv anti-TfR1 liposome complex is in Phase I and II.
Aptamers	a-Pegaptanib	-VEGF receptor	Possible to develop for any target	High production cost	a-Approved as Macugen (Pegaptanib Sodium) Injection.
Small molecules	a-Folate b-Galactose	-Folate receptor -Asialoglyco-protein receptor	Low production cost, low molecular weight; simple chemistry	Could reduce circulation time	a-Phase II. b-Not approved yet

For example, Miura and coworkers utilized PEG-poly glutamic acid and maleimide conjugated PEG-poly glutamic acid in the study. Integrins, abundantly expressed in angiogenetic areas and malignancies, were targeted with cRCD peptides in Figure 1.9. As a control experiment, the non-targeting ligand cRAD was also employed. When compared to micelles decorated with non-targeted ligand cRAD, confocal laser scanning microscopy studies revealed that cRGD linked polymeric nanoparticles gathered quickly and had high permeability from vessels into the tumor cell parenchyma, even though both cRGD and cRAD-linked micelles have similar size, surface charge, and amount of loaded drug [76].

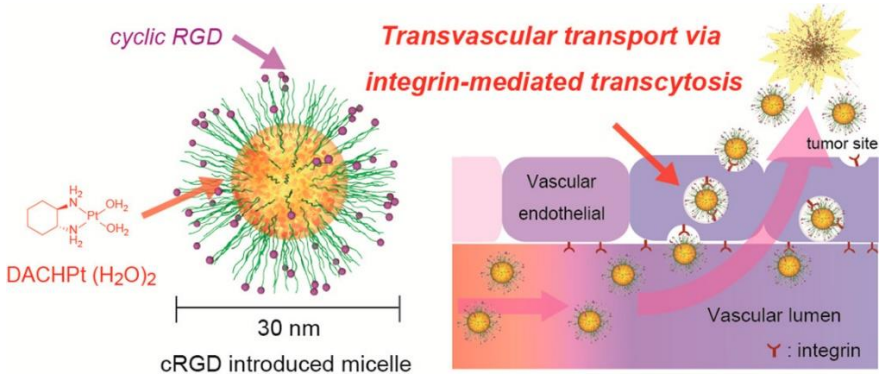

Figure 1.9. The design and synthesis strategy for the ligand-linked DACHPt/m is depicted in this diagram. Reprinted from [76].

1.3.2. Polymeric Nanocarriers in Cancer Treatment

Conventional chemotherapy agents comprised of small molecule cytotoxic agents are typically used to treat cancer. As chemotherapeutic drugs are toxic, they perform well, but they also harm healthy cells, causing side effects that can impair their overall effectiveness. Many drugs used in cancer treatment are hydrophobic and must be dissolved using a toxic solubilizer, which can cause adverse side effects. Hydrophobicity is also linked to poor kinetics, a high amount of protein binding, and thus a small apparent volume of distribution [77]. Because cancer medications are small molecules, they influence the entire body, including healthy cells. They can produce side effects such hair loss, nausea and vomiting, exhaustion, hearing loss, and infection susceptibility [78]. They also have a short half-life and undergo rapid clearance. As a solution to these challenges, incorporating chemotherapy agents within biodegradable nanomaterials through physical encapsulation or chemical linkages has been actively investigated.

Nanoparticles employed in medical therapy often have certain diameters, shapes, and surface composition since these three factors significantly impact the effectiveness of nanocarriers transport and hence therapeutic effectiveness control [79, 80]. Nanocarriers have been used for many years, and there are even those on the market in Figure 1.10. Nanomaterials with a size of 10 to 100 nm are commonly used in cancer treatment because they may carry medications efficiently and have an increased permeability and retention

(EPR) effect. Smaller particles can easily leak from normal vasculature, causing harm to normal cells, and can be quickly processed by kidneys (just under 10 nm in diameter), however particles bigger than 100 nm are more likely to be eliminated from circulatory by phagocytic cells. Furthermore, nanoparticle surface properties can affect bioavailability and half-life. Nanocarriers coated using hydrophilic materials like as polyethylene glycol (PEG), for example, reduce deposition and hence prevent immune system clearance. As a result, nanocarriers are frequently modified to render them hydrophilic, which prolongs drug circulation and improves drug permeation and retention in malignancies [81, 82]. Nanocarriers' therapeutic impact in cancer management is determined by their many features taken together.

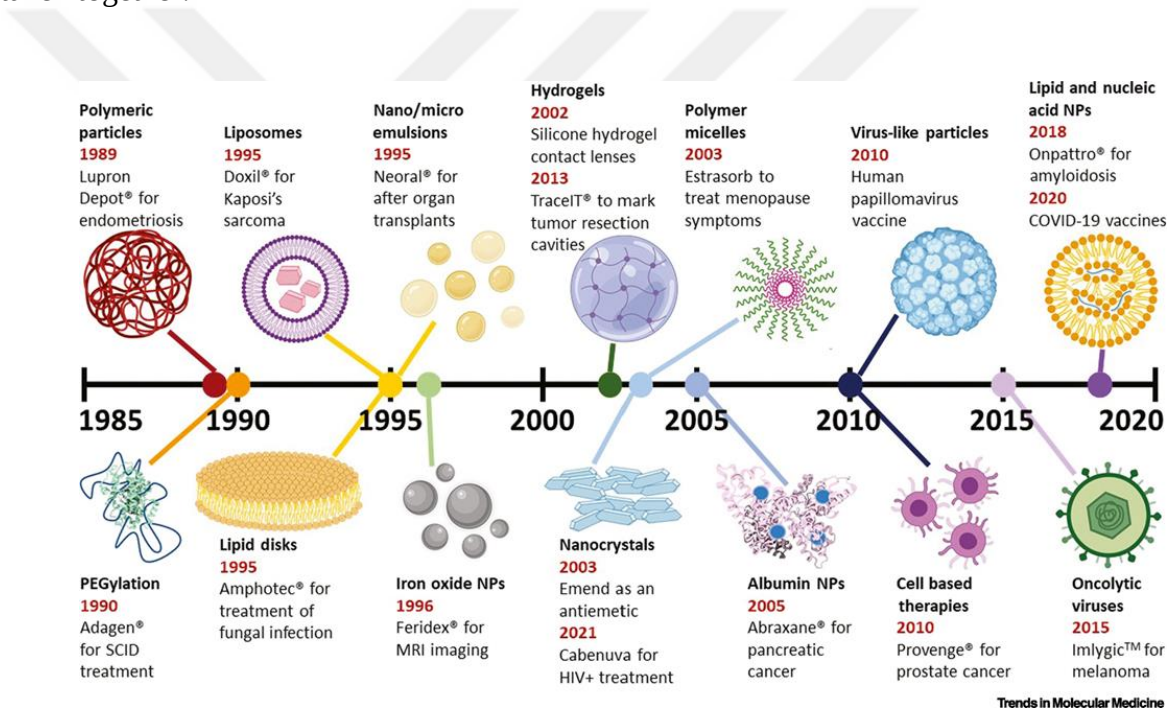

Figure 1.10. Timeline of FDA Approval of Therapeutic Nano and Microparticles. Reprinted from [83].

1.3.3. Polymer Dendron Conjugates as Drug Delivery Systems

The architectural perfection of dendritic structures distinguishes them from traditional polymers [84–86]. Dendrimers are spherical monodisperse macromolecules that are usually highly symmetric [87, 88]. Dendrimers and dendrons are tree-like branched polymeric

architectures in Figure 1.11 [89]. Depending on the generation, the size of dendrimer can be tuned from 1 to 10 nanometers. Dendrimers are made up of three major components: core, branches, and changeable periphery. These well-defined monodisperse architectures are synthesized using a stepwise manner using highly efficient organic reactions. Dendrimers can be made using one of the two methods: a divergent approach, or a convergent approach. In the divergent method, synthesis starts with a reactive core to generate generation, and then functionalize the molecule's periphery. Higher generation dendrimers are obtained by following these reactions in an iterative manner, usually requiring a protection-deprotection sequence.

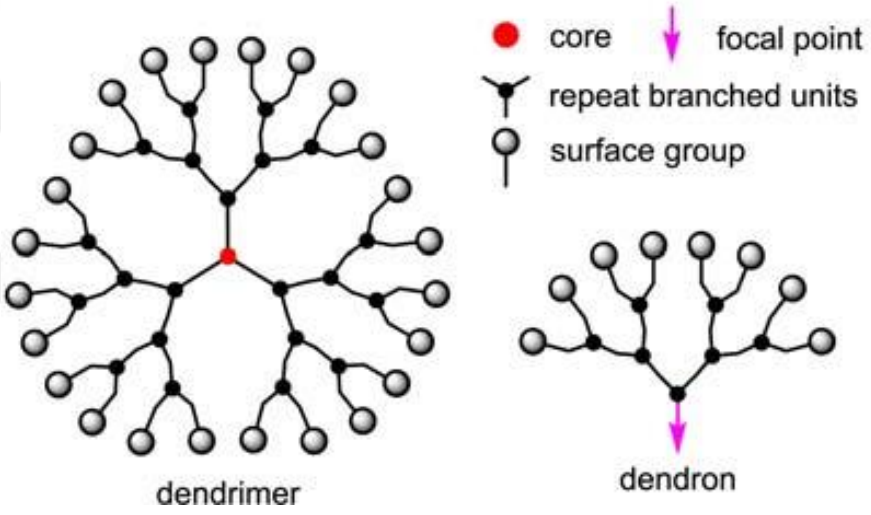

Figure 1.11. Schematic structural illustration of a dendron. Reprinted from [89].

In recent years, dendron-polymer copolymers have emerged as an attractive polymeric precursors for the fabrication of nanosized drug delivery systems in Figure 1.12 [90]. Dendrons can be combined with polymers to obtain architecturally different constructs [91], [92]. While linear polymers usually have a random-core structure, addition of dendrons onto the polymer backbone makes the structure more extended due to the steric hindrance. Thus, the conformation takes a cylindrical or rod like structure after attachment of several generations of dendrons to side chains or polymer ends. Dendron conjugated polymers have been widely used in drug delivery and pharmaceutical applications due to their improved physical properties and multifunctionality [93]. Among the possible structures, the dendron-

polymer conjugates such as linear AB diblock or ABA triblock copolymers have been extensively studied to assemble in micellar form.

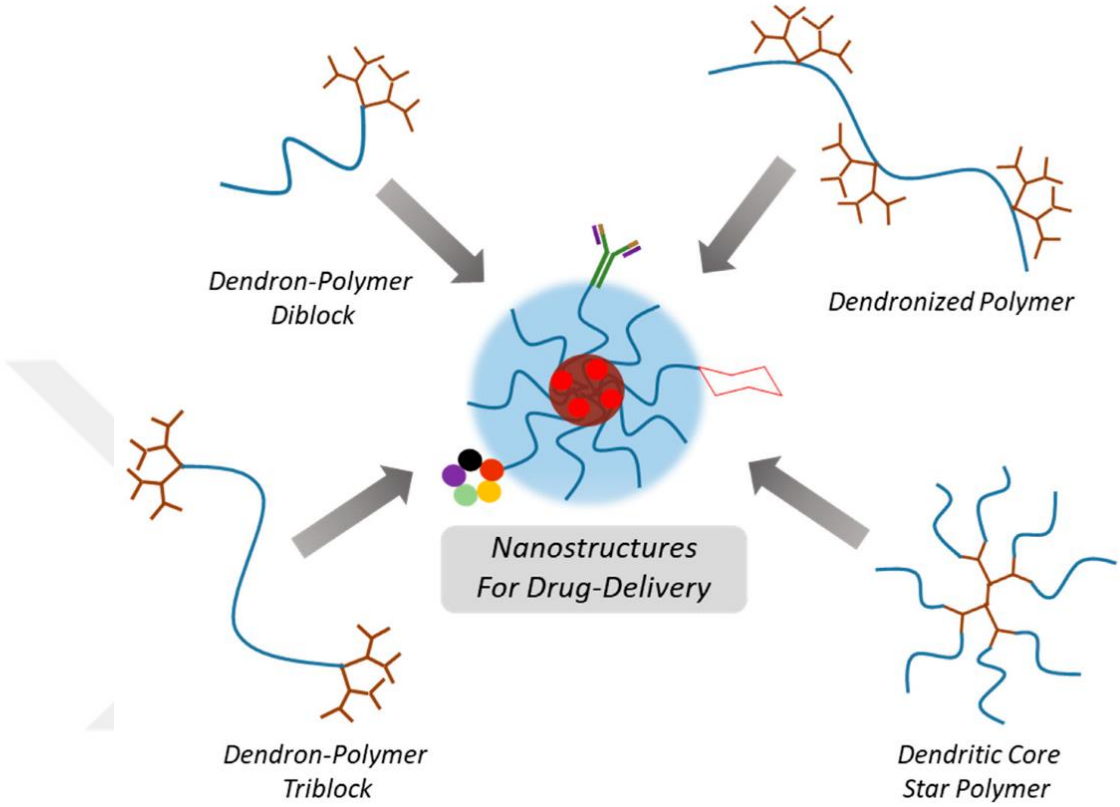

Figure 1.12. Various dendron-polymer conjugates utilized for fabrication of nanosized drug delivery systems. Reprinted from [90].

Polymeric micelles are an emerging class of promising platforms for cancer therapeutics. In general, amphiphilic macromolecules composed of a hydrophilic and hydrophobic block are used as building blocks for polymeric micelles [94]. Micellar drug formulation has been proven in preclinical and clinical research to have various advantages, including improved drug solubility, longer drug circulation duration, passive tumor targeting via EPR effects, and improved drug tolerance [95]. Moreover, targeting group can be used to improve accumulation of nanoparticle in tumor tissue. Since micelles are stabilized through non-covalent hydrophobic interactions, their stability can be compromised upon dilution, usually a situation confronted upon in vivo administration. To further improve their aqueous stability, core and shell crosslinked micelles have been investigated as pragmatic drug delivery systems.

An early example of dendron-polymer conjugate based DDS was reported by Pan and coworkers. When compared to a linear polymer-DOX conjugate, Pan and colleagues found that a dendronized polymer-doxorubicin (DOX) hybrid (DPDH) had better in vivo drug delivery efficiency for cancer therapy (LPDC). Since a larger proportion of DOX is released at pH 5.2 at a faster pace than at pH 7.4, the *in vitro* drug release pattern of DOX implies that DPDH exhibits pH-responsive drug release due to hydrazone bond cleavage. DPDH penetrates 4T1 cells efficiently and releases DOX, causing cytotoxicity and apoptosis. DPDH has a substantially longer blood circulation duration than LPDC because to its dendronzied structure. Cancer progression inhibition, TUNEL assessment, and histological analysis all show that DPDH significantly outperforms LPDC and free medication in suppressing tumor growth in a 4T1 breast cancer model. Hemolysis, body weight fluctuations following treatment, and pathological investigation all indicate DPDH's biosafety. This research shows that using dendronized polymer-DOX hybrids for specific drug molecules is a promising drug delivery method [96].

More recently, Sanyal and coworkers reported that two types of micellar systems using polymer–dendron conjugates in Figure1.13. AB type diblock build utilizing a 2K PEG and an ABA type triblock construct using a 6K PEG as the B block. The hydrophobic component used in both constructions was a fourth generation polyester dendron (block A). The micellar system was created with the ability to insert varying amounts of targeted ligands onto their surface. An additional dendron–polymer construct with a cyclic RGD targeting group was introduced to achieve this. The micellar carrier was utilized to encapsulate the widely used anti-cancer medication docetaxel, and the effect of the micellar carrier on treatment efficacy was tested *in vitro* on two RGD-sequence recognizing cancer cell lines, the MDA-MB-231 human breast cancer and the A549 human lung cancer. From this study it was deduced that micellar nanostructures with high degree of stability could be obtained by using an AB-type dendron-polymer conjugate by employing a fourth-generation dendron which provided an ideal hydrophilic-hydrophobic balance. Thus in this thesis, most of the constructs are fabricated using higher generation dendrons. Although, it should be noted that it is possible to obtain stable constructs with lower generation dendrons, provide the micellar structures are covalently crosslinked after their self-assembly.

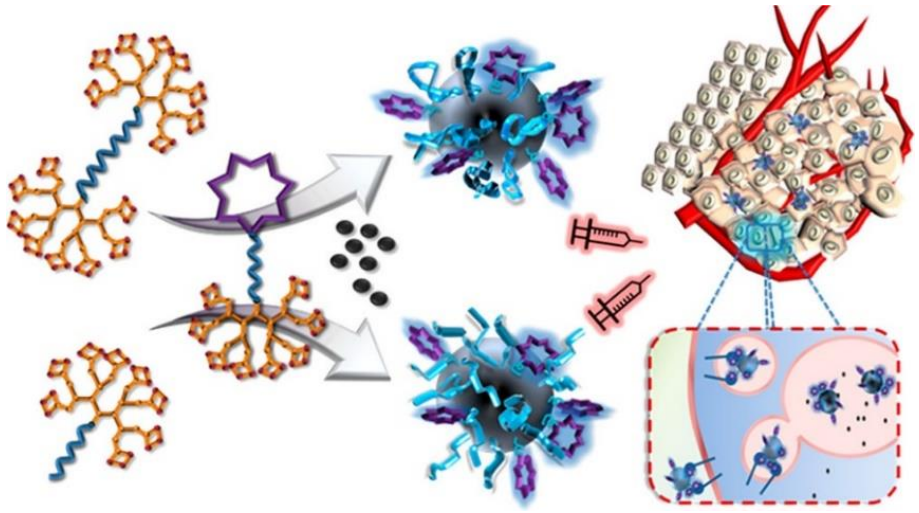

Figure 1.13. Micelles can be passively and actively targeted in the tumor environment. Reprinted from [97].

Micellar systems formed in PDC can also be designed to be sensitive to stimuli. Some variables, including as pH, reduction, and light intensity, are extremely sensitive to these polymeric micelles [98]. The pH of tumor tissues differs from that of normal tissue. The pH of tumor tissue is roughly 5.5. This acidic media allows polymers to disperse into unimers. In acidic environments, ortho ester, hydrazone, cis-aconityl, and acetal bonds, for example, are extremely vulnerable to breaking down, and thus can be used as linkages to conjugate the drug or stabilize the micellar constructs during transport and accumulation in the tumor.

1.4. Cryogels as an Emerging Scaffold for Biomedical Applications

Apart from soluble and dispersible polymeric supports, solid polymeric interfaces are also indispensable for various biomedical applications. In particular, hydrogels, a class of crosslinked hydrophilic polymers with high water uptake capacity is employed as bioimmobilization support for diagnostic applications, as drug delivery devices and scaffolds for tissue engineering. Although over the past several decades hydrogels have been investigated as scaffolds enabling therapeutic delivery of both small molecules and biomolecules, their performance can be limited due to lack of high porosity. Presence of large pores are often desirable so that biomolecules and cellular materials can infiltrate into the interior of the scaffold. This characteristic is especially important if these scaffolds are

utilized as scaffolds for biomolecular separations, where facile flow through the polymeric materials is advantageous. Likewise, macroporosity is an inherent requirement for scaffolds if they are going to be employed for tissue engineering. Cells should be able to spread throughout the polymeric materials to enable three-dimensional tissue formation. A special class of gels, termed as cryogels, provides a viable solution to many of the limitations of hydrogels. In recent years, cryogels (CGs) have emerged as a compelling alternative to hydrogels [99]. Figure 1.14 shows that cryogels are macroporous gel networks created by crosslinking of monomers and/or polymeric precursors at subfreezing temperatures. Cryogels have a larger porosity than typical hydrogels, resulting in improved swelling ability and, as a result, improved loading and release characteristics. Apart from simplicity of fabrication of cryogels, an added advantage is possibility of using aqueous solvents, depending on the choice of monomers. In spite of the highly porous nature of these materials, these materials possess adequate osmotic durability and mechanical strength, thus making them materials of interest for a number of biomedical applications.

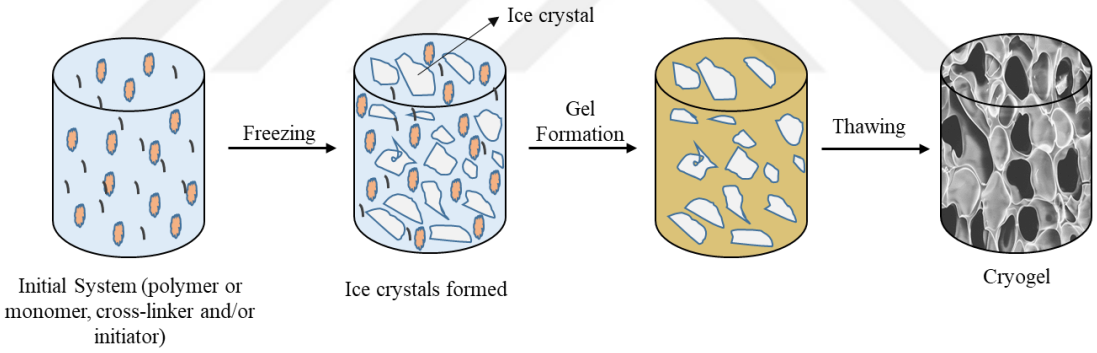

Figure 1.14. Schematic illustration of cryogelation technique.

Although there is renewed interest in these materials, early reports on cryogels dates back to 1908 [100]. Lottermoser was perhaps one of the first to describe the creation of honeycomb structures in materials when they were frozen. Bobertag *et al.* observed structural changes in the first frozen, then remelted material, which they explained as the result of expanding ice crystals exerting forces on the matter, which is expelled from the liquid carrier and trapped between the crystals as it freezes. According to the literature, the first few applications of cryogels was published by Lozinsky *et al*. They were focused on

the immobilization of bacterial cells and enzymes onto cryogel matrices. Citrobacter intermedius cells were entrapped in 10% poly(vinyl alcohol) cryogel beads [101].

Some of recent studies proved that cryogels outperform standard hydrogels for the conjugation and release of anti-cancer medicines in a study. Sanyal and coworkers reported that the development and testing of novel bulk hydrogels and cryogels with N-hydroxysuccinimide (NHS) activated carbonate moiety as reactive groups for drug molecule attachment and slow release via a hydrolyzable carbamate linker in Figure 1.15. Hydrogels and cryogels containing different ratios of reactive monomers were synthesized. When the water holding capacity and drug release profile of hydrogels are compared due to their nonporous structure, it was observed that they had worse water holding capacity and drug release than cryogels, as expected. Cryogels with very porous microstructures were created to achieve a significant level of drug release in a short period of time. Through the creation of a hydrolyzable carbamate link, the resulting cryogels were functionalized with the amine-containing anti-cancer medication doxorubicin. At somewhat acidic conditions, the release of doxorubicin from the cryogel was significantly boosted and sustained, according to the release studies [102].

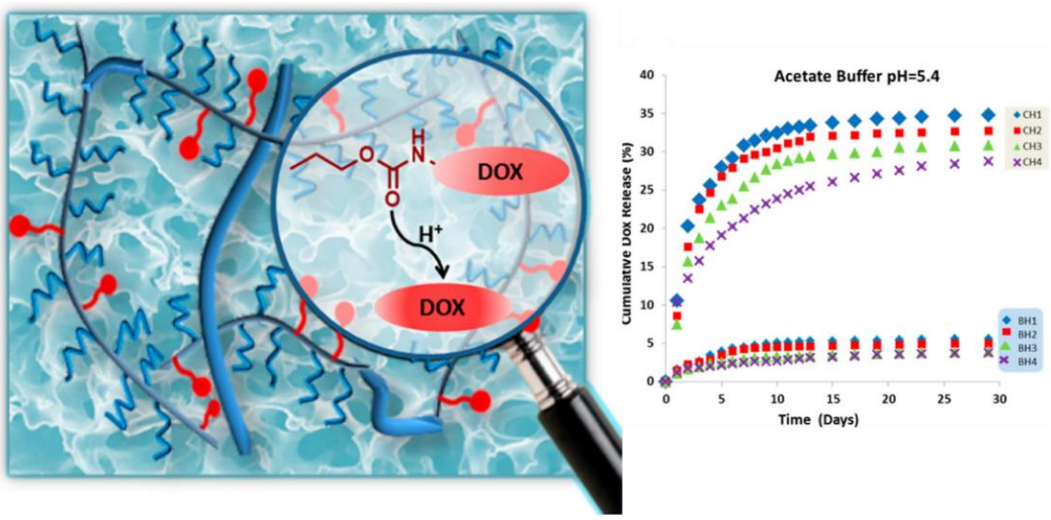

Figure 1.15. *In vitro* doxorubicin release profiles of cryogels and bulk gels in acetate buffer pH = 5.4. Reprinted from [102].

Apart from drug delivery scaffolds, cryogels can be used as polymeric interfaces for diagnostic purposes such as protein sensing. The macroporous nature of cryogels allows easy diffusion of large biomolecules and thus interact with the ligands throughout the gel matrix. In this regard, cryogels containing 'clickable' reactive groups are quite attractive since they can be decorated with ligands of interest in a facile and efficient manner. In a recent work, Sanyal and coworkers described cryogels with thiol-reactive maleimide groups for protein attachment and identification. They used furan-protected maleimide-containing monomers to introduce the reactive maleimide group into the cryogel matrix. The monomer contains a lengthy hydrophilic linker that acts as a spacer seen between thiol-conjugation domain and the cryogel matrices. The resulting cryogels were successfully prepared with a thiol-bearing protein, including such albumin, or with thiol-bearing ligands to provide ligand-targeted protein immobility or detection. The ability of cryogels to bind ligand-directed proteins including streptavidin as well as Concanavalin A (ConA) proves its viability as a protein detection platform. In particular, a comparison was made between hydrogels and cryogels to demonstrate that the higher matrix porosity of cryogels leads to their superior performance in Figure 1.16.

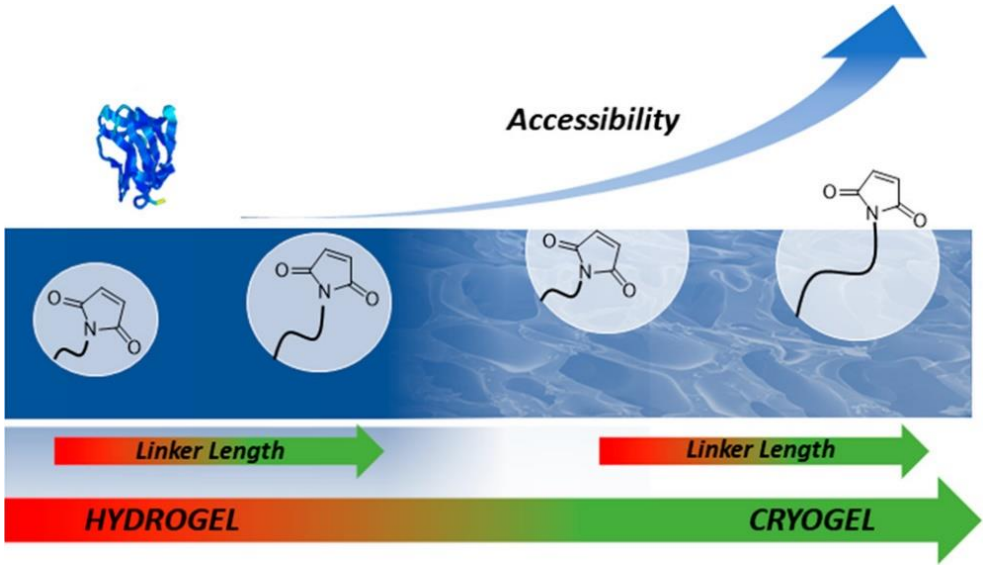

Figure 1.16. Schematic illustration of impact of linker length and porosity on the extent of biomolecule conjugation onto gel substrates. Reprinted from [103].

The short overview presented above suggests that polymeric materials play a vital role in providing solutions to many health-related areas. The increasing demands for functional materials in the health sector necessitate the design and fabrication of novel materials to meet present challenges. This thesis explores the fabrication of novel stimuli-responsive polymeric materials and assesses their preliminary performance in drug delivery and biomolecular sensing areas.

2. RESEARCH OVERVIEW

This thesis includes four research projects involving the design and synthesis of polymeric materials for biomedical applications. These projects can be classified under two broad topics: fabrication of dendron-polymer conjugate (DPC) based stimuli-responsive micellar nano-aggregates as drug delivery vehicles, and stimuli-responsive macroporous cryogel (CG) scaffolds for applications such as protein immobilization and cell culture.

The first three chapters focus on the fabrication and application of micellar structures derived from the self-assembly of DPCs in aqueous media. Obtained nano-aggregates are characterized and evaluated for loading and release of anticancer drugs. Also, in two chapters, cyclic peptides are integrated into DPC structures to enable targeted delivery to cancer cells that over-express specific receptors. A critical aspect of such delivery platforms is their stability upon dilution; a scenario faced upon intravenous administration. Two different approaches are evaluated in this thesis. The first approach involves stabilization through crosslinking of the self-assembled nanostructures. In the second approach, utilization of higher generation hydrophobic dendrons and changing the architecture of DPC from diblock to the side-chain dendronized copolymer. Furthermore, while the constructs in the first chapter are acid-sensitive degradation, the latter two chapters use a disulfide-based redox-responsive linkage between the dendron and the polymer.

In the final chapter, we employ disulfide-based chemistry to fabricate redox-responsive cryogels. It is demonstrated that scaffolds obtained using cryogenic photo-polymerization can be reversibly functionalized using thiol-containing small molecules and bioactive ligands. Selection protein immobilization/sensing on such scaffolds was evaluated. Cytocompatibility of such materials is also evaluated to assess their suitability for possible tissue engineering applications.

In conclusion, employing developments in contemporary organic and polymer chemistry, this dissertation describes the design and synthesis of novel micellar nanostructures and gel-based materials that can be adapted for various biomedical applications.

3. DENDRON-POLYMER CONJUGATE BASED CROSSLINKED MICELLES: A ROBUST AND VERSATILE NANOSYSTEM FOR TARGETED DELIVERY

The materials in this chapter have been adapted from the following article:

Calik, F., A. Degirmenci, M. Eceoglu, A. Sanyal, and R. Sanyal, "Dendron-Polymer Conjugate Based Cross-Linked Micelles: A Robust and Versatile Nanosystem for Targeted Delivery", *Bioconjug. Chem.*, Vol. 30, No. 4, pp. 1087–1097, 2019.

3.1. Introduction

Nanoparticle based drug delivery carriers are emerging as a viable platform since they are able to address many of the challenges faced in conventional cancer therapeutics such as high toxicity and non-specificity of drug molecules toward disease cells and their short residence time in the body. Nano-therapeutic platforms based on liposomes have been clinically administered for decades to elongate the residence time of therapeutic agents in the body, as well as reduce their systemic toxicity. Due to the fragile nature of liposomal constructs, investigations in recent years have focused on the evaluation of polymer based micellar structures. The enhanced stability of these nanostructures, coupled with the wide variety of possible structural and compositional variations make these promising candidates for drug delivery. As with most nanosized carriers, polymeric micelles benefit from preferential accumulation in tumor tissues due to the enhanced permeability and retention (EPR) effect. Furthermore, recent advances in design and synthesis of functionalizable polymers, allow conjugation of various receptor homing groups to allow ‘active’ targeting.

While micellar delivery platforms have many of the abovementioned positive attributes, several aspects still require further consideration and improvement [104]. One of the main challenges is the stability of such systems upon dilution. After intravenous administration, micelles are diluted and thus encounter risk of dissociation, which would

cause premature drug release before the micelles reach the target diseased tissue. Among several approaches toward further stabilization of micelles, core or shell crosslinking based strategies have been evaluated. Apart of resisting disassembly upon dilution, crosslinking of the structure may also modulate the drug release profile. An ideal micellar system would exhibit a large difference in release rates under physiological condition encountered during transport versus under in acidic or redox environment of cancerous cells.

Dendritic structures have been utilized as components that form the hydrophobic core to increase the stability of micellar constructs. In an amphiphilic dendron-polymer conjugate, the branched structure of hydrophobic dendrons leads to enhanced hydrophobic interactions which stabilizes the structure. Unfortunately, the requirement of high volume of the hydrophobic component to obtain a suitable amphiphilic balance calls for employment of high generation dendrons, unless very hydrophobic peripheral groups like aromatic ones are employed [105]. While micelles may be obtained with lower generation dendrons, they usually disassemble upon dilution. In this regard, core-crosslinking of micellar structures after their assembly has been exploited as a viable strategy to address this challenge. Thus, we envisioned that it should be possible to employ dendron polymer conjugates with a lower generation dendron, which upon crosslinking should gain the desired stability against dilution.

Herein, we report the fabrication of dendron-polymer conjugate based targeting group bearing core-crosslinked micellar structures as drug delivery vehicles in Figure 3.1. The dendron polymer conjugates are obtained using Huisgen type ‘click’ reaction based coupling of an orthogonally functionalizable dendron containing an alkyne unit at the focal point and alkene functional groups at the periphery with an azide terminated hydrophilic copolymer. Polyester dendrons were chosen due to their biodegradable and hydrophobic nature. Hydrophilic copolymers containing amine reactive activated ester groups as side chains and azide group at chain end were obtained using controlled/living polymerization. While the chain end azide unit provides conjugation with the alkyne containing dendron, the amine reactive groups were used as handles to install cyclic peptide based targeting moieties. Obtained peptide bearing dendron-polymer conjugates were evaluated for preparation of micelles loaded with doxorubicin, a clinically administered anticancer drug. The micellar structures were core-crosslinked with tetrathiol-based crosslinkers using the alkene groups

at the periphery of dendrons using the radical thiol-ene reaction. The non-crosslinked and crosslinked micelles were compared with regard to their stability and drug release under neutral and acidic conditions. Finally, *in vitro* cytotoxicity and internalization studies were carried out with the best micellar candidates against MDA-MB-231 breast cancer carcinoma cells.

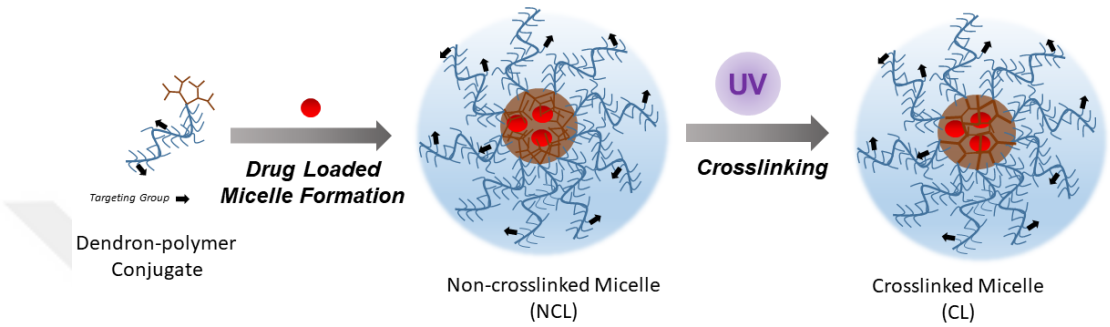

Figure 3.1. Illustration of fabrication of drug loaded core-crosslinked targeted micelles.

3.2. Experimental Section

3.2.1. Materials

2,2-Bis(hydroxymethyl)propionic acid, Dowex X50WX2, propargyl alcohol, 4-pentenoic anhydride and *N*,*N*-dicyclohexylcarbodiimide (DCC) were purchased from Alfa Aesar. Pentaerythritol tetrakis(3-mercaptopropionate), di(ethylene glycol) methyl ether methacrylate (DEGMA), *N,N,N′,N″,N″*-pentamethyldiethylenetriamine (PMDETA) and copper(I)bromide (Cu(I)Br) were purchased from Aldrich. 2,2-Dimethoxy-2-phenylacetophenone (DMPA) was obtained from Acros. Synthesis of cRGDfK was achieved through solid phase peptide synthesis (SSPS, PS3 Peptide Synthesizer, Protein Technologies Inc., USA) [106]. All solvents were purchased from Merck and used as obtained without further purification unless otherwise noted. Ultrapure water was obtained using Milli-Q Water Purification System (Milli-Q system, Millipore, Billerica, MA, USA). Azide functionalized initiator was synthesized according to literature procedures [107]. *N*–

hydroxysuccinimide methacrylate (NHSMA) monomer was synthesized using literature procedure [108]. Third generation polyester dendron containing alkyne unit at the focal point was synthesized according to literature [109].

3.2.2. Instrumentation

Chemical compositions of small molecules, dendrons and polymer were characterized using ^{1}H NMR spectroscopy (Varian 400 MHz). Micellar formations were characterized their critical micellar concentration and size using fluorescence spectrophotometer (Varian Cary Eclipse, Agilent, USA) and Zetasizer Nano particle analyzer (Malvern), respectively. The molecular weights of the polymers were estimated by size exclusion chromatography (SEC) analysis using a PSS-SDV (length/ID 8 × 300 mm, 10 µm particle size) Linear M column calibrated with polystyrene (PS) standards (1–150 kDa) using a refractive-index detector. Tetrahydrofuran (THF) was used as eluent at a flow rate of 1.0 mL/min at 30 °C. UVP Black-Ray B-100AP/R High Intensity UV lamp (100 Watt / 365 nm) was used for crosslinking experiments. During the internalization experiments, cells were visualized using Zeiss Axio Observer inverted fluorescence microscope (Carl Zeiss Canada Ltd, Canada). The dry micellar constructs were visualized on a holey carbon film coated 300 mesh Cu-grid (Pacific Grid Tech, USA) using a LVEM5 electron microscope on transmission electron microscopy (TEM) mode (Delong Instruments, USA).

3.2.3. Synthesis of cRGDfK Containing Polymer-Dendron Conjugate (PDC-R)

In order to attach targeting moiety, polymer dendron conjugate (PDC) was synthesis according to previously reported protocol [110]. After obtaining PDC, targeting group was utilized on it. In a 5 mL reaction flask, conjugate **(**5.0 mg, 0.00075 mmol), cRGDfK (10.8 mg, 0.018 mmol) and DMAP (12.8 mg, 0.104 mmol) were added, sealed and purged with N_2. The mixture was dissolved in anhydrous DMF (0.25 mL). The reaction was stirred at room temperature for 5 days. Then 1-amino-2-propanol (1.65 µL, 0.021 mmol) was added to the reaction mixture and stirred at room temperature 24 h, to convert the residual reactive groups. After evaporating DMF, residue was dissolved in water (2 mL) then acidified with

HCl solution (0.1 M, 0.25 mL). Polymer containing solution was dialyzed with deionized water to remove unbound cRGDfK. The solution in dialysis bag was freeze-dried to obtain the cRGDfK containing conjugate (70 % yield). For fabrication of non-targeting group containing micelles for control experiments, a polymer dendron conjugate (PDC-C) was synthesized by converting all NHS-groups by treatment with 1-amino-2-propanol using the abovementioned protocol (58% yield).

3.2.4. Micelle Formation from Polymer-Dendron Conjugate and Related Measurements

Co-solvent evaporation method was used to prepare micelle solution and measure critical micelle concentration (CMC). Briefly; various concentrations of the conjugate, ranging from 10^{-5} M to 10^{-9} M (in 3 mL water) were dissolved in 500 µL THF. Pyrene solution was added to all samples and the last concentration of pyrene was set to 6.10^{-7} M for each sample. Then, Milli-Q water (3 mL) was added to all samples dropwise and these mixtures were kept open to air to evaporate the organic phase. Fluorescence experiments were carried out for all samples to determine the CMC. Pyrene excitation spectra were recorded using a fluorescence spectrometer at emission wavelength of 390 nm. The excitation fluorescence at 300 and 360 nm was monitored. The intersection of the CMC values were calculated while extrapolating the intensity ratio I_{338} / I_{334}.

3.2.5. Core Crosslinking Experiments.

Polymer-dendron conjugate (PDC-R or PDC-C) (3×10^{-5} mmol) was dissolved in THF (300 µL). Concentration of copolymer was approximately 100 fold above CMC. In a separate dark vial, solution of pentaerythritol tetrakis(3-mercaptopropionate) (6×10^{-5} mmol) in THF (30 µL) and solution of DMPA (2.4×10^{-5} mmol) in THF (10 µL) were prepared and added into the polymer solution. Then, Milli-Q water (3 mL) was added dropwise. Mixture were kept open to air to evaporate the organic phase. The resulting solution was crosslinked by applying UV irradiation (365 nm) for 30 min from a distance of 10 cm.

3.2.6. Stability Experiments

In order to check the stability of micelle, size measurement was performed using dynamic light scattering (DLS). NCL and CL micelle samples at CMC concentrations were prepared using PDC-R. Samples were diluted to CMC x 10^{-3}. Then, size of micelles were examined using DLS. In addition, the colloidal stability of the CL micelles was also evaluated after 72 hours of incubation in 10% FBS solution.

3.2.7. Encapsulation and *in vitro* release of DOX

DOX was loaded into micelles using co-solvent evaporation method. The amount of DOX loaded was calculated by fluorescence spectrophotometer. For determination of drug loading content, the DOX-loaded NCL and CL micelles were freeze-dried and dissolved in DMSO and the DOX content was evaluated via fluorescence measurement using DOX calibration curve. The drug-loading capacity (DLC) were calculated as

DLC (wt%) = (weight of loaded drug/total weight of polymer with drug) x100%

and efficiency (DLE) as

DLE (%) = (weight of loaded drug/weight of drug in feed) x 100%.

To determine the release kinetics of DOX from CL and NCL micelles *in vitro,* dialysis membrane (MWCO 3500) was used under sink conditions with gentle shaking (260 rpm) at 37ºC in two different buffer media. Drug loaded CL and NCL micelle solutions (1 mg/mL) were prepared by co-solvent evaporation method. These solutions were placed into dialysis bags and immersed in 20 mL of acetate buffer (pH 5.4) and phosphate buffer (pH 7.4) separately and incubated at 37 °C for 30 hours. At predetermined time points, the outer phase of dialysis membrane was removed and replenished with an equal volume of fresh release media. The amount of DOX released was determined by using fluorescence spectroscopy (excitation at 485 nm). The release experiment results presented are average data with standard deviations.

3.2.8. *In vitro* Cytotoxicity.

In this study, MDA-MB-231 human breast cancer cells (purchased from ATCC (LGC Standards, Germany)) were used for cytotoxicity experiments. Cells were grown in RPMI medium according to manufacturer's culture method requirements and incubated at 37 °C in a humidified atmosphere of 5 % CO_2 and kept in logarithmic phase of growth throughout all experiments. The edge row and column wells of a 96-well plate was filled with distilled water (100 µL/well). The cells were seeded in rest of the wells, with a 5,000 cell/well density having medium (100 µL/well) in quadruplicates for each drug concentration.

After 24 h incubation, micelle solutions (in medium) containing DOX between 10^{-4} - 10^{-12} M, were placed onto the cells (100 µL/well). For free DOX treatment, DOX was dissolved in 1mL PBS buffer. After 48 h of incubation, CCK-8 assay was applied to determine cell viability. For this assay, CCK-8 solution (10 %) containing medium (60 µL/well) was applied and incubated for additional 2 h. The absorbance measurements were obtained with a plate reader (Multiscan FC, Thermo Scientific, USA) at 450 nm. Based on these absorbance values, EC50 values of different micelles and free DOX were calculated with Graph Pad Prism software by nonlinear regression analysis.

3.2.9. Cellular Internalization

For cellular internalization, MDA-MB-231 adenocarcinoma cells (75 000 cells/well) were seeded in 12-well plate as duplicate in culture media (1 mL). The cells were incubated at 37 ^{o}C for 24 h. Neutral doxorubicin (DOX), DOX-doped targeted and non-targeted micelles (0.04 mg/mL DOX concentration) were added onto the wells. For competitive internalization, free RGDfV was added as an inhibitor to another set of wells containing DOX-doped targeted micelles. After addition of micelles, cell media were removed at several time points (1, 3, 24 h) during incubation. Then, cells were washed with PBS (3 x 500 µL). Cells were fixed using 4 % formaldehyde solution for 10 min at 37 ^{o}C and incubated for 15 min for DAPI nuclei staining. Images of stained cells were obtained using Zeiss Observer Z1 fluorescence microscope and processed with AxioVision software.

3.3. Results and Discussion

3.3.1. Synthesis of Targeting Group Containing Polymer-Dendron Conjugate

Well defined hydrophobic dendron and hydrophilic polymeric building blocks were used for synthesis of the amphiphilic polymer-dendron conjugate. The hydrophilic copolymer segment also contained N-hydroxysuccinimide (NHS) activated ester groups to enable installation of the amine group bearing cyclic peptide based targeting ligand [111]. An orthogonally functionalizable dendron was designed to enable reactions in a selective manner at its focal point for conjugation to the polymer and its periphery for subsequent micellar crosslinking. Such dual clickable dendrons allow facile access to various multi-functionalizable polymer-dendron conjugates using click reactions [112]. The hydrophobic polyester dendron was synthesized from the third generation dendron containing an alkyne group at the focal point and hydroxyl groups at its periphery. Deprotection of the acetonide groups of the dendrons was achieved via treatment with DOWEX, H^+ yielding hydroxyl surface groups. Alkene units required for subsequent crosslinking of the micellar core was incorporated by treatment with an alkene-containing anhydride. The azide group containing hydrophilic polymeric segment was synthesized using atom transfer radical polymerization (ATRP) of di(ethylene glycol)methacrylate (DEGMA) and NHS-methacrylate (NHSMA). Number average molecular weight (Mn) for the DEGMA-co-NHSMA copolymer was deduced as 3.4 kDa from SEC analysis. The incorporation of the amine reactive NHS group on the polymer chain was confirmed from the presence of proton resonance at 2.77 ppm belonging to the methylene protons of the succinimide ring in the ^{1}H NMR spectrum.

To obtain the amphiphilic dendron-polymer conjugate, the two blocks were coupled using the Huisgen-type Cu(I) catalyzed alkyne-azide ‘click’ reaction. After purification of the conjugate by precipitation in ether to remove the unreacted dendron, the product was analyzed using ^{1}H NMR spectroscopy. As expected, a proton resonance at 7.70 ppm belonging to the triazole proton was observed, apart from the characteristic proton resonances from the polymer and dendron components in Figure 3.2. Additionally, a molecular weight increase to M_n = 5900 Da upon attachment of dendron to the polymer was

evident upon comparison of the SEC traces of the dendron, copolymer and the polymer-dendron conjugate (PDC) in Figure A2.

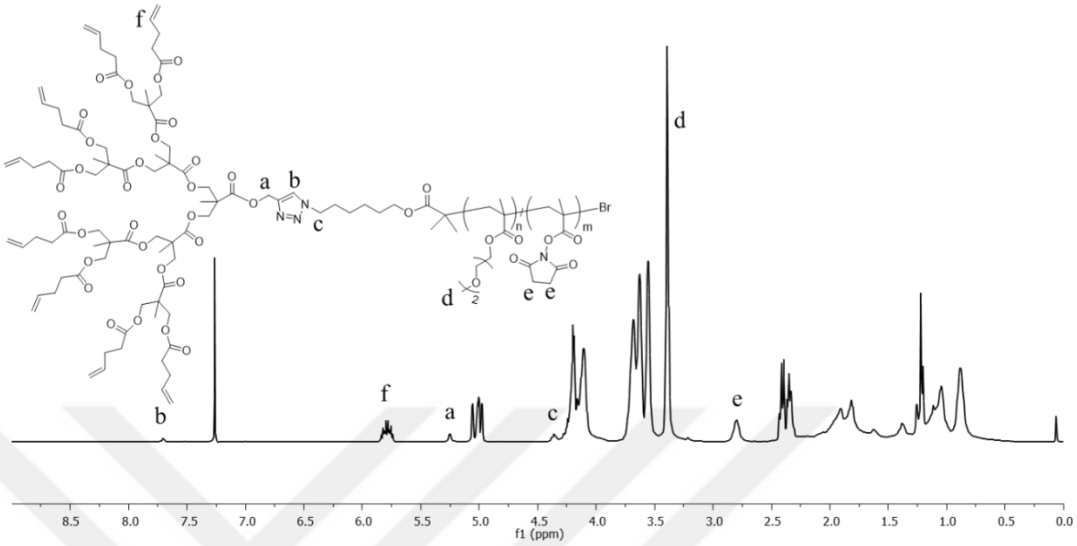

Figure 3.2. ^{1}H NMR spectrum of polymer-dendron conjugate

Thus obtained reactive PDC was utilized for attachment of cRGDfK using DMAP as a catalyst in DMF at room temperature in Figure 3.3. The residual peptide was removed through dialysis against water. Successful conjugation of the cyclic peptide onto the PDC to afford the targeting group containing construct PDC-R was verified by ^{1}H NMR spectroscopy in Figure 3.4. Residual NHS-activated ester groups on the conjugate were treated with 1-amino-2-propanol to eliminate any undesirable interaction in the biological media. The characteristic peaks of cRGDfK were clearly observed in the ^{1}H NMR spectra of PDC-R. The newly formed doublets between 7.23 ppm and 7.18 ppm belong to the protons of the phenyl group in cRGDfK. Extent of peptide functionalization was deduced as close to 10%, which was deemed to be sufficient since a micellar construct will possess a large number of polymeric chains, which would display multiple targeting motifs. For control experiments, a dendron-polymer conjugate (PDC-C) devoid of any targeting peptide was prepared where all activated ester groups were converted to unreactive form by treatment with 1-amino-2-propanol in Figure A1.

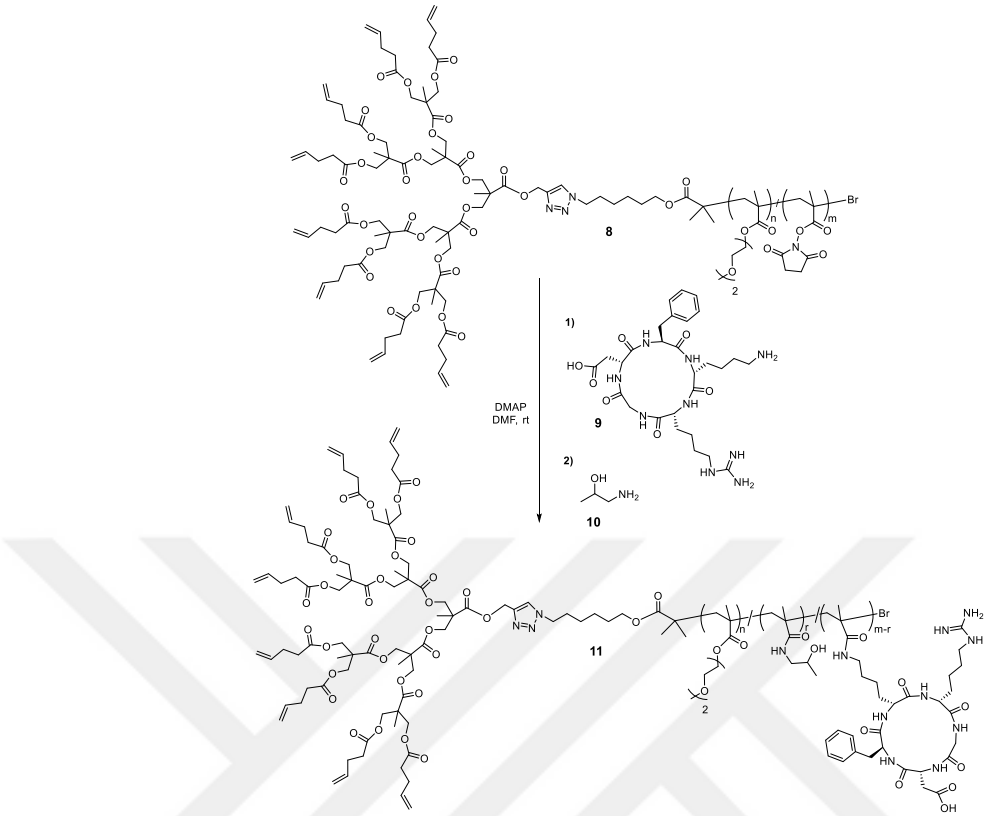

Figure 3.3. Synthesis of cRGDfK containing polymer dendron conjugate (PDC-R).

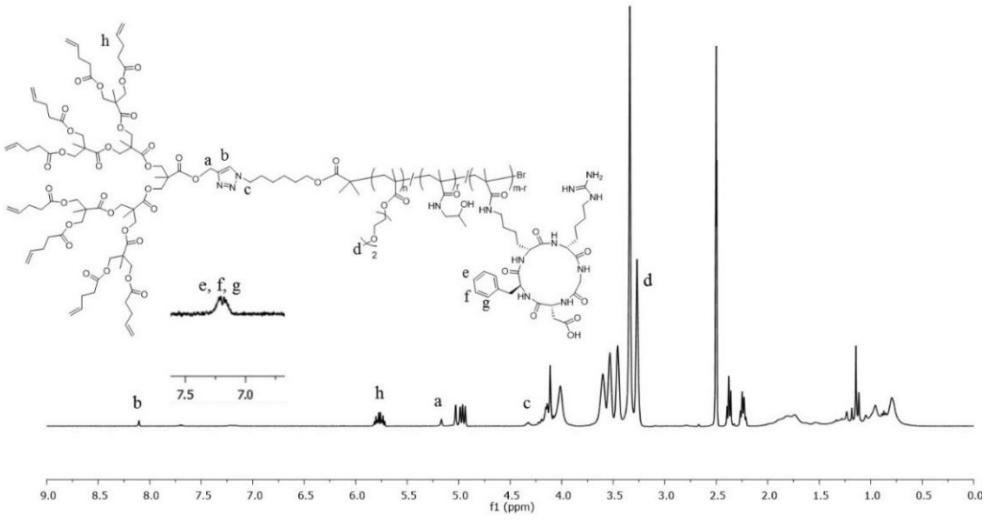

Figure 3.4. ^{1}H NMR spectrum of polymer-dendron conjugate PDC-R containing peptide.

3.3.2. Determination of Critical Micelle Concentration (CMC)

CMC of the PDC-R was determined using pyrene, a hydrophobic fluorescence probe. Micelle formation above a certain concentration of the amphiphilic conjugate in aqueous media, results in an increase in the amount of solubilized pyrene, which is accompanied by an increase in the intensity of the pyrene emission peak. In addition, the maxima of the peak shifts from 334 nm to 338 nm upon micelle formation. The CMC is calculated from the intersection when extrapolating the intensity ratio I_{338}/I_{334} at low and high concentration regions. Using this approach, CMC value of PDC-R and PDC-C constructs were determined as 7.47 x 10^{-7} M and 1.02 x 10^{-7} M, respectively in Figure 3.5 and Figure A3. The CMC values of the conjugates are close to each other since they have similar molecular weight and they both have the same hydrophobic core.

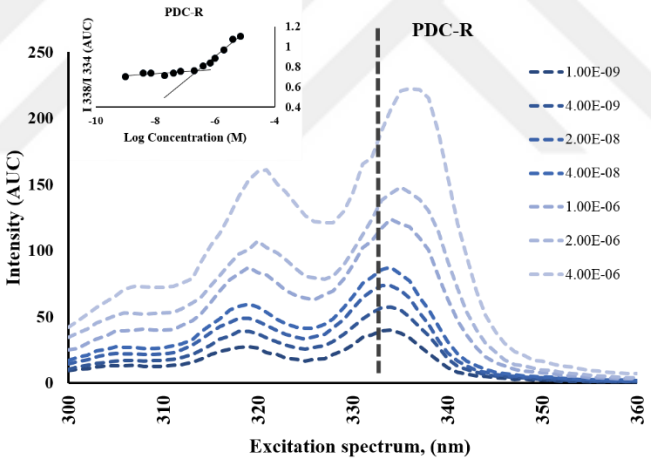

Figure 3.5. Pyrene excitation spectra of PDC-R based micelles. Left inset: I_{338}/I_{334} vs log concentration graph to calculate CMC value.

3.3.3. Preparation and Characterization of Crosslinked Micelles

Stability towards severe dilution as experienced upon injection into the bloodstream is an important aspect for consideration. Stability of micellar integrity also warrants minimal drug release before reaching the target tissue. Increased stability through core crosslinking was investigated in this study. After determination of the CMC of polymer-dendron

conjugates, thiol-ene chemistry was applied to undertake core-crosslinking. A hydrophobic tetra-thiol crosslinker and a photoinitiator 2,2-dimethoxy-2-phenylacetophenone (DMPA) was utilized for crosslinking under UV irradiation (365 nm) for 30 min in Figure 3.6.

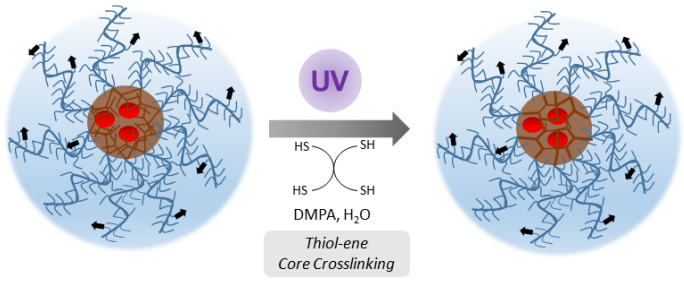

Figure 3.6. Synthesis of CL-R from copolymer PDC-R.

The diameter of micelles assembled from PDC-R with and without encapsulation of DOX were determined using DLS. Without any drug encapsulation, it was observed that targeting group containing non-crosslinked (NCL) micelles NCL-R were slightly larger in size when compared to the core crosslinked (CL) micelles CL-R, suggesting that crosslinking leads to decrease in their diameter in Figure 3.7a-e. It was also observed that drug loaded micelles possessed slightly smaller average size when compared with the empty ones (122.1 nm vs 126.6 nm). It can be postulated that this happens due to hydrophobic interactions between DOX, a hydrophobic drug, and the hydrophobic polyester dendron core. Size analysis of dry micellar constructs using TEM showed that drug loaded crosslinked micelles possessed a well-defined and slightly larger size than the non-crosslinked drug loaded micelles in Figure 3.7f. The average size of dry micelles from TEM were calculated as 29.8 nm and 50.4 nm for the drug loaded non-crosslinked and crosslinked micelles, respectively. As expected, the sizes of drug loaded micelles measured using DLS are larger than measured from TEM, since the micelles are in their hydrated state in the former measurement. The size difference in hydrated and dry states suggests that a more collapsed structure smaller in size in the dry state is formed for the drug loaded NCL micelles, while the drug loaded CL micelles shows less compaction upon drying, perhaps due to increased rigidity of the core due to crosslinking.

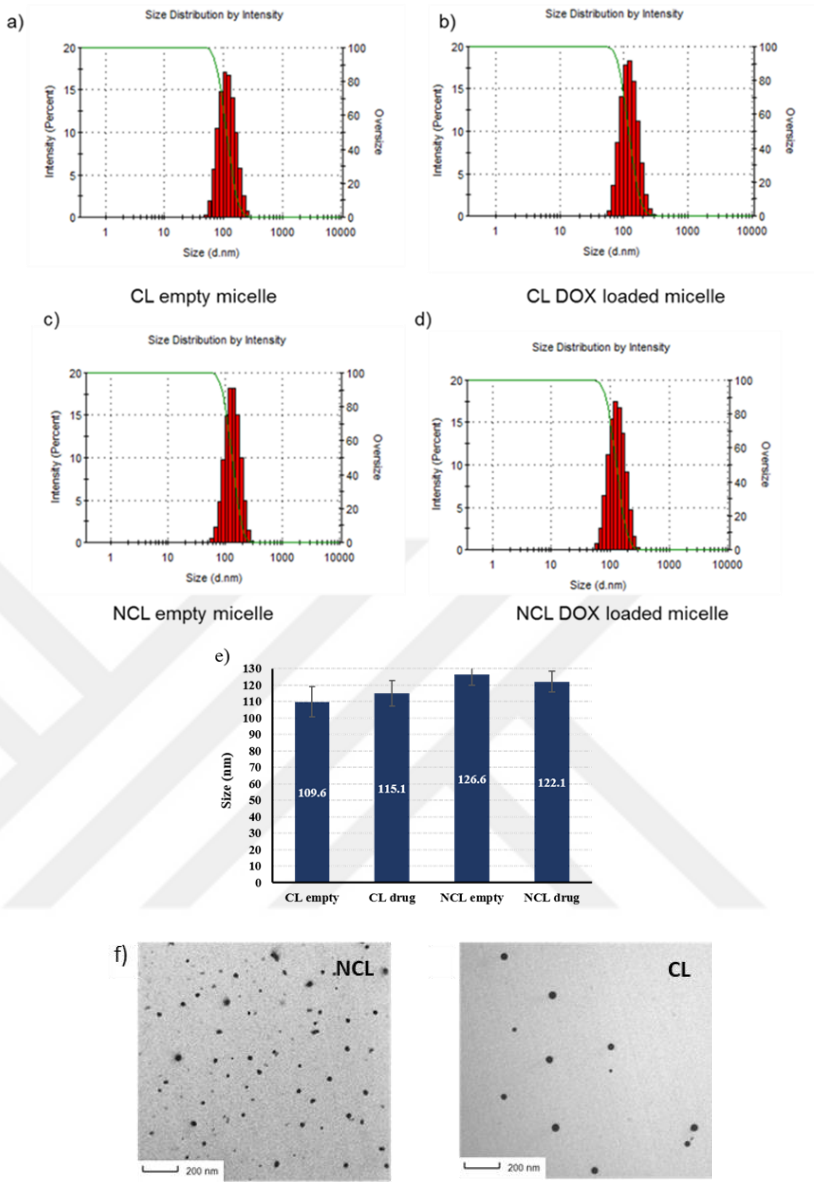

Figure 3.7. (a-d) Size distributions of drug loaded and empty crosslinked (CL-R) and non-crosslinked (NCL-R) micelles from PDC-R, (e) comparative Z-average diameter of micelles as determined by DLS at 37 ^{o}C, and (f) TEM micrographs of drug loaded NCL-R and CL-R micelles.

In order to check the colloidal stability of these micelles, DLS measurements were taken. Each of the samples was extensively diluted using water and the change in size with respect to concentration was monitored via DLS. Although CMC value of PDC-R is 7.47×10^{-7} M, upon dilution micelles remained stable even at 7.47×10^{-10} M, which suggests that the crosslinked micelles are quite resistant to severe dilution However, as expected, the

non-crosslinked micelle disintegrated into unimers below the CMC value in Figure 3.8a-b. Additionally, crosslinked micelles maintained their size upon exposure to 10% fetal bovine serum (FBS) solution, thus suggesting that they should remain stable in biological milieu in Figure A4.

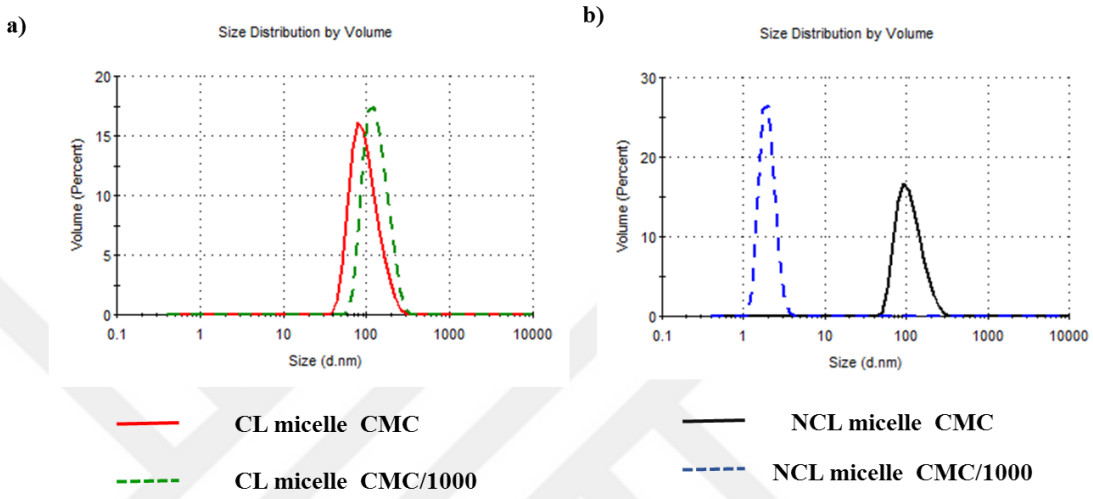

Figure 3.8. Stability of a) Crosslinked (CL-R) and b) Non-crosslinked (NCL-R) micelles from PDC-R against dilution as probed using DLS.

3.3.4. Drug Loading into NCL and CL Micelles and Release

Drug loaded micelles were obtained by dropwise addition of distilled water to a THF solution of DOX and PDC-R under stirring at room temperature, allowing complete evaporation of the organic solvent in the dark. The DOX-loaded micelles were crosslinked as described above using a tetra-thiol and a photoinitiator DMPA under UV irradiation. The drug loading capacity was determined by fluorescence spectroscopy, using a calibration curve of the drug at five different concentrations. A slightly higher amount of drug loading was observed for the NCL-R micelles compared to the CL-R micelles (10.72 ± 0.18 vs 7.25 ± 0.19) with corresponding drug loading efficiencies as 89.3 ± 1.5 and 60.4 ± 3.2, respectively. This can be expected due to the congestion of the micellar core after the crosslinking.

In vitro release behavior of DOX from NCL-R and CL-R micelles were studied simulating extracellular environment (pH 7.4) and lysosomal environment (pH 5.4) at 37ºC under sink conditions in Figure 3.9. As expected, the release of DOX from the carriers was observed to be pH dependent. For PDC-R micelles, DOX release was much faster and higher in acidic medium compared to release in neutral pH. Importantly, a much slower DOX release was observed from the CL-R micelles compared to NCL-R micelles at pH = 7.4 (12% vs 34% respectively at 8 h). While crosslinking of micelles decreased the overall drug release (ca. 50%), it is important to note that there was a significant decrease in the drug release at the extracellular condition (pH 7.4). Since the local drug concentration in the tissue is expected to be high upon selective accumulation, it is important that drug release from the carrier is minimum during its transportation to the tumor site. The remarkable change in the drug release profile due to core crosslinking of the micelles highlights the advantage for these systems [113].

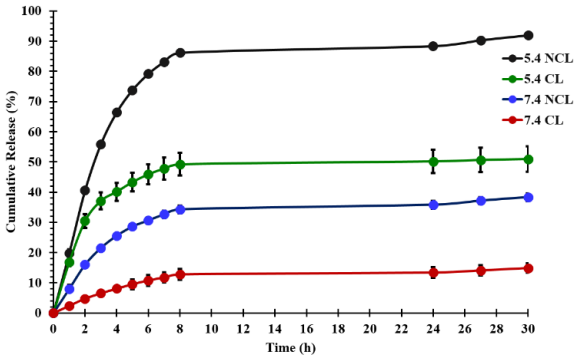

Figure 3.9. *In vitro* release of DOX at pH 7.4 and 5.4 from NCL-R and CL-R micelles.

3.3.5. *In vitro* Cytotoxicity and Cellular Internalization

In order to investigate the cytotoxic effect of DOX loaded polymeric micelle and targeting group-bearing micelle, *in vitro* cytotoxicity tests were performed using a human breast cell line, MDA-MB 231. The cells were exposed to a series of equivalent concentrations of free DOX or DOX encapsulated targeted and non-targeted micelles; drug concentration was varied between 10^{-4} M and 10^{-12} M. Cytotoxicity assays revealed that

while free DOX exhibited an EC50 = 5.698 x 10^{-8} M, the DOX loaded non-targeted micelles (CL-C) and targeting group bearing micelles (CL-R) possessed an EC50 of 7.67 x 10^{-7} M and 1.305 x 10^{-7} M, respectively in Figure 3.10. As expected, the free drug was found to be more active than drug loaded polymeric micelles i.e. DOX loaded micelles exhibited lower cytotoxicity when compared with free DOX for the same drug concentration. Faster diffusion of the free DOX into the cell nuclei might be the reason for this observation. Additionally, a slightly better cytotoxic effect was observed for the targeting group bearing construct (CL-R). Only slight increase observed in the *in vitro* experiments after 48 h is as expected since during this time period both the constructs get sufficiently internalized and release the drug. As expected from the benign chemical composition of the polymeric building blocks, the polymeric micelles formulated using PDC-R, devoid of any cytotoxic agent did not show any loss of cell viability.

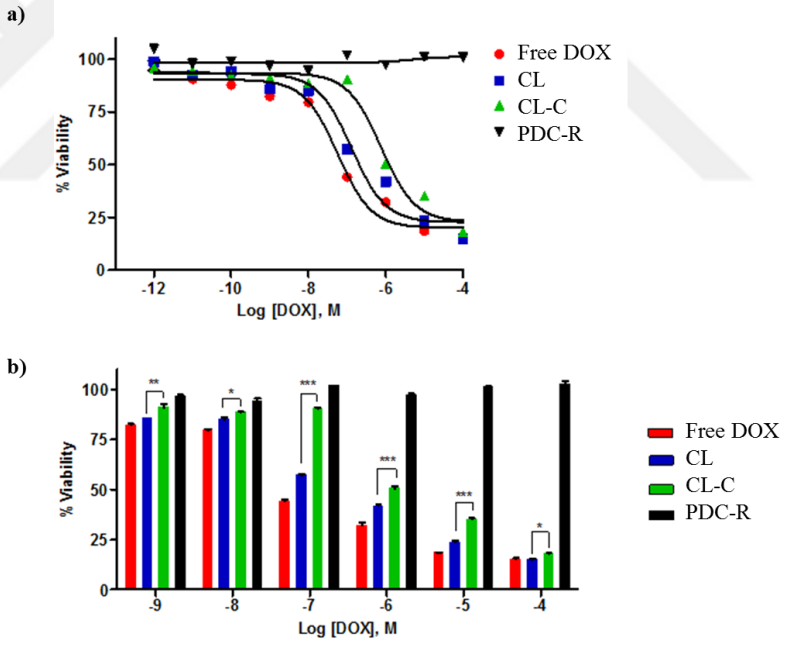

Figure 3.10. Viabilities of MDA-MB-231 cells incubated with polymer (PDC-R), DOX loaded non-targeted micelle (CL-C) and DOX loaded targeted micelle (CL-R), and free drug after 48h treatment as (a) dot plot and (b) as histogram.

The intracellular localization of free DOX and DOX-loaded polymeric micelles into the breast cancer cells were investigated using fluorescence microscopy. The MDA-MB 231 cells were incubated with free DOX, DOX loaded CL-C, DOX loaded CL-R, and DOX

loaded CL-R along with free cRGDfV peptide as a competitive ligand. Each group demonstrated different level of internalization. Figure 3.11 shows that after 3 h, free DOX exhibited strong fluorescence intensity in cell nuclei due to faster diffusion [114]. In contrast, DOX loaded polymeric micelles showed significant fluorescence intensity in the perinuclear region rather than the cell nuclei in Figure A5. This result demonstrate that DOX loaded micelles have to diffused into the cells through endocytosis. In addition to this, fluorescence intensity showed that targeting group bearing micelle (CL-R) showed higher internalization capacity when compared with drug loaded CL-C micelles. On the other hand, when free cRGDfV peptide was added with CL-R, since free competitive inhibitor group blocks the integrin receptors located on the cell membrane, it inhibits the interaction of micelles with cancer cells. These results clearly demonstrate that the cRGDfK peptide as a targeting moiety on the micelles facilitates intracellular uptake of DOX loaded micelles and aid transportation of the drug into the cell, raising the intracellular drug concentration.

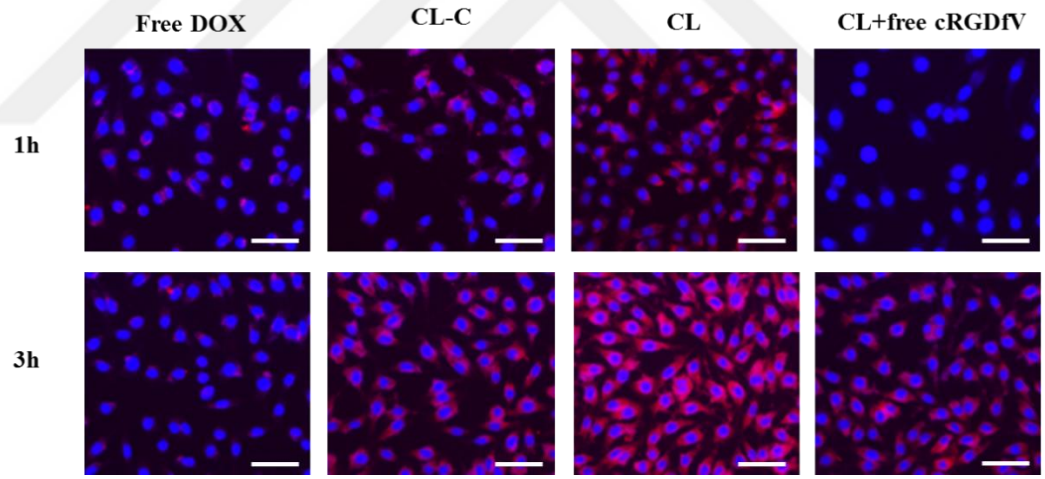

Figure 3.11. Fluorescence microscopy images of MDA-MB-231 cells treated with free DOX and DOX loaded non-targeted (CL-C) and targeted (CL-R) micelles. Cell nuclei were stained with DAPI (blue). Scale bar = 50 μm.

3.4. Conclusions

In summary, polymer-dendron conjugate based crosslinked micelles containing a peptide based targeting moiety were synthesized. The polymer-dendron conjugate was

synthesized by clicking an orthogonally reactive hydrophobic biodegradable polyester dendron together with an azide-terminated copolymer containing activated esters as amine reactive groups. This micelle precursor was appended with an amine group containing peptide based targeting group, namely cRGDfK, to fabricate micelles for targeting cancer cells with overexpressed integrin receptors. While the dendron-polymer conjugates assembled to provide micelles with low CMC, the constructs were not stable in highly dilute conditions. To add extra stability against dilution, the alkene bearing dendritic core of these micelles were crosslinked using the photochemical radical thiol-ene reaction. These drug loaded core crosslinked and non-crosslinked micelles showed appreciable drug release under acidic conditions, although slightly higher in case of the non-crosslinked ones. Importantly, lower drug release under neutral conditions was observed for the core crosslinked micelles compared to their non-crosslinked micellar counterparts. Thus, the core crosslinking not only provides very stable micellar constructs, but also suppresses drug release in neutral environment. Treatment of MDA-MB-231 breast cancer cells with non-targeted and targeted micelles demonstrated higher internalization of the targeted construct. Furthermore, *in vitro* cytotoxicity assay revealed that targeted micelles possessed higher cytotoxicity than the non-targeted crosslinked micelles. Additionally, the parent polymer PDC-R based construct devoid of any drug showed no appreciable cytotoxicity. These results suggest that these dendron-polymer based micellar constructs are benign and biocompatible drug delivery vehicles. Due to the modular design of the construct, any particular drug and targeting ligand combination can be incorporated to address different types of cancerous cells. Facile fabrication of this versatile drug delivery platform suggests that the construct bears potential for further exploration as a drug delivery vehicle.

4. REDOX-RESPONSIVE DENDRON-POLYMER CONJUGATES: VERSATILE BUILDING BLOCKS FOR FABRICATION OF STIMULI-RESPONSIVE TARGETED DELIVERY SYSTEMS

4.1. Introduction

Cancer is evolving into a widespread global health issue confronting humanity. It has a far greater mortality rate than many other diseases [115]. Chemotherapy is one of the most widespread therapeutic approaches for cancer treatment, aside from surgery and radiotherapy [116]. Unfortunately, most chemotherapy drugs have inherent weaknesses such as limited water solubility, poor bioavailability, poor distribution network, quick blood clearance, substantial side effects, and cancer cell drug resistance [117]. For this reason, designing a drug carrier that predominantly targets and delivers the drug to cancerous tissues has become an actively investigated approach in recent years. With a better understanding of the tumor environment in recent years, it has been established that the tumor tissue generally differs significantly from that of normal tissues, with a low pH and large amounts of glutathione (GSH) [118]. Besides their nanosized dimensions, attachment of cell-specific recognition unit and imparting stimuli responsiveness have gained significant attention in the development of DDS.

Among the stimuli-responsive polymeric materials studied to date, the most common ones are responsive to changes in the pH and/or redox environments. It is relatively simple to integrate such stimuli-responsive linkages in the precursors containing hydrophilic and hydrophobic block domains. In particular, acid-sensitive or reduction-sensitive units are employed when combining the two blocks at the junction point [119, 120]. If the structures sensitive to stimuli can be adjusted to disrupt the hydrophilic-hydrophobic balance when the polymeric assembly reaches a different pH and redox environment, cargo release will occur. Disulfide bonds are commonly used as a reduction-responsive linkage to aid in the quick and differential release of anticancer agents in tumor cells and improve antitumor effectiveness [121, 122].

Herein, we report the fabrication of redox-responsive dendron-polymer conjugate-based micellar structures as targeted drug delivery vehicles. The dendron polymer conjugates were obtained using the thiol-disulfide exchange reaction between a polyester dendron containing a thiol-reactive pyridyl-disulfide unit at the focal point with a thiol terminated hydrophilic linear PEG polymer. The choice of the hydrophobic component was polyester dendrons due to their hydrophobic and biodegradable characteristics. Micelles constructed using a PEG-thiol and third and fourth-generation dendrons were fabricated, and their stability in forming micelles was evaluated. After that, a hetero-telechelic PEG polymer containing a thiol- and carboxylic acid group at chain ends was then utilized to obtain dendron-polymer conjugates containing functional carboxylic acid group at one end of the PEG polymer. An activated ester of the carboxylic acids was employed to obtain peptide-bearing conjugates. A mixture of dendron-polymer conjugate with and without peptide was used to prepare a targeting group containing micellar aggregates. These constructs were loaded with doxorubicin, a clinically administered anticancer drug. Obtained micelles were evaluated for their stability and drug release under neutral and acidic conditions in the presence and absence of GSH. *In vitro* cytotoxicity and the cellular internalization of the drug-loaded aggregates were carried out against MDA-MB-231 breast cancer carcinoma cells.

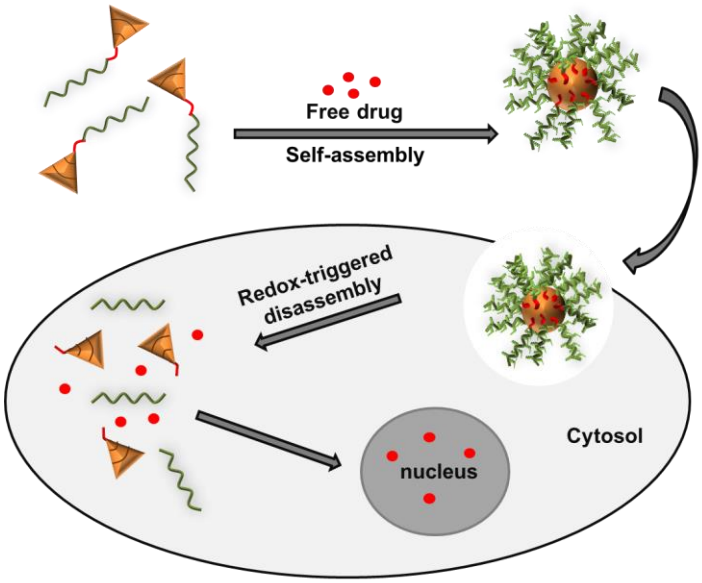

Figure 4.1.General scheme of cleavage of disulfide bond reductive environment.

4.2. Experimental Section

4.2.1. Materials

2,2-Bis(hydroxymethyl)propionic acid, Dowex X50WX2, *N*,*N*-dicyclohexylcarbodiimide (DCC) were purchased from Alfa Aesar. Synthesis of cRGDfK was achieved through solid phase peptide synthesis (SSPS, PS3 Peptide Synthesizer, Protein Technologies Inc., USA) [106]. Glutathione reduced ethyl ester (GSH-OEt) was purchased Cayman. All solvents were purchased from Merck and used as obtained without further purification unless otherwise noted. Ultrapure water was obtained using Milli-Q Water Purification System (Milli-Q system, Millipore, Billerica, MA, USA). Third generation polyester dendron containing pyridyl disulfide group at the focal point was synthesized according to literature [119].

4.2.2. Instrumentation

Chemical compositions of small molecules, dendrons and polymer were characterized using ^{1}H NMR spectroscopy (Varian 400 MHz). Micellar formations were characterized their critical micellar concentration and size using fluorescence spectrophotometer (Varian Cary Eclipse, Agilent, USA) and Zetasizer Nano particle analyzer (Malvern), respectively. The molecular weights of the polymers were estimated by size exclusion chromatography (SEC) analysis using a PSS-SDV (length/ID 8 × 300 mm, 10 µm particle size) Linear M column calibrated with polystyrene (PS) standards (1–150 kDa) using a refractive-index detector. Tetrahydrofuran (THF) was used as eluent at a flow rate of 1.0 mL/min at 30 °C. UVP Black-Ray B-100AP/R High Intensity UV lamp (100 Watt / 365 nm) was used for crosslinking experiments. During the internalization experiments, cells were visualized using Zeiss Axio Observer inverted fluorescence microscope (Carl Zeiss Canada Ltd, Canada). The dry micellar constructs were visualized on a holey carbon film coated 300 mesh Cu-grid (Pacific Grid Tech, USA) using a LVEM5 electron microscope on transmission electron microscopy (TEM) mode (Delong Instruments, USA).

4.2.3. Synthesis of 3rd Generation Polyester Dendron (DG3)

As previously described in the literature, a 3rd generation polyester dendron containing a PDS group at the focal point was synthesized [119].

4.2.4. Synthesis of 4th Generation Polyester Dendron (DG4)

According to the literature, a deprotected third-generation polyester dendron with a PDS group at the focal point was synthesized [119]. For protection of hydroxyl end groups of 3rd generation dendron with acetal groups, acetonide-2,2-bis(methoxy)propionic anhydride (3.82 g, 11.5 mmol) and DMAP (0.293 g, 2.30 mmol) were dissolved in 40 mL of CH_2Cl_2 in a round-bottom flask. Deprotected 3rd generation dendron (0.722 g, 0.73 mmol) in 10 mL of CH_2Cl_2 and pyridine (1.052 mL, 12.99 mmol) were also added into this mixture. The reaction was stirred for 48 h, then water (1.052 mL) was added to the reaction flask and stirring was continued for an additional 2 h. The reaction crude was extracted with 1 M $NaHSO_4$ solution (3 × 20 mL), then 10% Na_2CO_3 solution (3 × 20 mL), and with brine solution (20 mL). The organic layer was dried with solid anhydrous Na_2SO_4 before being filtered. To obtain pure product, the solvent was removed under reduced pressure. After that, the crude product was purified using a column chromatograph using silica gel as the stationary phase and ethyl acetate/hexane as the eluent. Under vacuum, the pure product was dried into a viscous colorless liquid (0.856 g, 72% yield).^{1}H NMR (400 MHz, $CDCl_3$) δ 8.48 (t, *J* = 7.2 Hz, 1H), 7.64 (dt, *J* = 57.9, 28.6 Hz, 2H), 7.18 – 7.06 (m, 1H), 4.41 (t, *J* = 6.3 Hz, 2H), 4.36 – 4.19 (m, 32H), 4.12 (t, *J* = 11.9 Hz, 19H), 3.61 (d, *J* = 12.2 Hz, 18H), 3.08 (t, *J* = 6.3 Hz, 2H), 1.56 (s, 18H), 1.40 (s, 27H), 1.34 (s, 28H), 1.30 (s, 4H), 1.27 (s, 13H), 1.25 (s, 6H), 1.14 (s, 27H) in Figure 4.2. ^{13}C NMR (101 MHz, $CDCl_3$) δ 173.48 (s), 171.83 (s), 171.73 (s), 171.42 (s), 159.36 (s), 149.85 (s), 137.15 (s), 121.02 (s), 119.98 (s), 98.10 (s), 66.32 (s), 65.95 (d, *J* = 5.2 Hz), 65.53 (s), 64.83 (s), 63.02 (s), 46.84 (s), 46.73 (s), 42.04 (s), 36.98 (s), 25.14 (s), 22.14 (s), 18.53 (s), 17.70 (s), 17.54 (s) in Figure A.6.

4.2.5. Conjugation of Linear PEG Dendron (PEGDG4, PEGDG3 and HOOC-PEGDG4)

PDS core of the G4 dendron (61 mg, 0.038 mmol) was reacted with thiol functional groups on mPEG2K-SH (50 mg, 0.025 mmol) in the presence of catalytic amount of CH_3COOH (37.5 µL) in 200µL DMF purge with N_2 20 minutes before the reaction. To get rid of the unreacted dendron, crude was precipitated twice in 40 ml of cold diethyl ether. The pure substance was dried into a white solid under vacuum (0.074 mg, 85% yield). ^{1}H NMR (400 MHz, $CDCl_3$) δ 4.39 (t, *J* = 6.5 Hz, 1H), 4.35 – 4.21 (m, 6H), 4.14 (d, *J* = 11.8 Hz, 4H), 3.65 (d, *J* = 5.3 Hz, 126H), 3.38 (s, 2H), 2.97 – 2.86 (m, 2H), 1.41 (s, 6H), 1.35 (s, 6H), 1.27 (s, 5H) in Figure 4.4. The same manner was applied to construct PEGDG3 in Figure A.7 and HOOC-PEGDG4 in Figure A.8.

4.2.6. Synthesis of cRGDfK Containing Linear Peg Dendron Conjugate

In a reaction flask, N-hydroxysuccinimide (NHS) (, 5.05 mg 0.044mmol), HOOC-PEGDG4 (55 mg, 0.011 mmol), 1-Ethyl-3-(3-Dimethylaminopropyl) Carbodiimide (EDCI) (10.51, 0.054 mmol) were dissolved in anhydrous CH_2Cl_2 (0.2 mL) and purged with N_2. After 24 hours, cRGDfK (9 mg, 0.015 mmol) was dissolved in DMF (0.2 mL) and added to reaction vessel. DIPEA (0.11 mg, 0.85 mmol) was added dropwise to the PEG solution, and the reaction mixture was maintained at 45 °C for 24 hours in Figure 4.6. Reaction mixture was diluted with MeOH (2 mL) and inserted in a 3.5 kDa cutoff dialysis bag. Dialysis was performed for 2 days using methanol to get rid of unbound cRGDfK and impurities. To get cRGDfK functionalized PEG dendron conjugate (R-PEGDG4), the solvent was evaporated and dried under *vacuo* (25mg, 74% yield).

4.2.7. Micelle Formation from Polymer-Dendron Conjugate and Related Measurements

Co-solvent evaporation was used to make three sets of pyrene doped micelles namely R-PEGDG4, PEGDG4 and PEGDG3. In order to calculate CMC values, 3 stock solutions

of conjugate were prepared. In 500 mL THF, various quantities of the conjugate were dissolved, ranging from 10^{-5} M to 10^{-9} M (in 3 mL water). Pyrene stock solution was added to all samples, and the final concentration of pyrene for each sample was adjusted to 6.10^{-7} M. The organic phase was then evaporated after adding Milli-Q water (3 mL) dropwise to all samples and leaving them open to air. To determine the CMC, fluorescence studies were performed on all samples. A fluorescence spectrometer was used to record pyrene excitation spectra at a wavelength of 390 nm. The excitation fluorescence was measured at 300 and 360 nm. While calculating the intensity ratio I_{338} / I_{334}, the intersection of the CMC values was calculated.

4.2.8. Stability Experiments

The size of micelles was measured using dynamic light scattering to ensure their stability (DLS). R-PEGDG4 and PEGDG3 were used to make 1 mL of micelle samples at 10^{-5} M. Using PBS was used to dilute the samples. The size of micelles was then investigated using DLS.

4.2.9. Release of NR from PEGDG4 in Response to Two Stimuli

The co-solvent evaporation approach was used to make NR doped micelles. Briefly, Nile Red solution in THF (50 µL, 0.6 mg/mL) was added to 1 mL of the PEGDG4 solution (6 mg/mL). 6 milliliters of water was then added dropwise to the solution and left open to air to allow it to evaporate. To get rid of unloaded nile red, the solution was filtered (0.45 µ PES filter) and divided into 6 equal parts. Each solution were mixed with 5mM, 10 mM GSH in PBS (pH = 7.4), acetate buffer at pH = 5.4, 5mM, 10 mM GSH in acetate buffer at pH 5.4 and PBS with pH 7.4 as control. Their fluorescence spectra were taken at specific times to track the intensity of fluorescence at its maximum wavelength.

4.2.10. Encapsulation and *in vitro* Release of DOX

Dox loaded micelles were arranged by co-solvent evaporation method. Filtration was performed to get rid of the unloaded dox in the prepared micelles. A fluorescence spectrophotometer was used to calculate the amount of DOX injected. DOX loaded micelles were freeze-dried and dissolved in DMSO to determine drug loading content, and the DOX content was determined by fluorescence detection using a DOX calibration curve. The following equations were used to compute the drug-loading capacity (DLC) as

DLC (wt%) = (weight of loaded drug/total weight of polymer and loaded drug) x 100%

and efficiency (DLE) as

DLE (%) = (weight of loaded drug/weight of drug in feed) x 100%.

A dialysis membrane (MWCO 3500) was utilized with gentle shaking (260 rpm) at 37°C in four different buffer media with or without 10mM GSH to assess the release kinetics of DOX from micelle solutions *in vitro*. The outer phase of the dialysis tubing was withdrawn and replaced with an equal volume of fresh release medium at predefined time intervals. Fluorescence spectroscopy has been used to calculate the amount of DOX emitted (excitation at 485 nm).The data reported in the release study are averages with standard deviations.

4.2.11. Procedure of GSH-mediated Cytotoxicity

MDA-MB-231 cells (6000 cells/well) were seeded in a 96-well plate in 100 μL DMEM supplemented with 10% fetal bovine serum (FBS) and incubated at 37 °C for 24 h for cells to adhere completely. After 24 hours, the cells were divided to three groups. Only one group cells were incubated with 5mM GSH-ester for 5 hours. End of 5 hours, GSH solution was removed and the cells were washed with 1xPBS (3 times). R-PEGDG-4 micelle dispersions and free DOX solutions with different DOX concentrations (10^{-4}-10^{-12} M) were prepared in DMEM. Free DOX and R-PEGDG4 micelle solutions were applied the cells. In

addition to this, GSH-ester treated cells were incubated with RPEGDG4 micelle solutions for 24 hours. After 24 hours incubation, micelle solutions were removed and the cells were washed with 1xPBS. CCK-8 solution (10 %) (100 μL) was added to every well and after incubation for 2h, absorbance values at 450 nm were measured using a microplate reader. Results were obtained by GraphPad prism software using in nonlinear regression mode.

4.2.12. Procedure for Internalization and Flow Cytometry

For the cellular internalization, MDA-MB-231 adenocarcinoma cells (75 000 cells/well) were seeded in 12-well plate as duplicate in 1 mL of culture media (DMEM). The cells were incubated at 37 ^{o}C for 24 h. Doxorubicin (DOX), DOX loaded PEGDG4-M and R-PEGDG4-M micelles (0.04 mg/mL DOX concentration) were added on the wells. For competitive internalization, free RGDfV and R-PEGDG4-M micelles were used. After addition of micelles, cell media were removed at several time points (1, 3, 24 h) during incubation. At each time point, cells were washed with PBS (500 μL) three times. Cells were fixed using 4% formaldehyde solution for 10 min. at 37 ^{o}C. After being washed with PBS three times, cells were incubated at 37 ^{o}C for 15 min. for DAPI nuclei staining. Cell images were collected using Zeiss Observer Z1 fluorescence microscope and processed with AxioVision software.

For flow cytometry experiment, the cells (200 000 cells/well) were treated similarly and after incubation periods, supernatants were discarded, cells were washed with PBS and cells are removed using trypsin. Intracellular Dox fluorescence intensities were determined by flow cytometry (Guava easyCyte) and results were processed on GuavaSoft software. The statistical processing of the data was done using one-way ANOVA analysis employing GraphPad Prism software.

4.3. Results and Discussion

4.3.1. Synthesis of Redox-responsive Polymer-Dendron Conjugates

Fabrication of redox-responsive dendron-polymer conjugates was undertaken by coupling a linear PEG polymer with a polyester dendron through a disulfide bridge in Figure 4.3. In particular, a thiol-containing linear PEG polymer was coupled with a polyester dendron containing a pyridyl-disulfide group at its focal point. The fourth-generation dendron was synthesized using a previously reported protocol with minor modifications. A well-established divergent synthetic approach used a bis-MPA unit as a building block to obtain the hydrophobic, acid degradable polyester dendron. A pyridyl disulfide containing alcohol was used as a starting material to install the thiol-reactive exchangeable group at the focal point. The purity of the fourth generation dendron was confirmed using ^{1}H and ^{13}C NMR spectroscopy in Figure 4.2 and Figure A.6. The peaks (8.48, 7.64, 7.18 – 7.06 ppm) belonging to the PDS unit on the focal point of dendron and characteristic peaks from the acetal group of dendron (between 1.56 and 1.14 ppm) were visible.

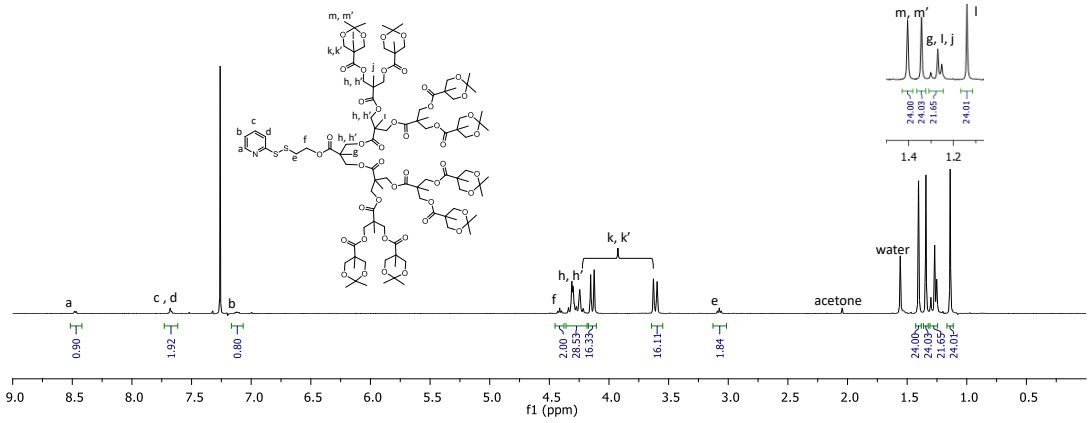

Figure 4.2.^{1}H NMR spectrum of generation 4 dendron.

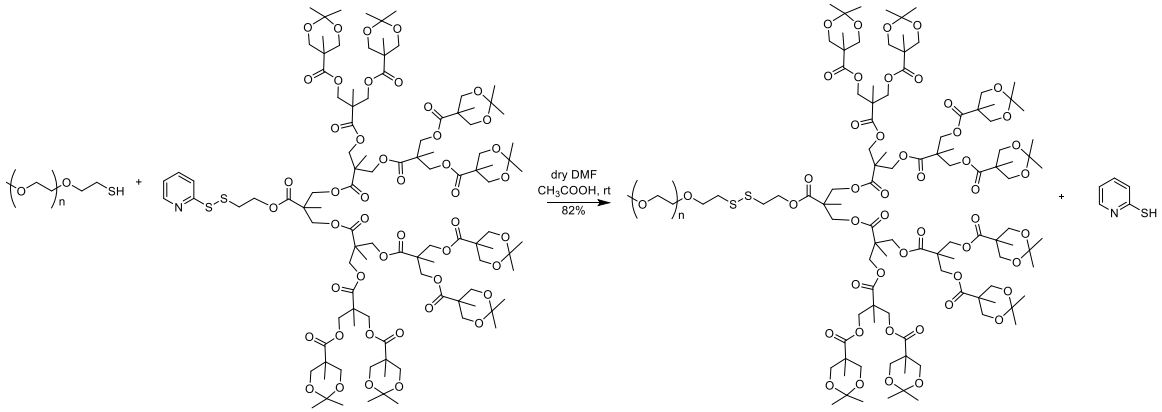

Figure 4.3. Representative synthesis of PEG-SS-DEN4.

Redox-responsive amphiphilic dendron-polymer conjugates were obtained through the disulfide-thiol exchange reaction. The displacement of the PDS group by the thiol-terminated PEG polymer was suggested by the change of color of the reaction mixture from clear to yellowish. The release of the thiopyridone unit was observable by UV-Vis spectroscopy, with its characteristic peak present at 343 nm in Figure A.7. The dendron-polymer conjugate was purified by precipitation in cold ether to remove the unreacted polyester dendron and the released pyridothione by-product. The purity of the obtained product was analyzed using ^{1}HNMR spectroscopy. As expected, while the methylene groups of the PEG at 3.37 ppm and characteristic resonances from the polyester dendron at 4.39, 1.41, 1.35, and 1.14 ppm were present, the proton resonances belonging to the pyridyl disulfide moiety were absent. A proton resonance belonging to methylene groups next to the newly generated disulfide was observed at 3.01-2.78 ppm, along with the conventional proton resonances from the polymer PEG and dendron components in Figure 4.4. Furthermore, an increase in the molecular weight of the obtained product to M_n = 4652 Da upon conjugation of dendron to the polymer as observed in the SEC trace also supported successful coupling of the dendron and polymer component in Figure A.9.

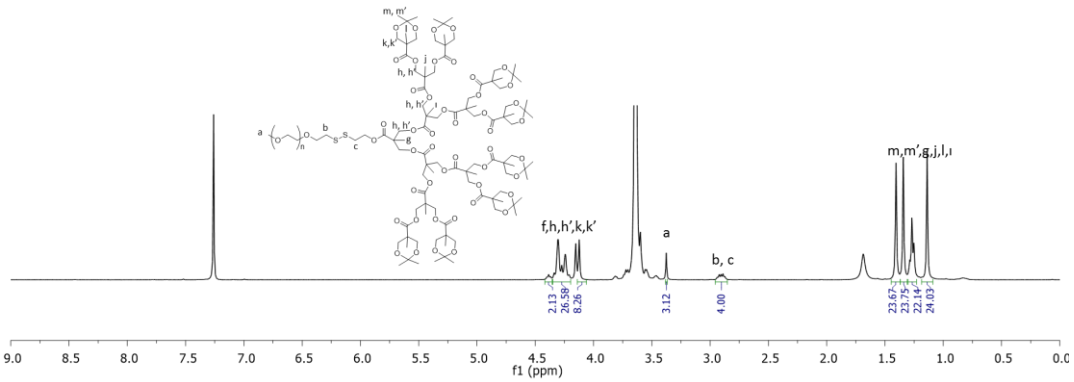

Figure 4.4. ^{1}H NMR spectrum of (PEGDG4).

After successfully synthesizing the dendron-polymer conjugate, the strategy was extended to synthesize the targeting group containing conjugate in Figure 4.5. We used a hetero-telechelic PEG containing an acid group at one end and a thiol group at the other end. Since we plan to use a substantial amount of this conjugate in the construction of the targeted micellar construct, we chose to make this also degradable under reducing environments; hence a conjugate similar in composition to the main building block was utilized. Coupling of the thiol- and carboxylic acid group-containing PEG with dendrons containing the pyridyl group at the focal point resulted in dendron-polymer conjugates in Figure A.10. The carboxylic acid group was activated to an NHS-ester, followed by the addition of an amine-containing cyclic peptide reaction to obtain the targeting group containing precursor.

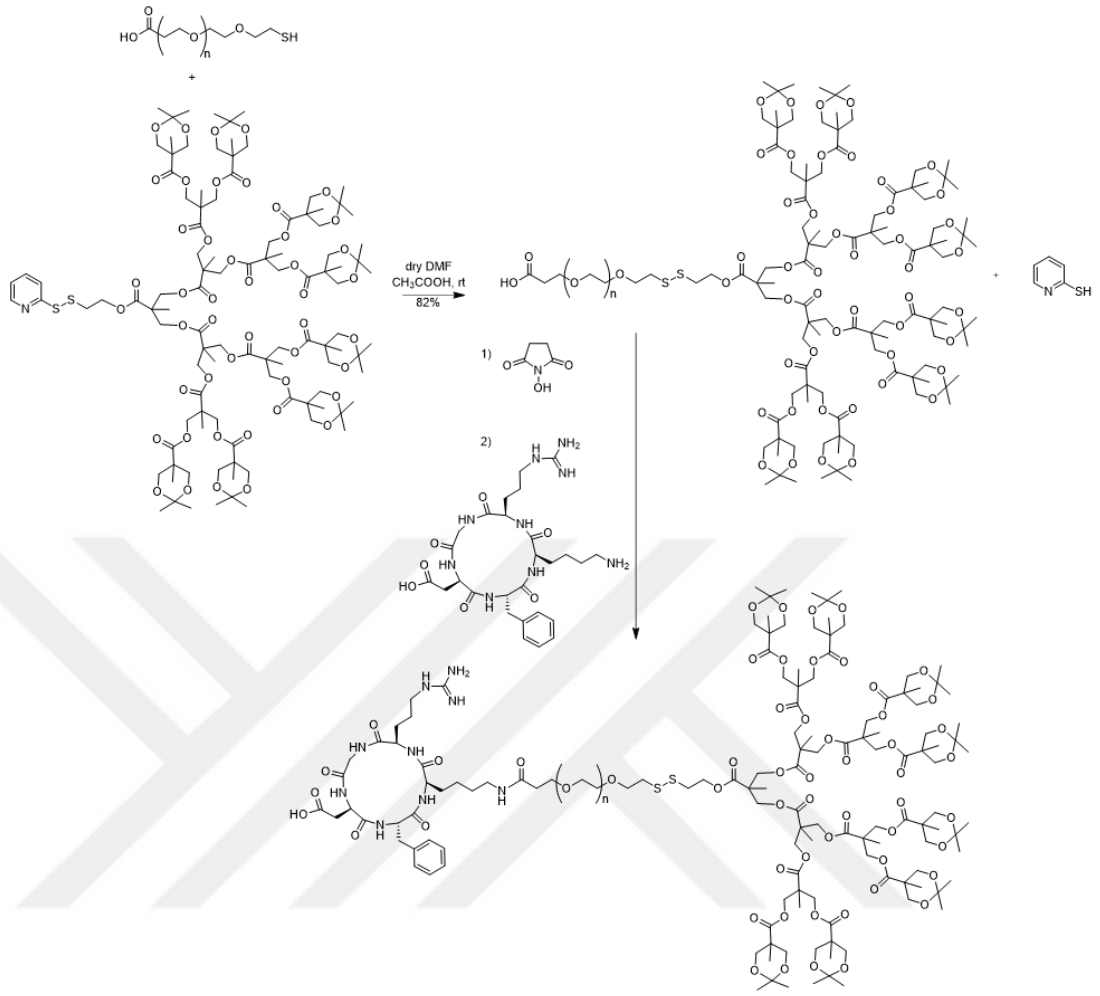

Figure 4.5. Synthesis of cRGDfK containing redox-responsive polymer dendron conjugate (R-PEGDG4).

The purity of the peptide-conjugated dendron-polymer conjugate was determined using ^{1}H NMR spectroscopy in Figure 4.6. The presence of characteristic proton resonances belonging to methylene units of PEG at 3.50 ppm and dendrons at 1.34, 1.21, and 1.01 ppm, along with the proton resonances from the peptide fragment at 7.27, 7.18 ppm, confirmed the composition of the peptide-containing dendron-polymer conjugate. Additionally, the increase in molecular weight was evident from SEC analysis in Figure A.11.

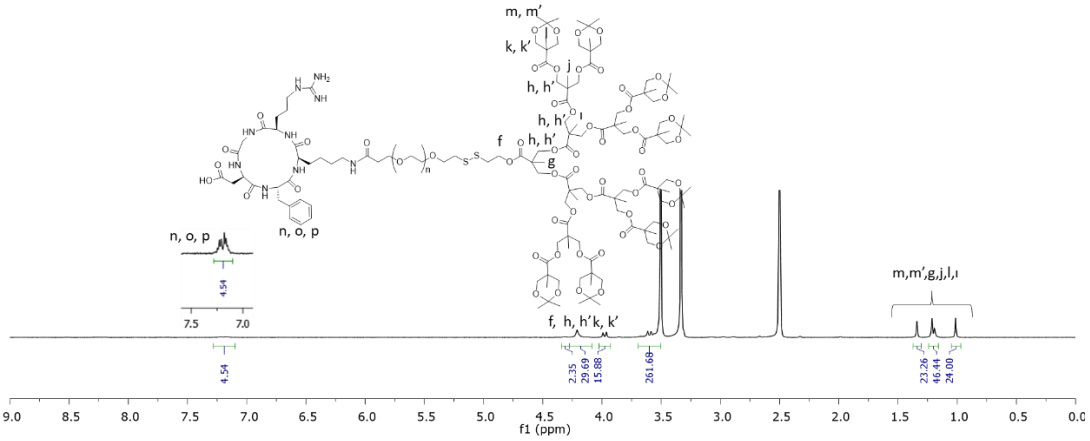

Figure 4.6.^{1}HNMR spectrum of polymer-dendron conjugate R-PEGDG4.

4.3.2. Determination of Critical Micelle Concentration (CMC)

Pyrene, a hydrophobic fluorescence probe, was used to evaluate the CMC of the PEG based conjugate. Micelle assembly in aqueous environments causes a rise in the amount of solubilized pyrene, as well as an increase in the intensity of the pyrene emission peak, above a specific concentration of the amphiphilic conjugate. Furthermore, as micelles form, the peak's maximum moves from 334 to 338 nm. When extrapolating the intensity ratio I_{338}/I_{334} at low and high concentration locations, the CMC is computed from the junction. Using this approach, CMC value of PEGDG3, PEGDG4 and R-PEGDG4 constructs were determined as 3.76×10^{-6} M, 1.62×10^{-6} M and 2.57×10^{-6} respectively in Figure 4.7.

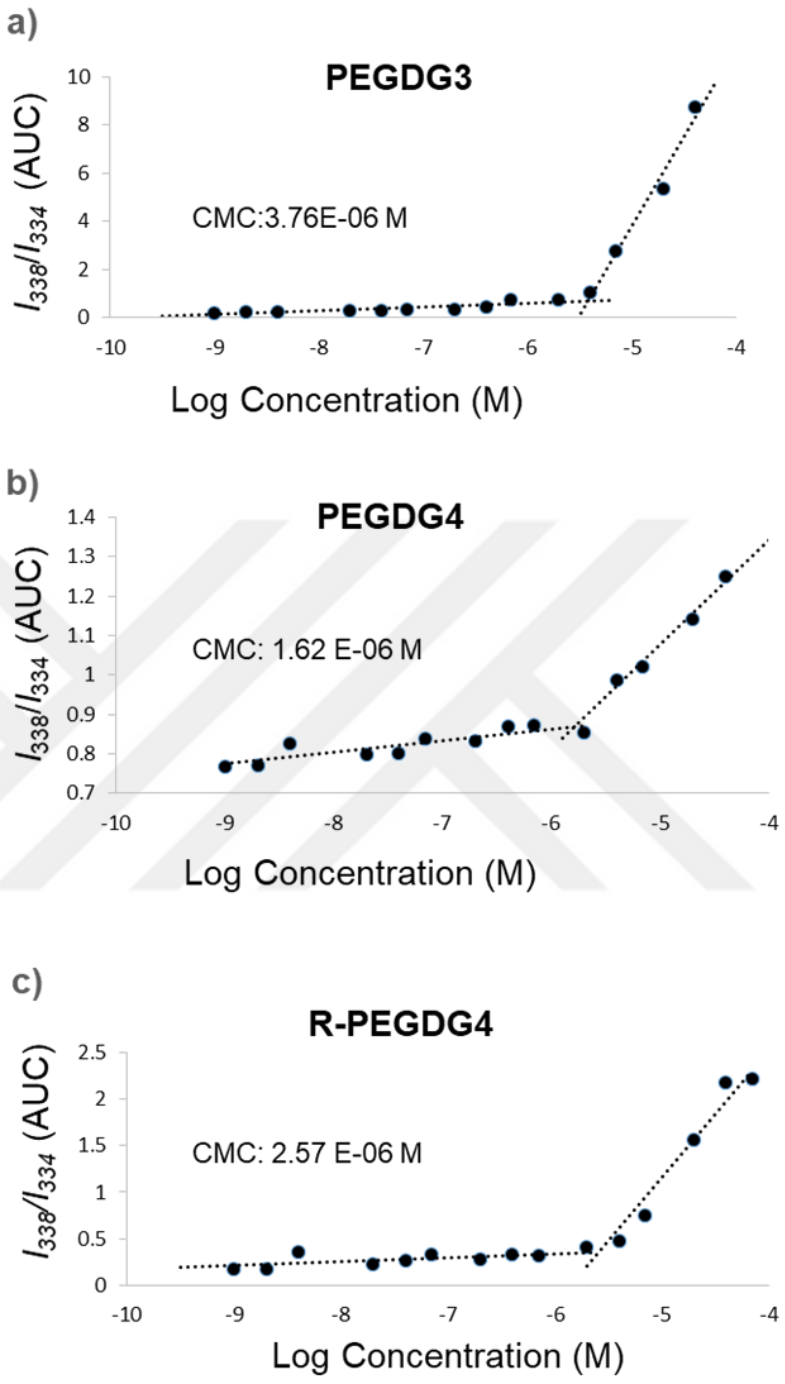

Figure 4.7. Pyrene excitation spectra of non-targeted producing PEGDG3, PEGDG4 and 20% RGD containing micelles R-PEGDG4. Insets: I_{338}/I_{334} vs log concentration graph to calculate CMC value.

4.3.3. Preparation and Characterization of RGD-containing Micelles

Micelles containing targeting group were obtained by mixing of PEGDG4 and R-PEGDG4 dendron polymer conjugates in a weight ratio of 80:20, respectively. Drop by drop addition of PBS to a THF solution of DOX, R-PEGDG4 and PEGDG3 separately under stirring at room temperature, enabling complete evaporation of the organic solvent in the dark, yielded drug-loaded micelles. While it was observed that the drug loading capacity was almost the same in the structures (8.69 ± 0.91 vs 8.7 ± 0.27) with and without the targeting group bearing micellar structures producing 4th generation dendrons, interestingly, it was observed that the drug loading capacity was half as much in the other structure prepared with the 3rd generation dendron compared to other structures (4.19 ± 0.92).This result can be predictable because of increasing in dendron generation makes the hydrophobic micelle core more stable, the drug loading capacity has also increased due to the hydrophobic interaction.

The diameter of the micellar structures prepared with the 3rd generation Dendron (126.2 nm) was smaller than the structures prepared with the 4th generation dendrons (168.5 nm). Presumably, the more branched higher generation hydrophobic dendron leads to micellar aggregates, which are larger in Figure 4.8 and Figure 4.9.

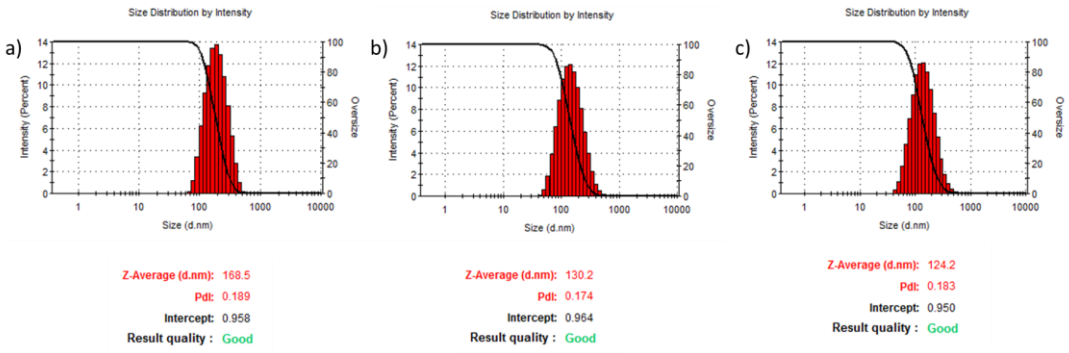

Figure 4.8. The diameters of (a) empty (b) DOX loaded (c) DOX loaded (after 2 days) micelles assembled from a mixture of R-PEGDG4 dendron-polymer conjugate.

On the other hand, a decrease in the micellar structure diameter was observed after drug loading. This may be due to the increasing hydrophobic interaction between the drug and the micelle core. R-PEGDG4 and PEGDG3-based aggregates' diameters after drug loading are 130.2 and 109.0 nm, respectively. Notably, no significant change was observed when the diameters were determined after 2 days.

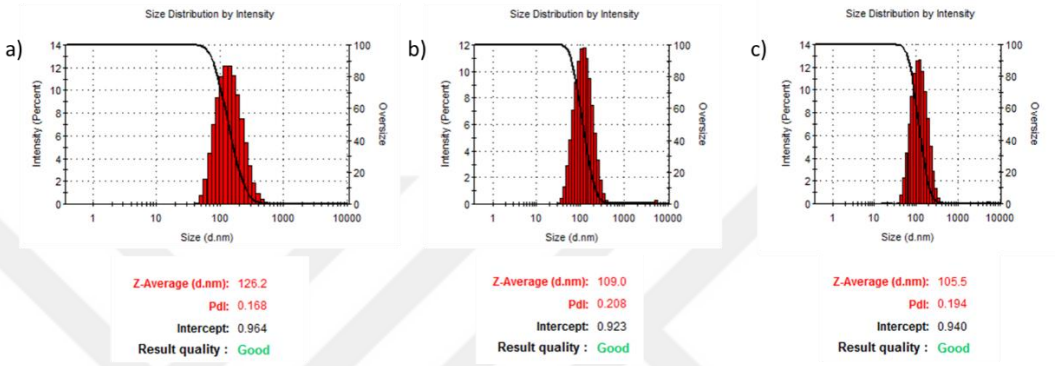

Figure 4.9. The diameters of (a) empty (b) DOX loaded (c) DOX loaded (after 2 days) micelles assembled from a mixture of PEGDG3 dendron-polymer conjugates.

At the same time, the images obtained from TEM mean that the micellar core is relatively small in the dry state in Figure 4.10. Size determinations smaller than those obtained using DLS can be expected since the micellar structures are likely to shrink considerably in the dry form.

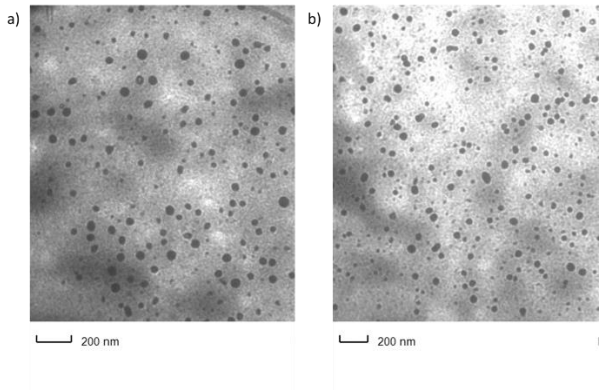

Figure 4.10. TEM micrographs of drug-loaded micelles fabricated using (a) R-PEGDG4 and (b) PEGDG3 dendron-polymer conjugates.

Using DLS measurements, the aggregates obtained by mixing R-PEGDG4 and PEGDG4 were investigated for their colloidal stability. Increasing amounts of PBS was added to nanoparticle samples with 1 x 10^{-5} M copolymer concentrations, followed by standard dilution with PBS in Figure 4.11. Even though the CMC values are very close to each other in each micelle structure, it was observed that the results are different. While the structure prepared with the 4th generation dendron was quite resistant to dilution, it was observed that the aggregate prepared with the 3rd generation conjugate started to disperse at higher concentrations. Based on this information, it was deduced that the PEGDG4-based dendron polymer conjugates possessed higher stability and were deemed suitable for further studies.

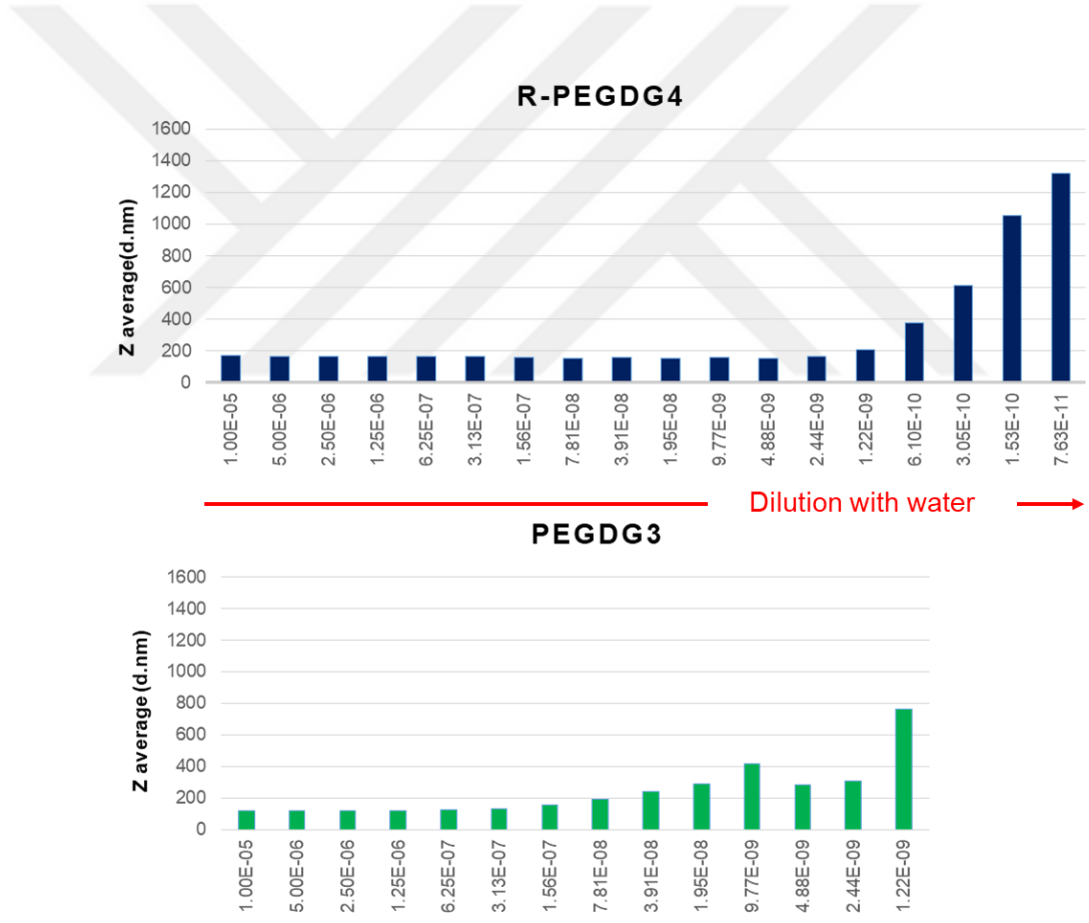

Figure 4.11. Stability under dilution in aqueous environment.

4.3.4. Drug Release Studies and *in vitro* Studies.

Combined acidic pH/reduction-responsive disintegration was investigated with aqueous micelles in diverse stimuli-responsive environments. Standardized fluorescence intensity stayed unchanged for the control structure, implying no significant micelle breakdown and consequently no NR release. For this purpose, six different solutions were prepared, and the intensity of each solution with FL was measured at predetermined intervals in Figure 4.12. While a decrease in NR intensity was observed in solutions containing either GSH or an acidic pH of 5.4, the most dramatic degradation was observed in solutions containing GSH (10 mM) and with a pH value of 5.4. Most likely, this exposure to dual stimuli caused the hydrophilic and hydrophobic blocks to separate from each other by breaking of the disulfide bond, while the acidic environment caused the acetal groups in the dendron to disintegrate, causing the structure to separate into its complete components.

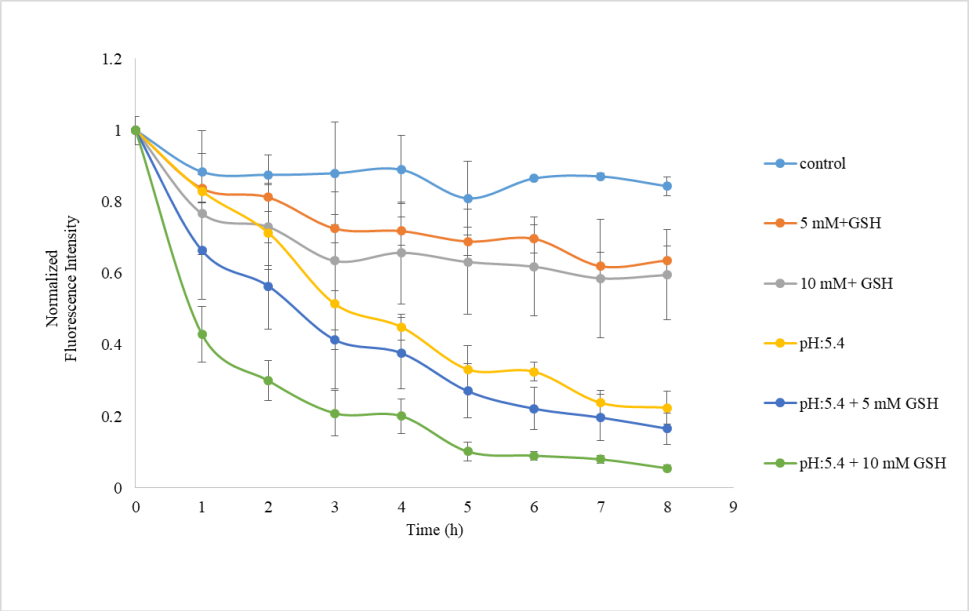

Figure 4.12. Change in the fluorescence intensity of NR-loaded micelles after incubation with and without 5/10 mm GSH at pH = 7.4 and 5.4.

Fluorescence spectroscopy was used for *in vitro* release of DOX from the micellar structures. Dox release over time in the presence of dual pH = 5.4 and 10 mM GSH, vs single stimuli (pH = 7.4 and 10 mM GSH) and a control (pH: 7.4) without stimuli. It was observed

that drug release studies led to a result similar to the NR dispersion study. In the environment containing GSH where the pH value is 5.4, the drug release reaches almost 100% in both structures, while the most striking difference was seen at pH 7.4. While 60% of the drug was released at the physiological pH value in the structure prepared with the 3rd generation dendron, it is seen that this value remains at 20% in the structure prepared with the 4th generation dendrons in Figure 4.13. Drug release occurs up to a point in an environment with a single stimulus, while a remarkable increase in drug release occurs when two stimuli are used together.

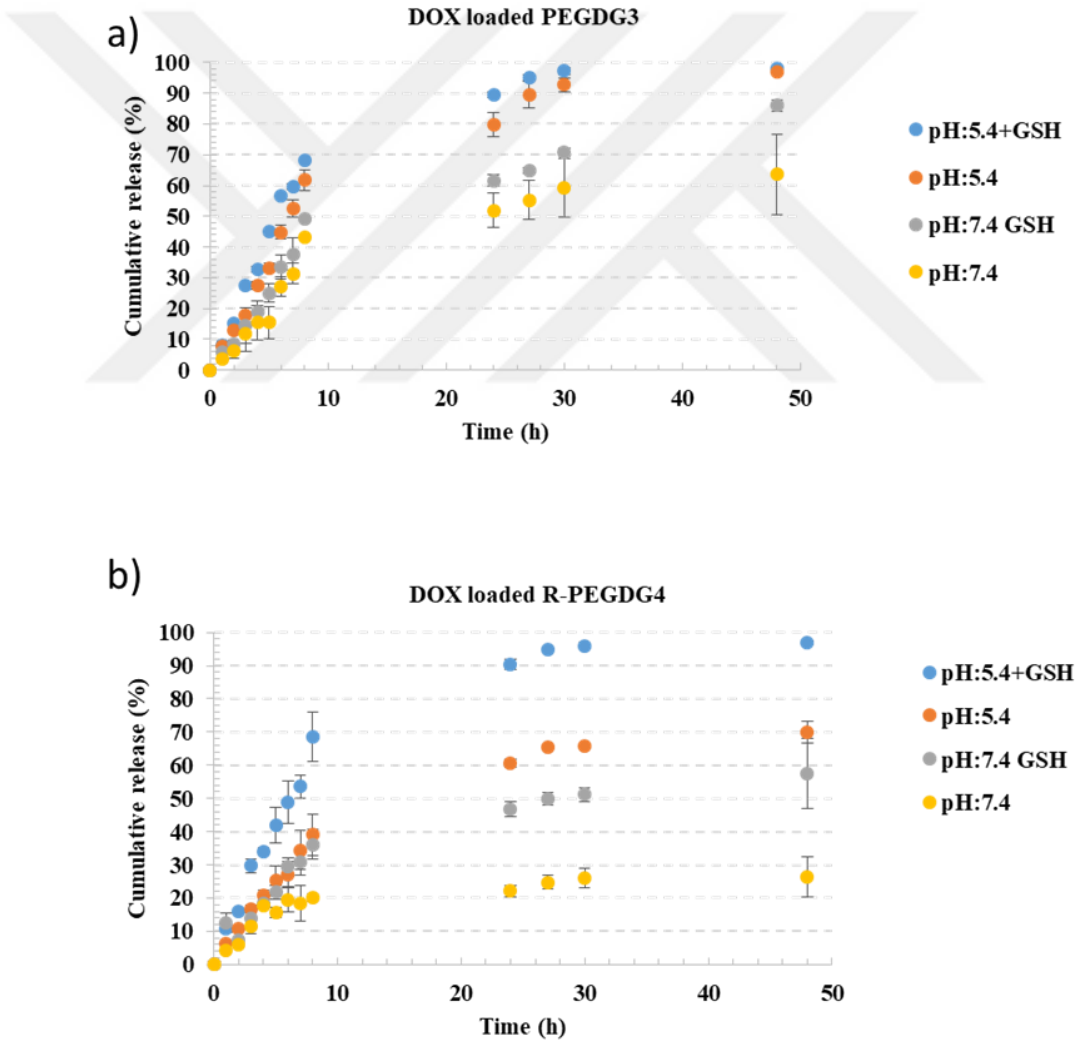

Figure 4.13. *In vitro* release of DOX at pH 7.4 and 5.4, with and without 10 mM GSH from micelles.

4.3.5. *In vitro* Cytotoxicity and Cellular Internalization.

The obtained micelles were first tested as efficient nanocarriers of antitumor drugs via redox induced intracellular transport of therapies in sensitivity to GSH. Fluorescence microscopy was used to analyze the intracellular location of free DOX and DOX-loaded polymeric micelles in breast cancer cell line, MDA-MB 231. The cells were exposed to a series of comparable concentrations of free DOX or DOX loaded targeted micelles with and without GSH-OEt, with drug concentrations ranging from 10^{-4} to 10^{-12} M. First of all, the cell line demonstrated almost 100% viability for all concentrations of the free polymer. This leads to the conclusion that the main structure is not cytotoxic in Figure 4.14a. Cellular GSH ethyl ester (GSH-OEt) can cross cellular membranes and swiftly achieve a high intracellular GSH content in biological systems. To ensure a known maximum internalized content of GSH, MDA-MB 231 cells were incubated with a 10 mM aqueous GSH-OEt solution. They were then cultured for 48 hours with different quantities of DOX-loaded micelles. Cells that had not been injected with GSH-OEt were also treated with DOX-loaded micelles and free DOX for comparison. While free DOX had an EC50 of $6.53E^{-6}$ M, DOX loaded targeted micelles with and without GSH-OEt had EC50 of $2.78E^{-5}$ M and $4.92E^{-6}$ M, respectively, according to cytotoxicity tests in Figure 4.14b. As expected, the free drug is more active than DOX loaded micelles. DOX-loaded micelles are less cytotoxic to breast cancer cells when compared to the same concentration of drug. This discovery could be due to faster diffusion of free DOX into the cell nucleus. Additionally, when MDA-MB 231 cells were incubated with GSH-OEt in the presence of DOX-loaded micelles, viability was much lower than when the cells were not treated with GSH-OEt. The presence of increased GSH in MDA-MB 231 cells causes quick and regulated liberation of DOX to useful therapeutic levels with disulfide linkage cleavage, resulting in decreased viability of MDA-MB 231 cells.

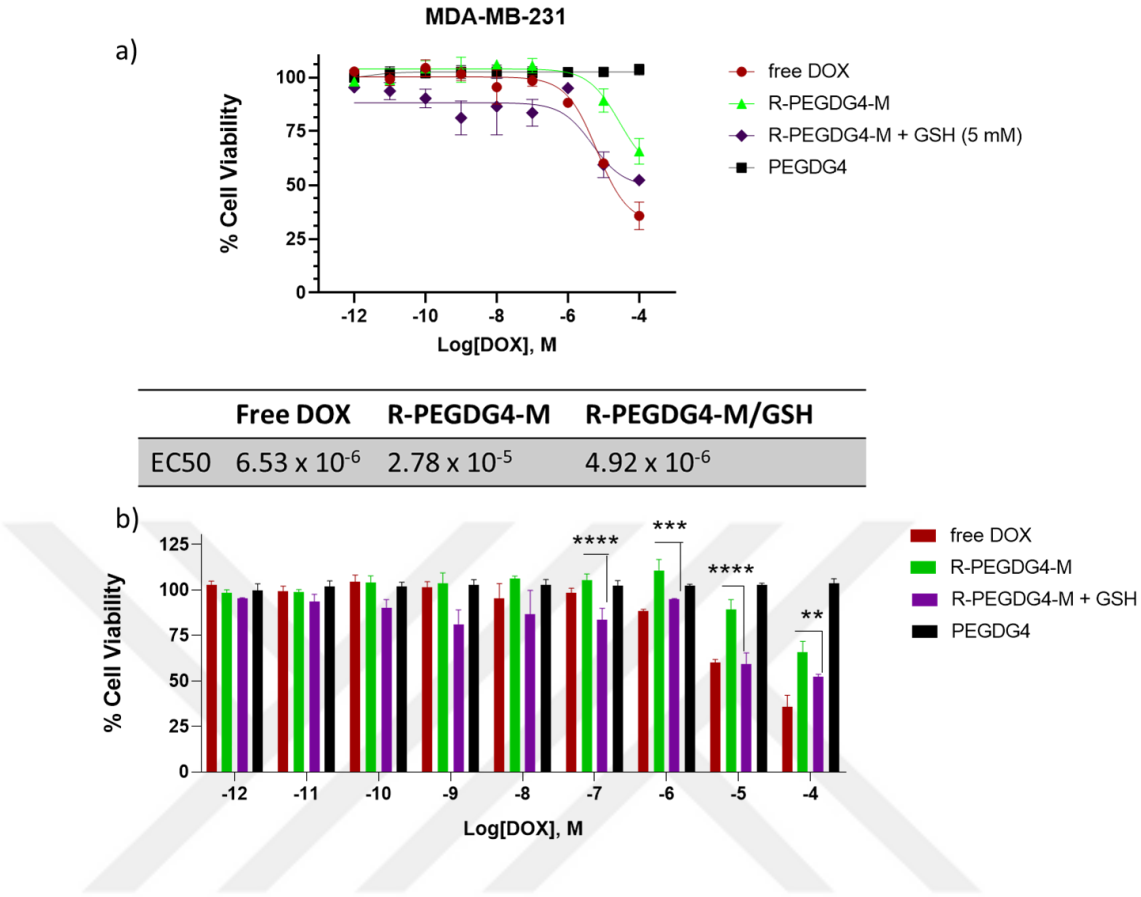

	Free DOX	R-PEGDG4-M	R-PEGDG4-M/GSH
EC50	6.53×10^{-6}	2.78×10^{-5}	4.92×10^{-6}

Figure 4.14. Viabilities of MDA-MB-231 cells incubated with polymer free DOX, DOX loaded targeted micelle R-PEGDG4 with or without GSH and free drug after 48h treatment as (a) dot plot and (b) as histogram.

Fluorescence microscopy was used to analyze the intracellular location of free DOX and DOX-loaded micellar structures in breast cancer cells. Free DOX, DOX loaded PEGDG4, DOX loaded R-PEGDG4, DOX loaded R-PEGDG4, and DOX loaded R-PEGDG4 were treated with free cRGDfV peptide as a competitively ligand in MDA-MB 231 cells. High internalization was observed even at the end of the first hour in the targeting group-bearing micellar structure in Figure 4.15. DOX-loaded polymeric micelles, on the other hand, showed significant fluorescence intensity in the perinuclear region rather than the nuclei of the cells in Figure A.11 when compared with free DOX. This finding indicates that DOX-loaded micelles must diffuse into cells via endocytosis.

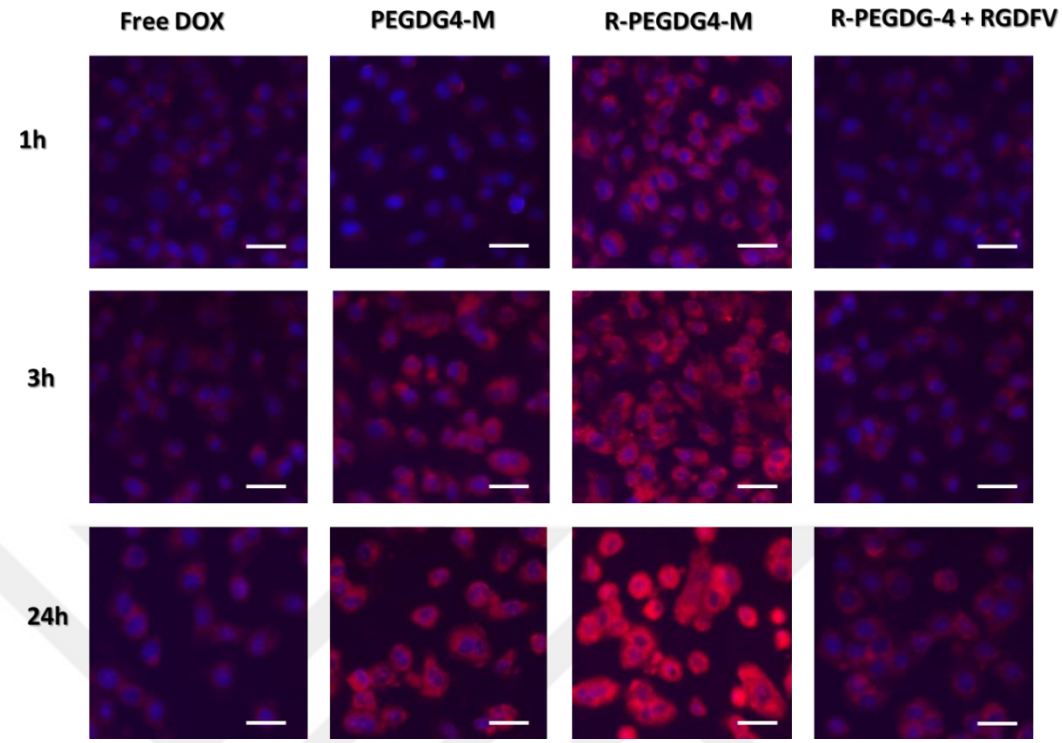

Figure 4.15. Fluorescence microscopy images (scale bar = 50 μm).

Flow cytometry was used to study the cellular uptake of DOX loaded targeted and non-targeted micelles. The free cyclic peptide cRGDfV was used as a selective antagonist of conjugated cRGDfK for integrin binding to illustrate the RGD dependent internalization in Figure 4.15. It is well known that cRGDfV binds to integrin regions on cell surface membrane with a higher affinity, hence addition of this free peptide should diminish the enhanced uptake of the targeted micelle s can be seen from the flow cytometry plots and histograms showing comparative fluorescence, even after 1 hour, the targeting group-bearing construct showed a higher mean fluorescence intensity compared to the other constructs and free drug in Figure 4.16. As expected, addition of free peptide as a competitive inhibitor of the integrin receptors leads to decree in the uptake of the targeting group bearing micelles.

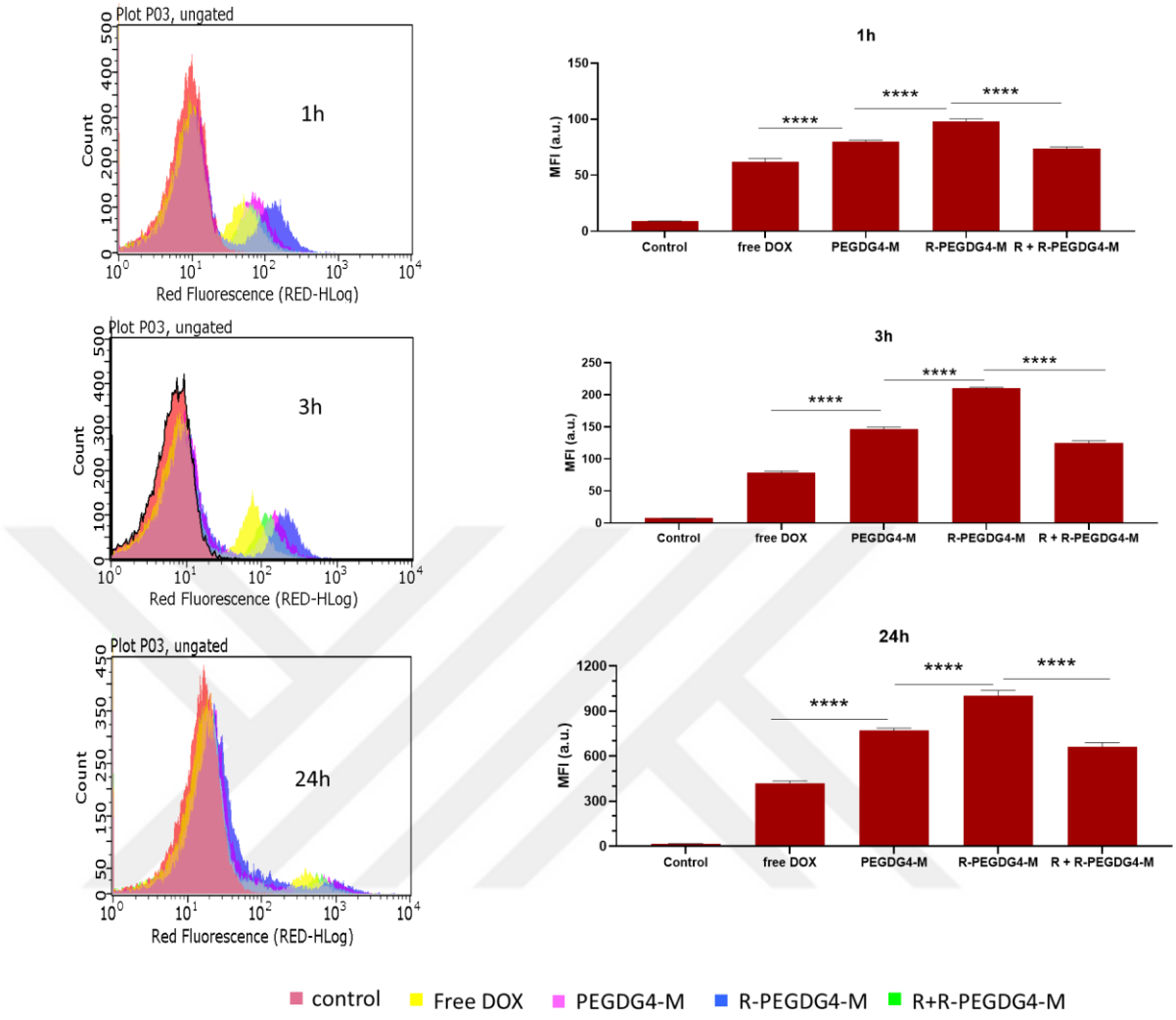

Figure 4.16. Flow cytometry histograms, of MDA-MB-231 cells treated with free DOX and DOX targeted micelles with and without GSH.

4.4. Conclusion

In summary, redox-responsive polymer-dendron conjugate-based micelles containing a cyclic peptide targeting moiety were synthesized. The polymer-dendron conjugate was synthesized using the thiol-disulfide exchange reaction. Disulfide bonds were introduced between the hydrophilic PEG segment and the hydrophobic dendron. When the micellar structures were compared, although there was no significant difference between the CMC values, it was observed that the structure prepared with the 4th generation dendron was more resistant to dilution. In addition, it was observed that the structure prepared with 4th

generation dendron was very stable at physiological pH. MDA-MB-231 breast cancer cells treated with micellar structures containing targeting groups showed very high internalization. Furthermore, *in vitro* cytotoxicity assay revealed that targeting group-bearing drug-loaded micelles was more cytotoxic under a reducing environment. These findings show that dual stimuli-responsive cleavable linkages in polymeric building block-based micellar precursors allow engineering DDS with improvised drug release characteristics.

5. MICELLAR TYPE NANOCARRIER FOR DRUG DELIVERY SYSTEMS FROM DENDRONIZED POLYMERS

5.1. Introduction

The use of polymeric nanomaterials as drug delivery systems has considerably increasing in recent years. Polymer-based nanomaterials find a wide variety of applications, especially in the area of smart drug delivery systems for disease diagnosis and treatment. It is well established that combining existing drugs with nano-sized carrier (NC) physically or chemically increases the effectiveness of drugs. Carrying the drug as cargo in a nano-sized structure increases the water solubility of the drug molecules which are mostly hydrophobic. The comparatively large size of the NC positively affects the plasma elimination half-life, tumor accumulation and renal excretion rate. As a result, targeting the transport of various therapeutic agents with NCs to reduce the overall toxicity and increase their efficacy has been exploited using polymeric NCs.

Conjugates containing dendritic structures among NC systems have attracted considerable attention in recent years. Dendrimers have a synthetically repetitive branched polymeric architecture. Dendritic molecules are characterized by their structural perfection. Dendrimers and dendrons are monodisperse and are usually highly symmetrical branched compounds. Since their discovery, considerable research has been done on dendritic macromolecules for the last 20 years, and many challenges related their synthetic and analysis have been resolved.

The conjugation of dendrons to polymeric structures imparts them with additional properties such as clustered multi-valency, and depending on the nature of the blocks enables their self-assembly into nanostructures. The two parts of the polymer-dendron conjugates may have different chemical and physical properties, and nanocarriers designed by utilizing these different offer a unique DDS. Dendron polymer conjugates can be designed as AB diblock, ABA triblock, star polymers with dendritic core or dendronized polymers.

Dendronized polymers carry more dendrons in the polymer backbone than AB type diblock and ABA type triblock polymer dendron conjugates, and thus provides more opportunities to benefit from the structural advantages of the dendron. Catalysis, biosciences, synthesis of hierarchically structured materials for optoelectronic applications are some of the main areas benefiting from dendronized polymers. However due to the steric bulk of the dendritic groups it is challenging to conjugate them along the side of polymers. Basically, the complex interactions that occur with the growth of dendron size, the distance between dendrons, and polymer backbone flexibility or stiffness, and solvent dendron interactions may make synthesis very difficult. However, if these difficulties are overcome, a unique structure that finds application in many areas emerge.

Herein we report a class of new dendronized copolymers comprised of a PEG-based hydrophilic polymeric chain appended with hydrophobic biodegradable dendrons that are connected through a redox-responsive disulfide linkage in Figure 5.1. Synthesis of such constructs starts with biodegradable and biocompatible poly(ethylene glycol) methyl ether methacrylate (PEGMEMA) based copolymers containing pyridyl disulfide (PDS) groups as side chains. Thus obtained copolymers were modified with polyester dendrons containing thiol groups at their focal point. The highly reactive PDS group undergoes efficient thiol-disulfide exchange reaction with the thiol-containing dendrons to yield dendronized copolymers. After their synthesis, formation and stability of self-assembled nanosized aggregates in aqueous environment was evaluated. Finally, drug loading and release, and cellular internalization and cytotoxicity of these DDS were evaluated.

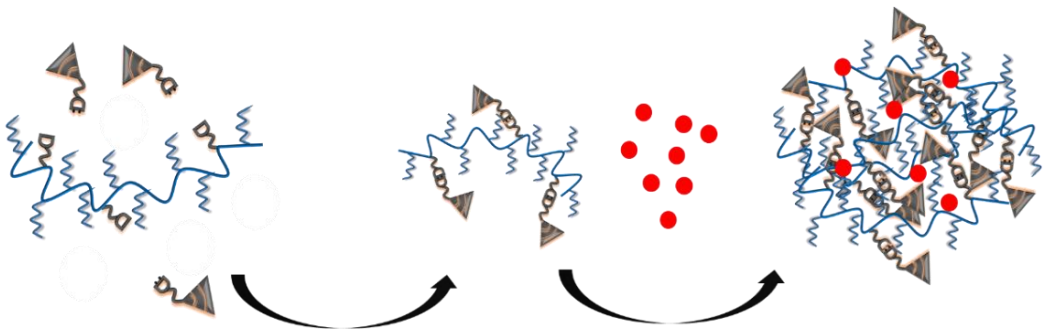

Figure 5.1. Illustration of fabrication of dendronized polymer-based nanoaggregate.

5.2. Experimental Section

5.2.1. Materials

2,2-Bis(hydroxymethyl)propionic acid, Dowex X50WX2, propargyl alcohol, and *N*,*N*-dicyclohexylcarbodiimide (DCC) were purchased from Alfa Aesar. All solvents were purchased from Merck and used as obtained without further purification unless otherwise noted. Ultrapure water was obtained using Milli-Q Water Purification System (Milli-Q system, Millipore, Billerica, MA, USA). Azide functionalized initiator was synthesized according to literature procedures [107]. Third generation polyester dendron containing alkyne unit at the focal point was synthesized according to literature [120].

5.2.2. Instrumentation

Chemical compositions of small molecules, dendrons and polymer were characterized using ^{1}H NMR spectroscopy (Varian 400 MHz). Micellar formations were characterized their critical micellar concentration and size using fluorescence spectrophotometer (Varian Cary Eclipse, Agilent, USA) and Zetasizer Nano particle analyzer (Malvern), respectively. The molecular weights of the polymers were estimated by size exclusion chromatography (SEC) analysis using a PSS-SDV (length/ID 8 × 300 mm, 10 µm particle size) Linear M column calibrated with polystyrene (PS) standards (1–150 kDa) using a refractive-index detector. Tetrahydrofuran (THF) was used as eluent at a flow rate of 1.0 mL/min at 30 °C. UVP Black-Ray B-100AP/R High Intensity UV lamp (100 Watt / 365 nm) was used for crosslinking experiments. During the internalization experiments, cells were visualized using Zeiss Axio Observer inverted fluorescence microscope (Carl Zeiss Canada Ltd, Canada). The dry micellar constructs were visualized on a holey carbon film coated 300 mesh Cu-grid (Pacific Grid Tech, USA) using a LVEM5 electron microscope on transmission electron microscopy (TEM) mode (Delong Instruments, USA).

5.2.3. Synthesis of Thiol group Containing Polyester Dendron

According to the literature, acetal-protected first, second, and third generation polyester dendrons with a thiol unit at the focal point were produced [120]. Briefly, at room temperature, 2-hydroxyethyl disulfide (0.93 g, 6.04 mmol) and 4-(dimethylamino)pyridine (DMAP) (0.589 g, 4.86 mmol) were dissolved in pyridine (1.46 mL) and CH_2Cl_2 (4.5 mL).The solution was spiked with acetonide-(2,2-bis(hydroxymethyl)propionic anhydride) (6 g, 18 mmol). After synthesizing generation 1 polyester dendrimer general acetonide deprotection-protection and cleavage of the disulfide bond procedures were applied to obtain reactive dendron containing thiol unit. A solution of protected dendron 2 (1.0 g, 0.97 mmol) and Dowex X50WX2 spatula tip in methanol (15 mL) was heated to 40 °C and stirred for deprotection. The end of the reaction was followed by TLC. Dowex was then removed through filtration, followed by methanol evaporation under decreased pressure. Disulfide-containing substances were dissolved in CH_2Cl_2 before being purged with nitrogen gas. The solution was spiked with DTT (2 eq) and triethylamine (4 eq). Extraction was done twice with $NaHSO_4$ once complete cleavage was achieved. The solvent was evaporated after the organic phase was dried on Na_2SO_4. Column chromatography was used to purify the crude product.

5.2.4. Synthesis of p(PEGMEMA)-b-p(PDSM) Block Copolymer

The PEGMEMA-b-PDSM block copolymer was made by via reversible addition–fragmentation chain transfer RAFT copolymerizing PEGMA and PDSM monomers in dry DMF utilizing AIBN as the initiator. PEGMEMA (0.4 g, 1.3 mmol) and PDSMA (48 mg, 0.19 mmol), were dissolved in anhydrous DMF (0.2 mL). To the polymer solution was added CTA (14.9 mg, 0.053 mmol) as chain transfer agent and AIBN (0.97 mg, 0.0059 mmol) as initiator. Reaction mixture was stirred under N_2 for 30 min. Reaction was sealed and heated 70 °C reaction was left at 21 hours. Following that, the polymer was then precipitated in cold Et2O after evaporation of DMF to a minimal amount. Ether was decanted after the mixture was kept in the cold to aid precipitation. Copolymer was dried under vacuo to yield pink substance Molecular weight and PDI of polymer were checked by gel permeation chromatography (GPC). (0.358 g, 70 % yield). The ratio of incorporated monomers in the

copolymer was determined from ^{1}H NMR spectrum as [PEGMEMA]:[PDSM]= 85:15. ^{1}H NMR (400 MHz, CDCl3) δ 8.51 (s, 9H), 7.90 (s, 2H), 7.73 (s, 18H), 7.55 (s, 2H), 7.38 (s, 3H), 7.17 (s, 9H), 4.18 (d, J = 58.0 Hz, 125H), 3.63 (d, J = 40.7 Hz, 792H), 3.41 (s, 146H), 3.07 (s, 18H) in Figure 4.4. $M_{n\ SEC}$ = 9.4 KDa, $M_{n\ NMR}$ = 15.6 KDa, Mw/Mn = 1.3.

5.2.5. Synthesis of Dendronized Polymer (DP)

Reactive PDS monomer including copolymer (50 mg 5.31 mmol) was mixed in DMF (1 mg/mL), then thiol reactive polyester dendrons (G1,G2,G3) and TEA (7.26 mg, 0.071 mmol) were added to the solution and stirred at room temperature for 24 hours. To obtain the required dendronized polymer, any unconjugated dendron was removed by dialysis against THF (MWCO 3500) after the process. The stoichiometric ratio of reactive monomer on co-polymer and dendron was adjusted to 1:10 for each conjugation.

5.2.6. Obtaining Micellar Nanoparticles from Dendronized Polymers

Micelle solutions were prepared and critical micelle concentration (CMC) were measured using the co-solvent evaporation method. Various quantities of the conjugate were dissolved in 500 µL THF in order to adjust final concentration of DP from 10^{-5} M to 10^{-9} M (in 3 mL water). Nile red solution (0.03mg/mL, 50µL) was added to all samples and then 3 mL PBS was added drop wise in a genteelly manner. The organic phase was evaporated by leaving the mixtures open to the air. Fluorescence measurements were taken with a fluorescence spectrophotometer at a wavelength of 550 nm for excitation and 580 to 660 nm for emission. While extending the intensity ratio, the intersection of the CMC values was calculated.

5.2.7. Stability Experiments

The size of the micelle was measured using dynamic light scattering to ensure that it was stable (DLS). DP was used to make P-SS-G1, P-SS-G2, and P-SS-G3 micelle samples at CMC concentrations. Each micelle solution was diluted at 1000 times its original concentration. The micelle size was then measured using DLS. After the micelles were prepared, 10 mM DTT was added to the solution and the stability of the micelles was checked in both DLS and GPC.

5.2.8. Encapsulation and *in vitro* release of DOX

The co-solvent evaporation approach was used to load DOX into micelles. Fluorescence spectrophotometry was used to calculate the amount of DOX loaded. The DOX-loaded P-SS-G2 and P-SS-G3 micelles were freeze-dried and dissolved in DMSO to determine drug loading content, and the DOX content was determined by fluorescence detection using a DOX calibration curve. The following equations were used to compute the drug-loading capability (DLC) as

DLC (wt%) = (weight of loaded drug/total weight of polymer and loaded drug)x100%

and efficiency (DLE) as

DLE (%) = (weight of loaded drug/weight of drug in feed) x100%.

Dual acidic pH/reduction-responsive disintegration and drug release were studied in micelles. Dialysis membrane (MWCO 3500) was utilized under sink circumstances with gentle shaking (260 rpm) at 37°C in four different buffer media to investigate the release profile of DOX from P-SS-G2 and P-SS-G3 micelles *in vitro*. Dox-loaded micellar aliquots (1.5 mg mL1, 2 mL) were transferred into dialysis bag (MWCO=3500 g mol1) and immersed in outer buffer solutions (20 mL) prepared under different conditions: aqueous PBS at pH = 7.4 and aqueous acetate buffer solution at pH = 5.4 with and without 10 mM GSH. The outer phase of the dialysis membrane was withdrawn and replaced with an equal volume of fresh

release medium at predefined time intervals. Fluorescence spectroscopy (excitation at 485 nm) was used to determine the amount of DOX emitted. The data reported in the release experiment are averages with standard deviations.

5.2.9. Cellular Internalization

MDA-MB-231 adenocarcinoma cells (100 000 cells/well) were seeded in 12-well plate as duplicate in 1 mL of culture media (DMEM). The cells were incubated at 37ºC for 24 h. Nile Red-loaded SCM-G3 micelle solution and free Nile Red were added on the wells with the same concentration (0.05 mg/mL). After 1h, 3h and 24 incubation process, Nile Red and micelle solution were removed from cells and the cells were washed with 1 x PBS (1 mL x 2 times). Cells were fixed by using 3.7% formaldehyde solution at 37ºC for 10 min. After fixation process, cells were washed with 1 x PBS (1 mL x 2 times). Then cell nuclei were stained by DAPI for 15 min at 37ºC. After washing the cells, cell images were taken using Zeiss Observer Z1 fluorescence microscope and processed with Zeiss Zen Blue lite software.

5.2.10. *In vitro* Cytotoxicity

Cytotoxicity of DOX-loaded SCM-G3 micelle was determined using CCK-8 assay. MDA-MB-231 human breast cancer cells (purchased from ATCC (LGC Standards, Germany) were used for cytotoxicity experiments. The cells were grown in DMEM supplemented with 10% fetal bovine serum and incubated at 37 ºC. MDA-MB-231 cells (7000 cells/well) were seeded in a 96-well plate in 100 µL DMEM and incubated at 37 ºC for 24 h to adhere completely. After 24 h incubation, free DOX and DOX-loaded SCM-G3 micelle solutions (10^{-4} and 10^{-12} M) were separately placed onto the cells (100 µL/well). For GSH mediated cytotoxicity, the cells were treated with glutathione ethyl ester (GSHOEt, 5 mM) for 5 hours. After that, GSH solution was removed from cells and the cells were washed with 1 x PBS (1 mL x 3 times). Then the cells were treated with DOX-loaded SCM-G3 micelle solutions. After 48 h incubation, drug solutions were removed from cell containing wells, and the wells were washed with PBS (1 mL x 2 times). CCK-8 solution %10 in

DMEM was added onto cells (100 μL/well) and incubated for 2h. The absorbance measurements at 450 nm were done with a plate reader. EC50 values of DOX-loaded SCM-G3 micelles and free DOX were calculated using Graph Pad Prism software.

5.3. Results and Discussion

5.3.1. Synthesis and Characterization of Dendronized Polymer

Three different dendronized polymer structures namely P-SS-G1, P-SS-G2 and P-SS-G3 were synthesized using a 'graft-to' approach. In this approach, well-defined dendrons with a thiol group at focal point were grafted to a PDS group containing copolymer. Different generations of thiol group containing polyester dendrons were produced in accordance with the literature [120]. Briefly, to obtain the 1st generation dendrimer, first, 2-hydroxyethyl disulfide was reacted with bis-MPA anhydride, followed by acetal deprotected by treatment with acidic Dowex resin. The same procedure was continued until the 3rd generation dendrimer was obtained in Figure 5.2. Using this methodology, generation 1, 2 and 3 acetal-protected polyester dendrons were obtained. The purity of each dendron was verified by ^{1}H NMR spectroscopy in Figure A13, Figure A14 and Figure A15.

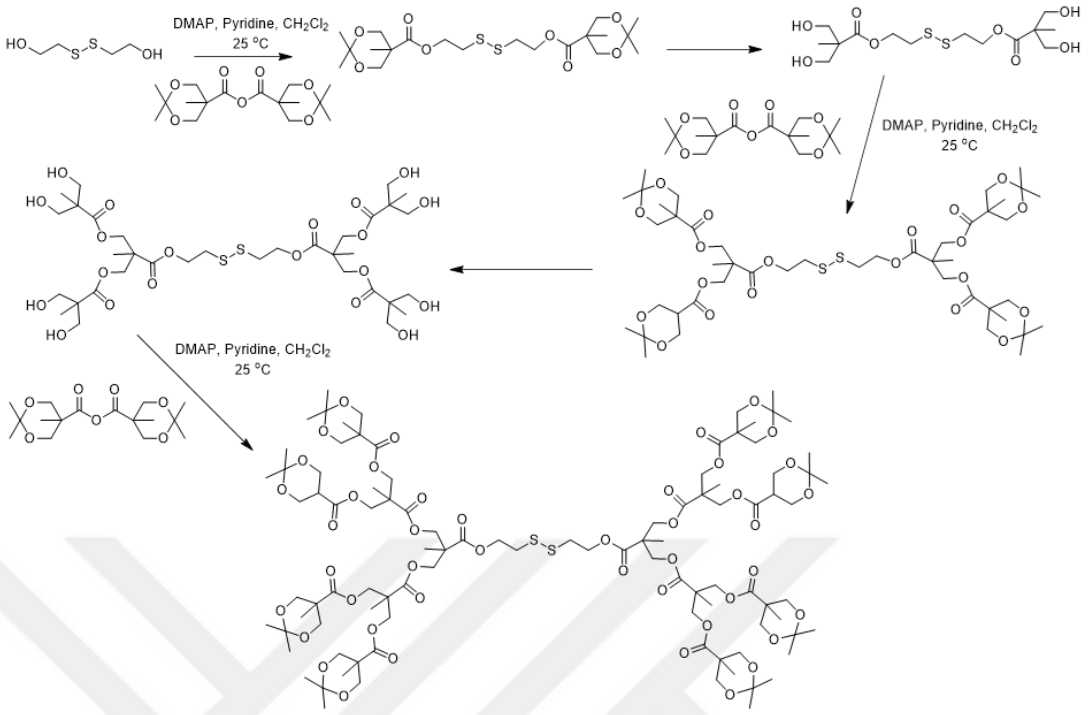

Figure 5.2. Synthesis of 1st, 2nd and 3rd generation polyester dendrimers.

The above protocol to obtain thiol-containing dendrons circumvents any side reactions with thiol group by using a disulfide group. The disulfide group can be viewed as a protected thiol group, which can be reduced to obtain thiol-containing dendrons by simple reduction prior to their utilization. To obtain the thiol containing dendrons, the 1st, 2nd and 3rd generation dendrimers were treated with 1,4-dithiothreitol (DTT) in dichloromethane in Figure 5.3.

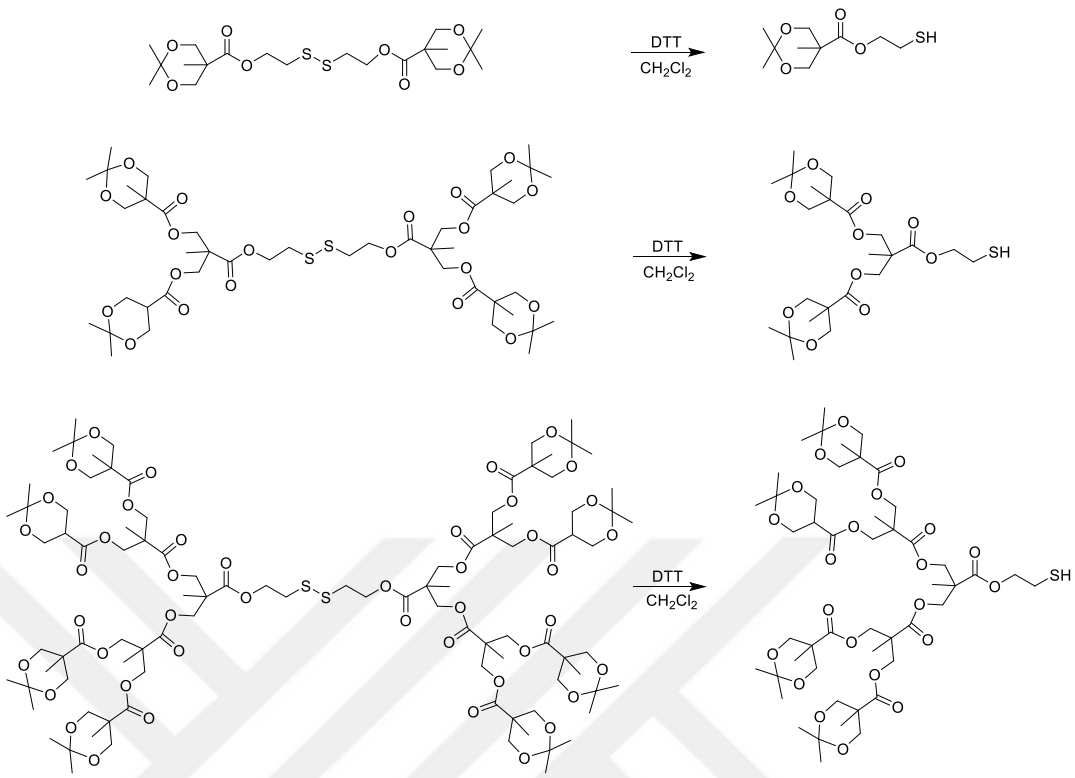

Figure 5.3. Synthesis of 1st, 3rd and 2nd generation thiol-containing polyester dendrons.

The purity of the dendron blocks was confirmed using ^{1}HNMR spectroscopy. Notably, in all of the ^{1}H NMRs, the characteristic triplet peak from the proton in the thiol group at 1.48 ppm is clearly observable. Additionally, a multiplet around 2.76 ppm belonging to the protons from the methylene group adjacent to the thiol group also supports successful disulfide cleavage in Figure 5.4.

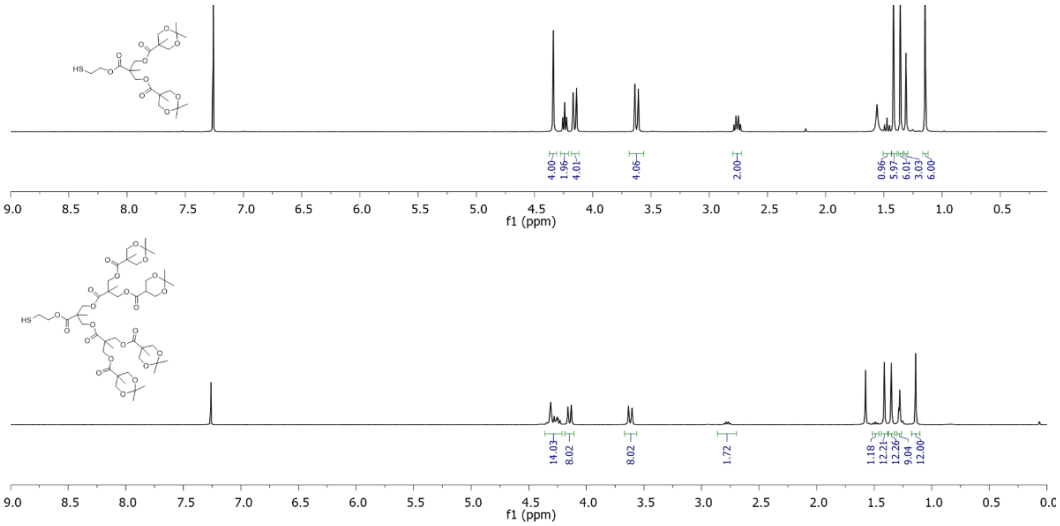

Figure 5.4. ^{1}H NMR thiol group containing 1st and 2nd generation polyester dendron.

5.3.2. Synthesis and Characterization Copolymer

Commercially available 2,2′-dithiodipyridine (Sigma-Aldrich) reacted with mercaptoethanol to yield product 1. The resulting pyridyl disulfide ethanol was reacted with methacryloyl chloride dropwise to a trimethylamine-containing dichloromethane solution to obtain pyridyl disulfide ethyl methacrylate (PDSM) monomer in Figure 5.5. The PDSM structure was confirmed by from the presence of proton resonances at 7.14, 7.48 and 7.70 ppm belonging to the protons of the PDS group in the ^{1}H NMR spectrum in Figure 5.6.

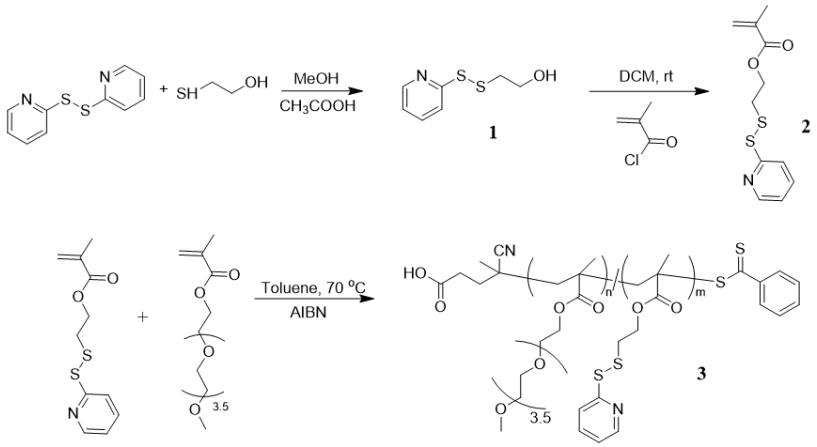

Figure 5.5. Synthetic route of PDSM bearing random copolymer.

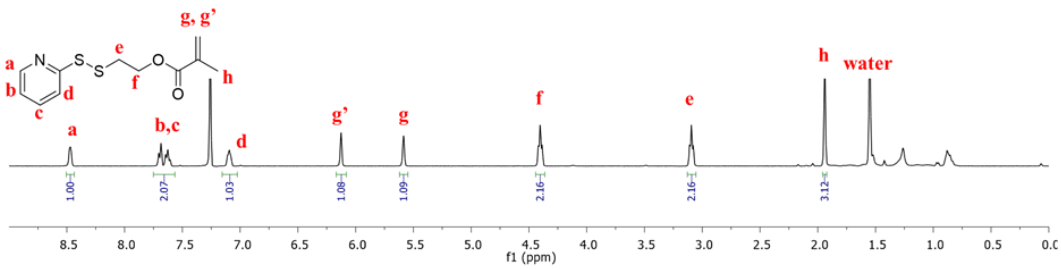

Figure 5.6. ^{1}H NMR spectrum of pyridyl disulfide ethyl methacrylate (PDSM) monomer.

Desired block copolymer was synthesized by RAFT polymerization utilizing PDSM and hydrophilic monomer PEGMEMA. First, PDS group bearing copolymer was synthesized *via* AIBN initiated RAFT polymerization in DMF. Synthesized copolymers were characterized by using ^{1}HNMR spectroscopy to determine individual monomer compositions in the copolymers in Figure 5.7. The existence of proton resonance at 7.14, 7.48 and 7.70 ppm refer to the aromatic protons of the ring in the ^{1}H NMR spectrum showed the insertion of the reactive PDS group along the polymer chain. Furthermore, the molecular weight (9.4 KDa) and distribution (1.3) of resulting copolymers were determined through size exclusion chromatography (SEC). Ratio of incorporation of monomers were determined using 1H NMR spectroscopy as 85:15 for PEGMEMA and PDSM respectively.

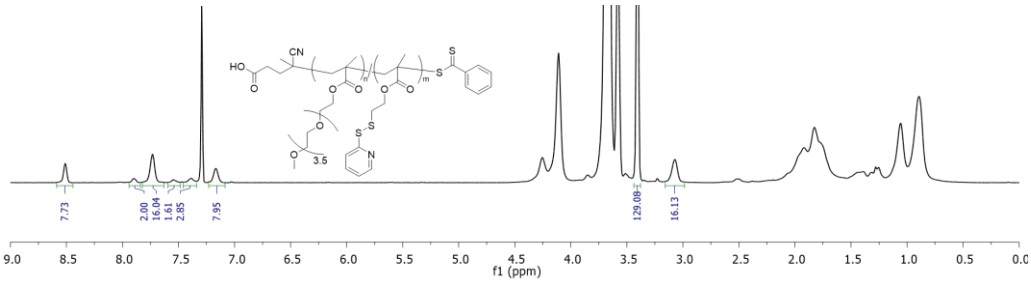

Figure 5.7. ^{1}H NMR spectrum of random copolymer.

5.3.3. Synthesis of Dendronized Polymer

Thiol-containing dendrons were attached to the polymer backbone with the reactive PDS group in their side branches by the thiol-disulfide exchange reaction. Successful conjugation of the dendrons onto the polymeric backbone was confirmed using ^{1}HNMR spectroscopy. The copolymer containing PDS group was dendronized with the three generations of thiol-containing dendrons to yield three dendronized copolymers with variation in the side-chain residues in Figure 5.8.

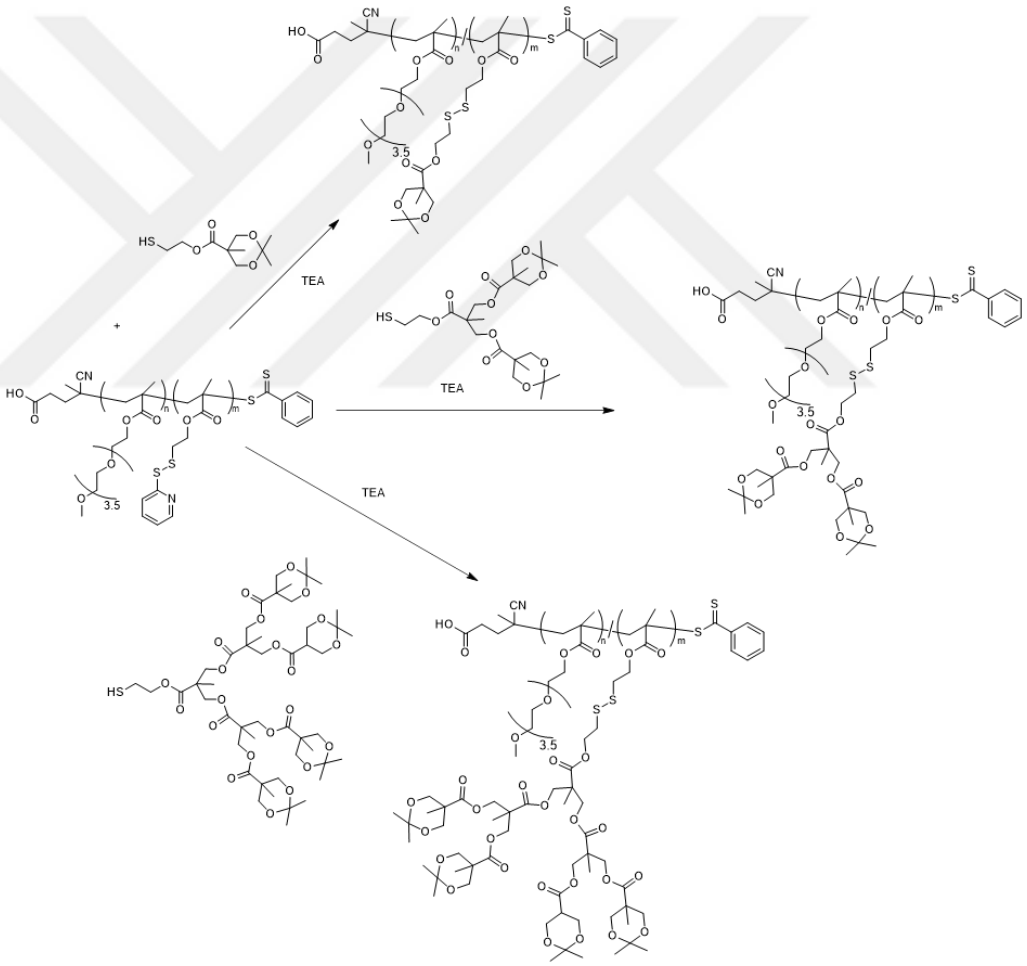

Figure 5.8. Synthesis of dendronized polymer using 1st, 2nd and 3rd generation polyester dendron.

Successful conjugation was demonstrated by ^{1}H NMR. As a result of the thiol-disulfide exchange reaction in the main polymer, it was observed that the peaks from the PDS disappeared and the new peaks from the dendron appeared. (1ppm-1.5 ppm) in Figure

5.9. The increase in the generation of the attached dendron brings with it the result that the acetal group protons coming from the dendron become more prominent in the ^{1}HNMR spectrum. The increase in molecular mass after the main polymer has become dendronized has been demonstrated by size exclusion chromatography (SEC) in Figure 5.10. While the molecular mass of the main polymer is 9.4 KDa, P-SS-G1, P-SS-G2 and P-SS-G3 have a molecular weight of 11.2 KDa 14.3 KDa 17.7 KDa, respectively.

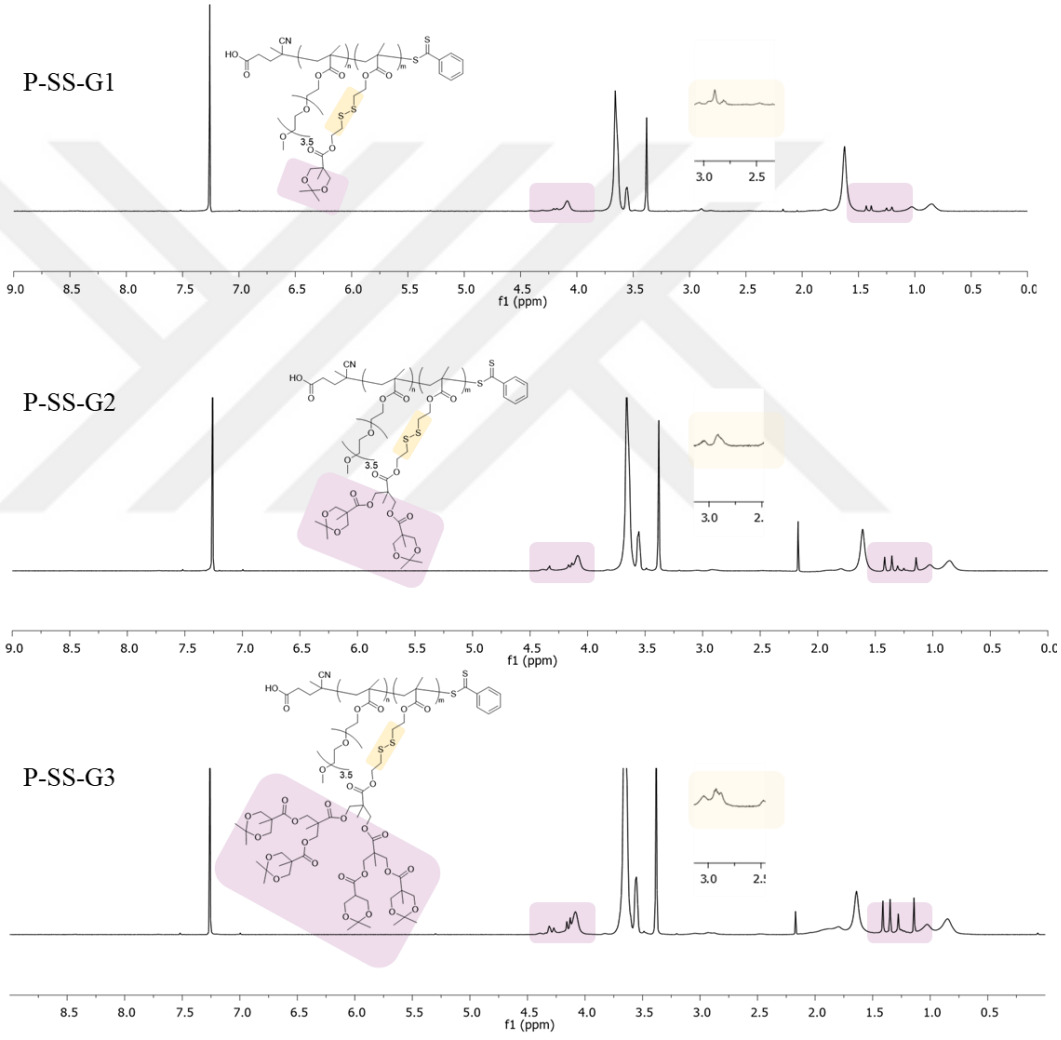

Figure 5.9. ^{1}H NMR spectra of dendronized copolymers P-SS-G1, P-SS-G2, and P-SS-G3.

The product was examined using ^{1}H NMR spectroscopy after purification of the conjugate by precipitation in ether to eliminate the unreacted dendron. Apart from the typical proton resonances from the polymer and dendron components, a proton resonance at 2.91

ppm belonging to methylene groups next to the newly produced disulfide was discovered. When comparing the SEC traces of the parent polymer and dendronized polymer constructs, a molecular weight rise to Mn = 10KDa was seen when dendron was attached to the polymer.

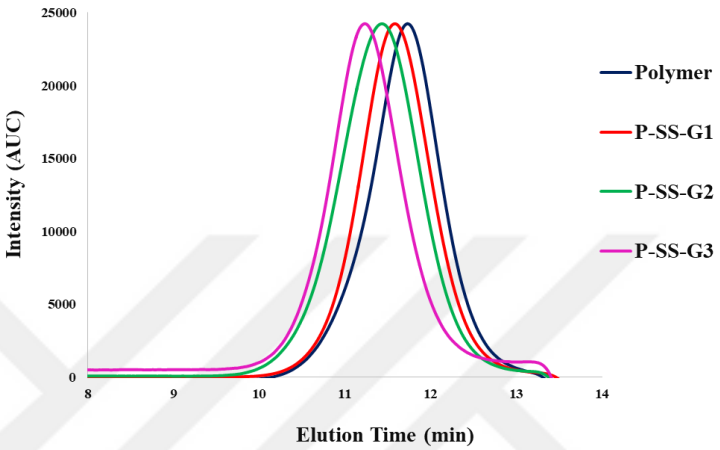

Figure 5.10. SEC traces of parent polymer and dendronized polymers.

5.3.4. Preparation and Characterization of Micelles.

After synthesizing the conjugates containing dendrons in the side branches, the critical micelle concentration (CMC) of each conjugate was calculated. The CMC of the conjugate was determined using pyrene, a hydrophobic fluorescent probe. Above a certain concentration, micelle formation makes pyrene soluble and causes an increase in the emission peak. In addition, the peak of the peak changes from 334 to 338 nm after micelle formation. CMC values of dendronized polymers are given in table 5.1 in mg/mL in Figure 5.12. It is clearly seen that the CMC value decreases as the dendron generation used increases in Figure 5.11.

The CMC values of the block copolymers were determined by measuring the fluorescence intensity of pyrene as a parameter of polymer concentration to determine the minimum needed concentration of amphiphilic polymers to produce micelle type polymeric nanoparticles by self-assembly.

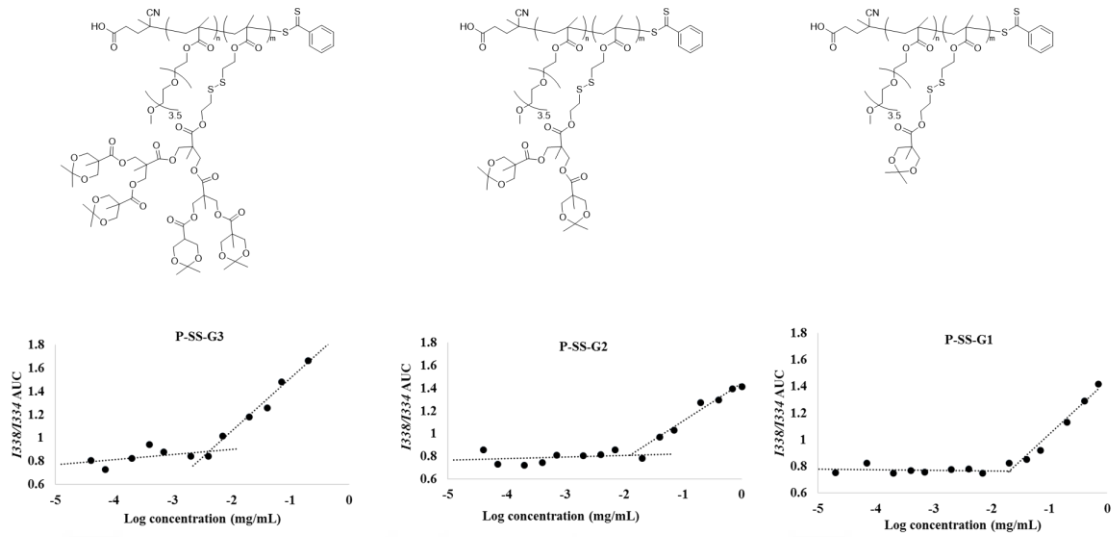

Figure 5.11. I_{338}/I_{334} vs. log [mg/mL] graph to calculate CMC value.

When the P-SS-G3 dendronized conjugate is compared with the other conjugates, the CMC value is 0.00417 mg/mL. On the other hand P-SS-G2 and P-SS-G1 have higher CMC value 0.01267 and 0.01867 mg/mL respectively. This value indicates that it will be highly resistant to dilution conditions, especially after drug loading. It shows that dendronized conjugates obtained using 3rd generation and 2nd generation dendrons are more suitable for forming micellar structure.

DLS was used to estimate the diameter of micelles made from P-SS-G3 with and without DOX encapsulation. It was discovered that drug-loaded micelles had a somewhat smaller average size than empty micelles (134.4 nm vs 100.1 nm). This is thought to occur due to hydrophobic interactions between DOX and the hydrophobic polyester dendron moiety. When the drug-loaded micelles were held at room temperature for a week and measured again using DLS, it was discovered that the micelles remained stable with a low PDI in Figure 5.12.

When the sizes of the structures prepared with every 3 generations are compared, it is seen that the size of the micelles increases as the generation of the dendron used increases. While average size of P-SS-G3 was 135.8 nm, P-SS-G2 and P-SS-G1 had slightly smaller size (124.5 nm and 114.7 nm). P-SS-G3 micelles had a well-defined and somewhat bigger size than P-SS-G2 micelles, according to TEM investigation of dry micellar constructions.

Since the micelles are in their wet environment in the former measurement, the diameters of drug loaded micelles assessed using DLS are bigger than those measured using TEM in Figure 5.13. This may be explained by the increased generation of dendrons causing greater accumulation. When micelles with CMC concentration were diluted 1000 times below the CMC concentration with PBS, it was observed that the micellar structures prepared with P-SS-G3 preserved their stability and size, while dispersion was observed in the other two structures. This situation brings with it the result that the micellar structure prepared with the increase of dendron generation is more resistant to harsh dilution circumstances in Figure 5.14.

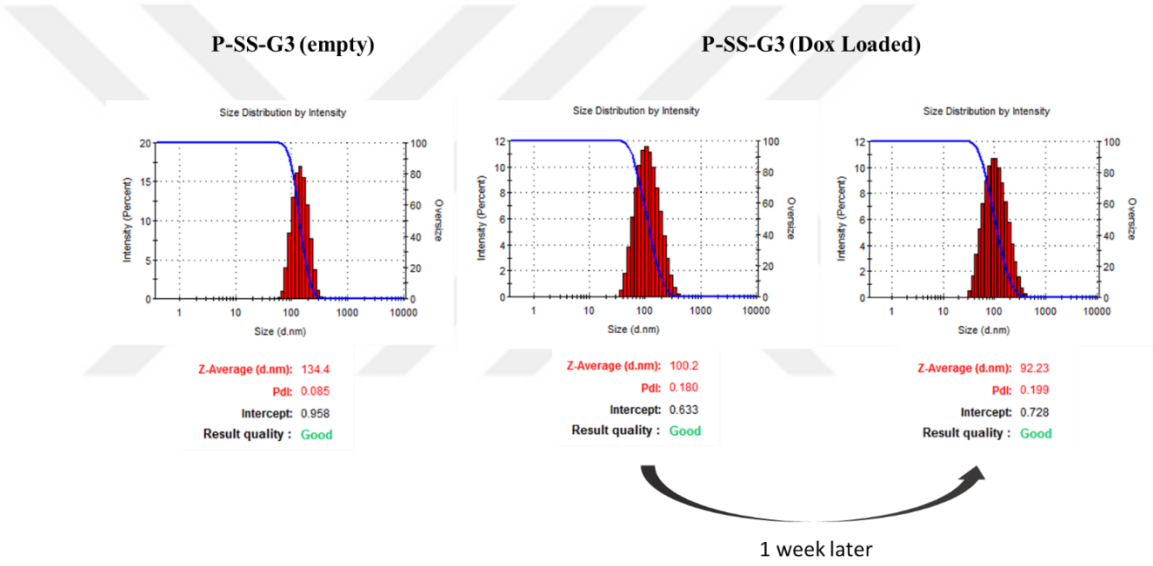

Figure 5.12. Effective size diameters of empty and DOX loaded P-SS-G3 micelles

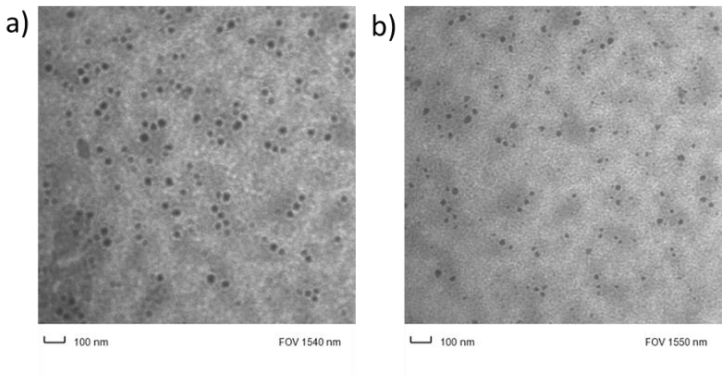

Figure 5.13. TEM micrographs of a) P-SS-G3 b) P-SS-G2 dendronized copolymer based micellar nanosized aggregates.

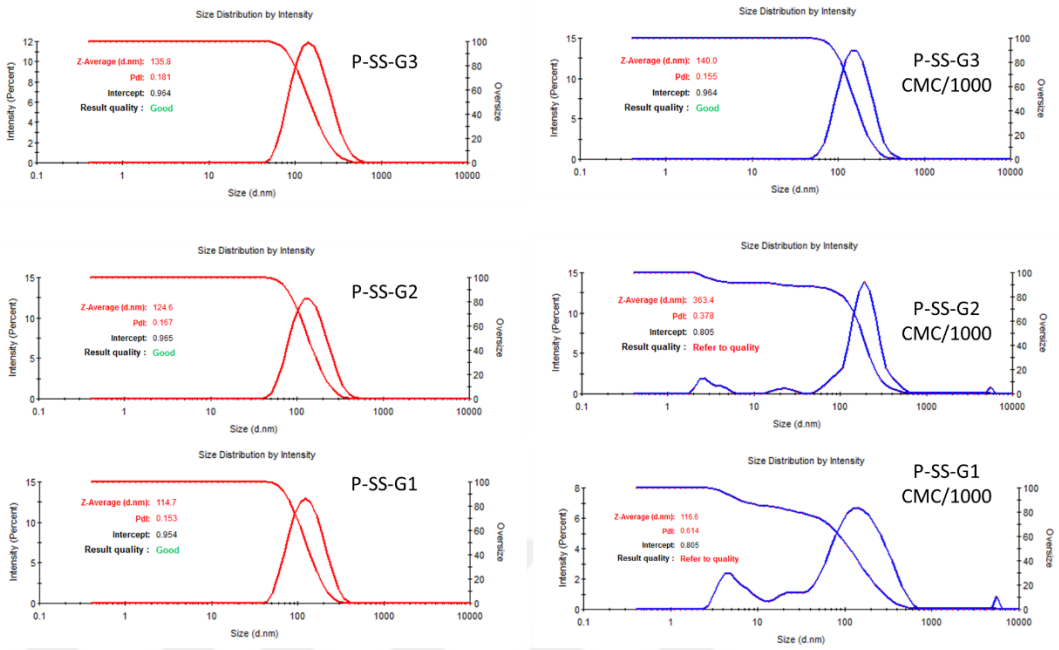

Figure 5.14. Stability of micelles from P-SS-G3, P-SS-G2 and P-SS-G1 against dilution as probed using DLS.

Extra stability studies were performed using DTT. After micellar solutions were prepared, 10 mM DTT was added to it. When checked with DLS after 1 hour, it was seen that the micelles could not maintain their stability in the reducing environment in Figure 5.15. When the same situation was tested for the P-SS-G3 structure in GPS, it was observed that the sample, which was normally seen as a single peak, was divided into two different structures in Figure 5.16.

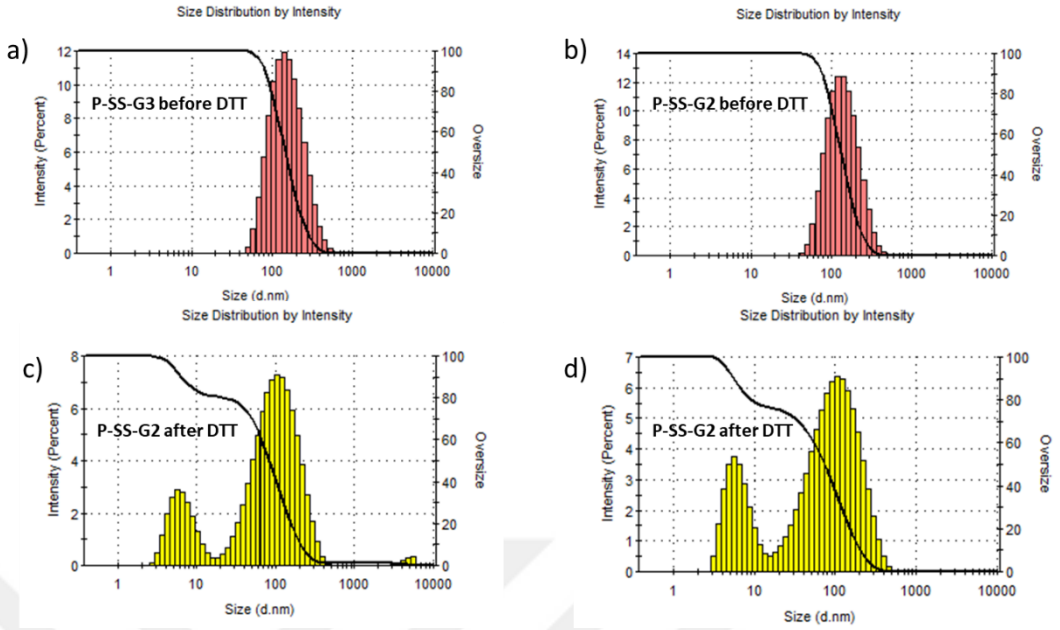

Figure 5.15. Stability of micelles from P-SS-G3, P-SS-G2 (a-c) before (c-d) after DTT treatment.

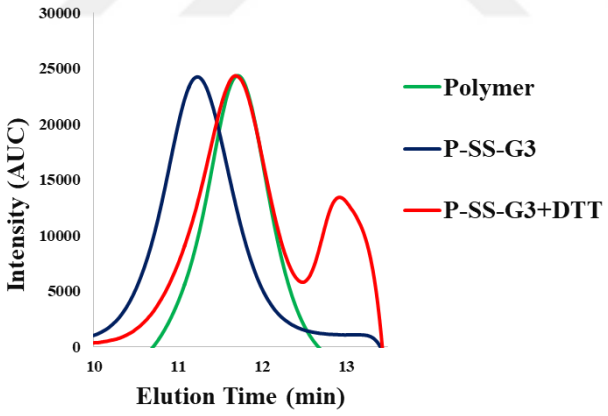

Figure 5.16. SEC traces of parent polymer and P-SS-G3 before and after DDT treatment.

5.3.5. Drug Loading and Release into Micelles Obtained from Dendronized Polymers

After calculating the CMC values, drug-loaded micelles were prepared with neutralized doxorubicin (DOX). DP and drug were dissolved in organic solvent (THF) and

distilled water was added dropwise. The organic solvent was then allowed to volatilize in the dark at room temperature. The drug loading capacity was determined by fluorescence spectroscopy, and the calibration curve of the drug was prepared using solutions containing drugs at different concentrations. The drug loading capacity was found to be considerably higher in the structure obtained using 3rd generation dendrons compared to the structure prepared using 2nd generation dendrons (9.7 ± 1.25 vs 6.2 ± 0.69). This result may be actually an expected situation. Since 3rd generation dendrons strengthen the hydrophobic structure in the dendronized structure, it may cause the drug in the hydrophobic structure to be loaded more by physical interaction.

The *in vitro* release of the hydrophobic drug DOX, P-SS-G2 and P-SS-G3, was studied. For drug release studies, four different pH environments were prepared. A pH:7.4 PBS was used to simulate the extracellular environment, and a pH:5.4 acetate buffer solution was used to mimic the lysosomal environment. While preparing the other two buffer solutions, 10mM buffer solutions were prepared with glutathione (GSH), which is more abundant in cancer cells than in the extracellular medium. As expected, the release of DOX was dependent on the pH environment and it was observed that it was higher in the acidic environment compared to the neutral environment. In the acidic environment, the acetal groups of the dendrons are broken and the structure becomes completely hydrophilic, and thus the drug release is more. In addition to all these, it is seen that the release is quite high in the solution containing 10mM GSH in an acidic environment. This result is very important for the drug-loaded micelles to carry cargo stably in the extracellular environment. The maximum drug release in the P-SS-G3 dendronized conjugate structure was observed in the solution containing 10mM GSH at pH=5.4. When this structure was compared with P-SS-G2, it was observed that the drug release was very low in the extracellular environment. In addition, the micelle structures degrade quite rapidly in the reducing (GSH) environment, releasing their cargo in Figure 5.17.

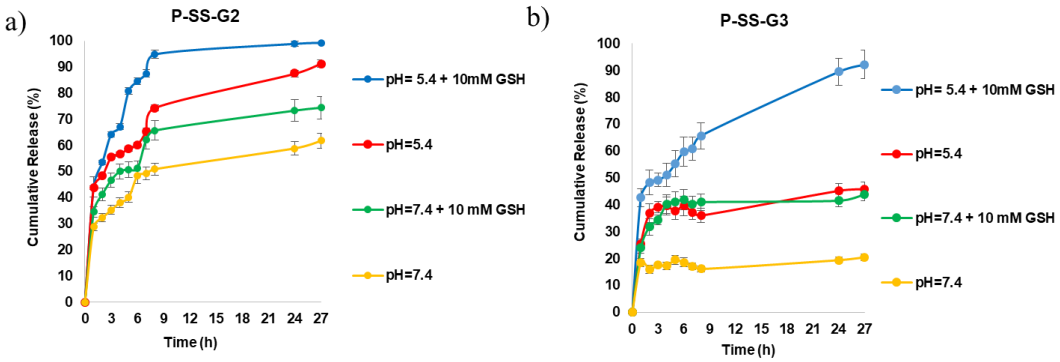

Figure 5.17. *In vitro* release of DOX at pH 7.4 and 5.4 with and without GSH for a) P-SS-G2 and b) P-SS-G3 dendronized copolymers.

5.3.6. Cellular Internalization and *in vitro* Cytotoxicity

P-SS-G3 micelles were treated with MDA-MB-231 human breast cancer cells to determine cellular internalization. Micelles were doped with a hydrophobic dye, Nile Red, in visualizing internalization of the cargo. After 1 hour of incubation, the treated cells with micellar carriers showed an increase in NR intensity when compare to control well, wherein NR was introduced to cell containing media without any micelles. The NR signal increased significantly in all wells excluding the control after 3 hours, demonstrating that cell internalization of NR was greatly improved once encapsulated into micelles, and uptake increased over time in Figure 5.18.

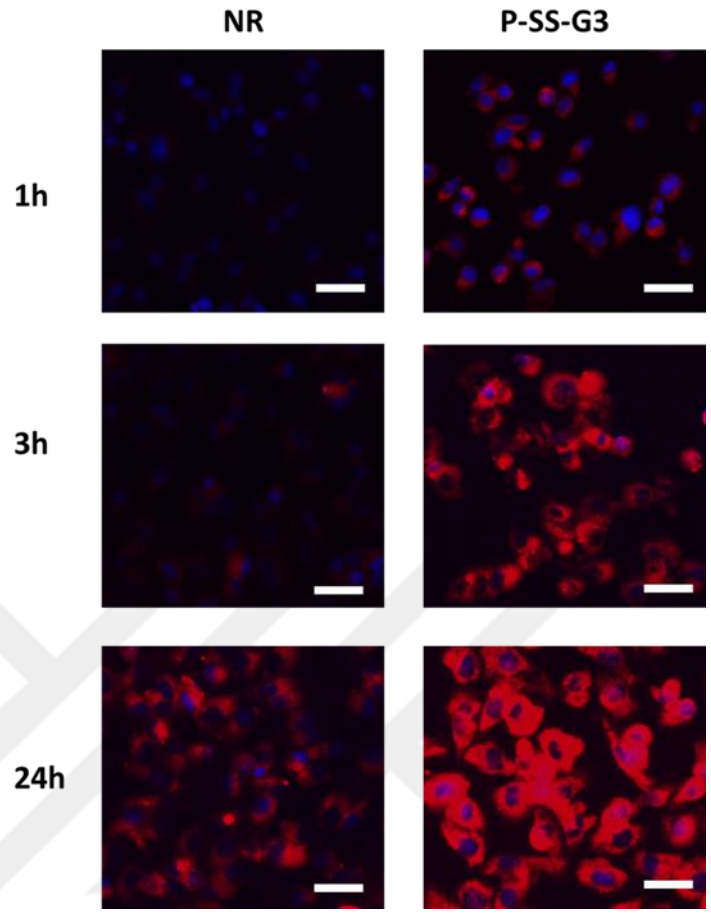

Figure 5.18. Fluorescence microscopy images showing the comparison of internalization of Nile Red and Nile Red-loaded micellar aggregate by MDA-MB-231 human breast cancer cells. Scale bar is 100 μm.

In vitro cytotoxicity assays were performed on a human breast cell line, MDA-MB 231, to explore the cytotoxic effect of DOX loaded polymeric micelles. The cells were subjected to a range of comparable doses of free DOX or DOX-loaded micelles, ranging from 10^{-4} to 10^{-12} M. The cytotoxicity of DOX-loaded micelles was also investigated in the context of GSH-responsive degradation. Cellular GSH ethyl ester (GSH-OEt) can cross cellular membranes and swiftly achieve a high intracellular GSH content in biological systems [121]. While free DOX had an EC50 of 5.69×10^{-8} M, the DOX loaded micelles P-SS-G3 and the same structures with GSH had an EC50 of 1.01×10^{-6} M and 7.24×10^{-7} M, respectively, according to cytotoxicity tests in Figure 5.19. The vitality of the cells reduced as the amount of free and encapsulated DOX increased, implying that DOX inhibits cell proliferation. When MDA-MB 231 cells are treated with GSH-OEt in the presence of DOX

loaded particles, a further lowering of viability was observed. The presence of increased GSH concentration in the MDA-MB 231 cells causes quick release of DOX to efficient therapeutic levels upon disulfide linkage cleavage, resulting in decreased viability of MDA-MB 231 cells.

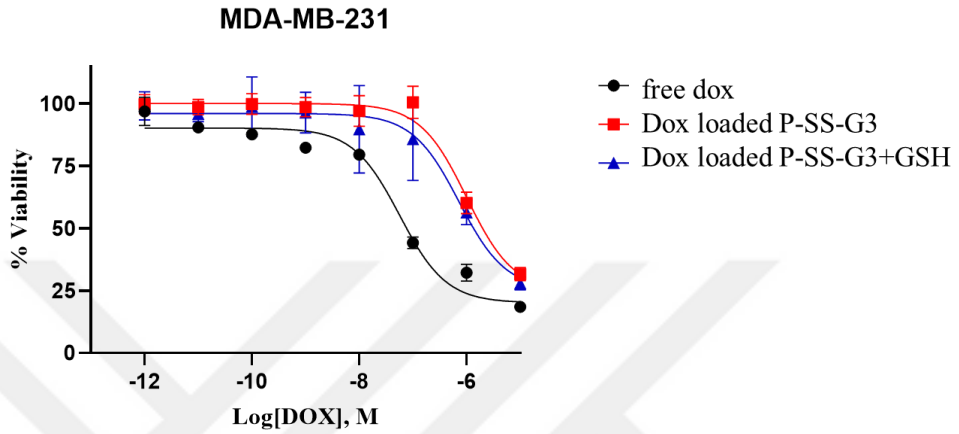

Figure 5.19. Viabilities of MDA-MB-231 cells treated with DOX loaded P-SS-G3 under normal and redox environments.

5.4. Conclusion

In this project, redox-sensitive polymer-dendron conjugates that can respond to the reducing environment in diseased tissues were fabricated. In these dendronized polymers, the dendrons in the side chains are connected to the main polymer backbone by disulfide bonds. While the polymer is hydrophilic, the attached dendrons were selected to be hydrophobic. This construct yield nanosized micellar aggregates when dispersed in an aqueous environment. Synthesized micellar structures were evaluated for drug delivery studies, and there performance was evaluated under reducing environment and at various pH values. The drug carrying capacity of the structures prepared with 3rd generation polyester dendrons was found to be 1.5 times higher than the structures with 2nd generation dendrons. Thus, the increase in dendron generation increases the drug loading capacity of the multiplex structure. Importantly, it was observed that the drug release was very low at physiological pH for the 3rd generation dendronized copolymer. The P-SS-G2 and P-SS-G1 constructions also assembled to micellar with low CMC, but they were unstable in excessively dilute

environments. On the other hand, the micellar constructs obtained using generation G3-dendrons were stable upon dilution. Cellular internalization of hydrophobic agents was facilitated by encapsulation in these micellar constructs, as demonstrated with internalization of Nile red into MDA-MB-231 breast cancer cells treated with dye-loaded P-SS-G3 micelles. Overall, the redox-responsive macromolecular structure designed in this study offers an attractive candidate for creating micellar nanocarriers responsive to endogenous stimulus, and is capable of effectively transporting therapeutically active agents. One can envision that the design of the present construct can be further improved to obtain specific targeting, as well as administration of multiple drugs in a synergistic fashion to address some of the challenges encountered in combating complex diseases.

6. ‘CATCH AND RELEASE’ CRYOGELS: FABRICATION, FUNCTIONALIZATION AND REVERSIBLE PROTEIN IMMOBILIZATION

6.1. Introduction

Three-dimensional polymeric scaffolds such as cryogels (CGs) are emerging as an attractive alternative to traditional hydrogels as hydrophilic crosslinked soft material in enabling a wide range of biomedical applications, such as diagnostics, drug delivery to tissue engineering scaffolds [123–125]. While their important role is indisputable, for some applications, traditional hydrogels require further structural refinements to improve their suitability. One important attribute that governs performance of these crosslinked polymeric scaffolds in several applications is the porosity of these materials. Imparting macroporosity to hydrogels is not trivial, and one has to often resort to approaches like utilizations of porogenic agents to enhance porosity. While this approach can increase the porosity of these materials, it not only introduces other components during hydrogel fabrication which would be needed to be removed, but also may compromise the preservation of the macroporous structure after their removal [126, 127]. In this regard, cryogels, macroporous crosslinked polymeric networks have emerged as an attractive alternative. It is a simple approach, where gelation occurs at subzero temperatures, the frozen solvent domains act as porogens [128–133]. Thawing the material post-crosslinking and removal of the solvent provides access to a highly interconnected polymeric network with macroscopic voids. While there has been renewed interest in these macroporous materials, their suitability in applications such as acting a cell scaffolds and stationary phase for separation and purification of proteins have been long recognized [134]. In both of the aforementioned applications a highly porous structure with interpore connectivity is desirable. To further enhance the properties of cryogels as scaffolds various functional groups have been introduced as reactive handles for conjugation of bio-relevant ligands, which as promote specific interactions between the biological entities such as proteins and cells with the polymeric matrix.

A survey of functionalizable cryogel scaffolds which have been reported in recent years for applications involving protein attachment and their release, reveals that reactive functional groups such as epoxide, hydroxyethyl methacrylate, acrylamide and maleimide have been utilized [135]. For example, Ingavle and coworkers reported that the possible use of macroporous monolithic cryogels for biotoxin removal using anthrax toxin protective antigen (PA). Using covalent immobilization technic, cryogel adsorbents with different containing hydroxyl and epoxy-derivatized physical and mechanical properties for binding of anthrax toxin specific antibodies [135]. While most of these examples utilize permanent conjugation of a bioactive ligand, one can utilize reversible linkages to the polymeric matrix. In this regard, the thiol-group based thiol-disulfide exchange chemistry has been exploited since thiol-groups are either inherently present in several proteins, or can be introduced using site-directed mutagenesis. In particular, sephadex microbeads containing thiol-reactive pyridyl disulfide group has been commercialized for protein purification [136]. While disulfide-containing reactive handles have been used for reversible conjugation on polymeric interfaces such as surface coatings and hydrogels to the best of our knowledge, this reactive functional group has not been exploited as a reversible handle in cryogels. Given the increasing adaptation of cryogels in many areas, one can envision that fabrication of cryogels that can be reversibly functionalized using the efficient thiol-disulfide exchange chemistry will further expand their utility.

Herein, we report fabrication of reversibly thiol-reactive cryogel scaffolds and demonstrate their application in biomolecular immobilization, protein detection and purification using a catch and release strategy. To this end, a pyridyl disulfide group containing oligoethylene glycol based methacrylate monomer was synthesized, and subjected to cryogelation using polyethylene glycol (PEG) based co-monomers and crosslinker. Cryogels with varying amount of the reactive PDS group could be obtained by varying the monomer compositions in the cryogel precursors. Obtained cryogels were characterized in terms of their morphology, water uptake capacity and chemical composition using various analytical techniques. Reversible attachment on the cryogels is demonstrated through attachment and release of fluorescent dyes, and proteins such as Streptavidin and Concanavalin A (Con A). Finally the non-cytotoxic nature of these materials is demonstrated through successful culture of fibroblasts on these macroporous scaffolds.

6.2. Experimental Section

6.2.1. Materials

2,2-dipyridyldisulfide was purchased from TCI chemicals. Methacryloyl chloride, DTT, cysteamine were purchased from Alfa Aesar. Biotin−thiol (Biotin−SH), and mannose−thiol (Man−SH) were manufactured in relation to the literature [137]. Poly(ethylene glycol) methacrylate (PEGMEMA, Mn= 360 g mol−1) and poly(ethylene glycol) dimethacrylate (PEGDMA, Mn = 550 g mol−1) were purchased from Sigma-Aldrich and purified by passing it via an activated aluminum oxide column prior to usage. D-(+)-mannose were purchased from Alfa-Aesar. Concanavalin A (FITC conjugate) was purchased from ThermoFisher. Sigma-Aldrich provided the 2,2-dimethoxy-2-phenylacetophenone (DMPA). Pierce provided rhodamine-conjugated streptavidin (TRITC-Streptavidin). Silica gel 60 (4360 m, Merck) was used for column chromatography. Silica gel plates were used for thin layer chromatography (Kieselgel 60 F254, 0.2 mm, Merck). All gelation processes were carried out at a distance of 10 cm using a UV lamp with a 100 W spot bulb (absorbance maxima ca. 365 nm). All solvents were purchased from Merck and used as obtained without further purification unless otherwise noted. Ultrapure water was obtained using Milli-Q Water Purification System (Milli-Q system, Millipore, Billerica, MA, USA).

6.2.2. Instrumentation

Chemical compositions of small molecules were characterized using ^{1}H NMR spectroscopy (Varian 400 MHz). A Thermo Scientific Nicolet 380 FT-IR spectrometer was used to obtain Fourier transform infrared (FTIR) spectra. We used an ESEM-FEG/EDAX Philips XL-30 (Philips, Eindhoven, The Netherlands) scanning electron microscopy (SEM) apparatus operating at 10 kV to characterize the cryogel morphology. Prior to SEM examination, cryogel samples were swelled in water and lyophilized. A fluorescent microscope was used utilized to confirm the attachment of FITCBSA and TRITC-

Streptavidin to the cryogels (HBO100 ZEISS Fluorescence Microscope, Carl Zeiss Canada Ltd., Canada).

6.2.3. Synthesis of 2-(pyridin-2-yldisulfanyl)ethanamine (PDS-NH_2)

Pyridyl disulfide ethylamine was synthesized according to reported procedures [6]. Briefly, in a round bottom flask equipped with a magnetic stirrer, 2,2-dipyridyldisulfide (415 mg, 4.54 mmol) was dissolved in methanol (3 mL) and acetic acid (0.26 mL, 5.54 mmol) was added into solution and the mixture was stirred under N_2. Cysteamine (143 mg, 1.26 mmol) was dissolved in methanol (2 mL) and added dropwise to the reaction flask. Then, it was allowed to stir at room temperature for 3 hours to give desired compound. After the formation of pyridyl disulfide ethylamine, solvent was evaporated in order to obtain a yellow liquid. Reaction mixture was added to cold diethyl ether dropwise. White solid product 2 was precipitated and collected by filtration method (300.21 mg, 73.5 % yield).

6.2.4. Synthesis of PEG-Based 2-(acryloyloxy)ethyl methacrylate

Poly(ethylene glycol) methacrylate (1.11 g, 3.08 mmol) was dissolved in anhydrous CH_2Cl_2 (20 mL) and triethylamine (0.85 mL, 6.16 mmol) was added to the solution. The mixture was cooled to 0^oC in an ice bath under N_2. Methacryloyl chloride (0.37 mL, 4.62 mmol) was added dropwise with continuous stirring into the mixture. The reaction was stirred at room temperature for 24 hours. After completion of reaction mixture, 30 mL CH_2Cl_2 was added and extraction was done using with $NaHCO_3$ (2x10 mL) and with brine (2x10 mL).Organic layer was collected and dried over anhydrous Na_2SO_4. In order to obtain pure product **1** column chromatography was used.

6.2.5. Synthesis of PEG-Based Pyridyl-Disulfide Group Containing Methacrylate (PDS-PEG-MA) Monomer

PEG-Based 2-(acryloyloxy) ethyl methacrylate (0.312g, 0.75 mmol) was dissolved in ethanol (5mL) then triethylamine (0.11mL, 0.82 mmol) and pyridyl disulfide ethylamine (0.18mg, 0.81 mmol) were added to the reaction flask and stirred at room temperature for 24 hours. Thereafter, reaction solvent was evaporated and mixture was diluted with CH_2Cl_2 (20mL) and extracted with brine solution (3 × 30mL). Organic layer was dried by adding solid anhydrous Na_2SO_4 and then it was filtered. Solvent was removed under reduced pressure to yield pure product. (0.368 g, 82% yield).^{1}H NMR ($CDCl_3$, δ, ppm) 8.47 (d, J = 3.5 Hz, 1H), 7.77 – 7.56 (m, 2H), 7.10 (d, J = 5.0 Hz, 1H), 6.13 (s, 1H), 5.57 (s, 1H), 4.40 – 4.15 (m, 4H) in Figure 6.1. ^{13}C NMR ($CDCl_3$, δ) 167.36, 166.16, 136.01, 131.35, 131.01, 128.29, 128.01, 126.09, 125.74, 63.88, 63.70, 62.36, 62.18, 18.32 in Figure A.16.

6.2.6. Fabrication of PDS-PEG-MA Functionalized Cryogels

For production of PEG-PDS-MA cryogel (30% reactive monomer), a classic method is followed. PEGMEMA (55.14 mg, 0.183 mmol), poly(ethylene glycol) dimethacrylate (144.42 mg, 0.262 mmol), PEG-PDS-MA monomer (50.00 mg, 0.078 mmol), and DMPA (3.36 mg,0.013 mmol) 1,4-dioxane (1.8 mL) were placed into glass vial and sonicated for 1 minute to provide a homogeneous transparent solution. The reaction vessel containing (0.6 mL) was then placed in a cryostat at -13 °C and treated to UV light (365 nm) from 15 cm away (1 h). After gelation procedure, cryogels were cleaned with ethanol in order to remove unreacted substances and rinsed carefully washed with water and dried under vacuum. The same procedure was applied to obtain 20% and 10% reactive monomer containing cryogel.

6.2.7. Fabrication of Control Cryogel

Control cryogels were fabricated in a parallel method as overhead without using reactive monomer.

6.2.8. Water up taking of Cryogels

Swelling measurements were carry out by taking certain amount of cryogel in a vessel having distilled water at ambient temperature. At predetermined intervals the change in mass of the cryogel samples were recorded up to the point where the mass of the cryogel no longer changed. The percentage weight variation was calculated from fractional weight change using the simple equation as

Percentage of Swelling (%) = $(W_{wet} - W_{dry}) / W_{dry} \times 100$,

where W_{wet} and W_{dry} refer to the weight of wet and dry cryogels respectively.

6.2.9. Pyridothione Release Studies

The cryogels sample were placed into a DTT solution (3 mL, 10 mM in PBS) in vial and incubated at 37 °C. At predetermined time points, 0.3 mL samples were taken from the solution and replaced with the same amount of fresh DTT solution. UV−vis spectrum of the solution was note down to decide the absorbance at 343 nm, fitting to the free pyridothione fragment. The total pyridothione amount was calculated on the basis of the molar extinction coefficient of pyridothione, and the percent release was obtained using the equation below as

n_{rel} (%) = $(n_{act}/n_{theo}) \times 100$,

where n_{rel}, n_{act}, and n_{theo} represent the released, actual, and theoretical molar amounts of pyridothione.

6.2.10. Scanning Electron Microscopy (SEM)

The morphology of dried cryogels were characterized with scanning electron microscopy (SEM) using an ESEM-FEG/EDAX Philips XL-30 (Philips, Eindhoven, The Netherlands) instrument with an accelerating voltage of 10 kV.

6.2.11. Direct immobilization of BODIPY-SH

Different mol ratio pyridyl disulfide reactive group containing cryogel samples were immersed in BODIPY-SH (the stoichiometric ratio of pyridyl disulfide to thiol was 1:1.1) solution in DMF and catalytic amount of acetic acid was added over the reaction solution at room temperature. After 18 hours, gels were washed using DMF several times to remove unreacted. As a control experiment, cryogel preparing without reactive monomer was treated with a solution containing BODIPY-SH and acetic acid with the same approach. All cryogels were analyzed using fluorescence microscopy for evaluating dye attachment.

6.2.12. Catch and Release of Streptavidin onto the Biotinylated

Cryogels. Pyridyl disulfide containing cryogels were treated with Biotin-SH (1mg/mL) in MeOH/THF (1:1) containing trace amount of acetic acid for 18 hours at room temperature. Afterwards, the gels were washed several times with the identical solvent to get rid of unbounded Biotin-SH. Swollen biotinylated cryogels was treated with a solution of TRITC−streptavidin (1 μg/mL in PBS) for 20 min. Fluorescence microscopy was used to examine protein-immobilized cryogels that had been extensively washed with PBS. To demonstrate the least amount of nonspecific interactions with the cryogel, a cryogel without a biotin attachment was employed as a reference. Cryogels incubated with DTT solution (10mM, 3mL) at room temperature for 3 hours to release streptavidin. Cryogels samples were visualized using fluorescence microscopy after and before DTT treatment. Cryogels samples were visualized using fluorescence microscopy after and before DTT treatment.

6.2.13. Immobilization ConA from Lectins Mixture.

Cryogels containing pyridyl disulfide were treated with a mixture of mannose-SH in methanol. Pyridyl disulfide to thiol has a stoichiometric ratio of 1:1.1.After allowing the gels and mannose to react overnight, they were carefully cleaned with methanol and distilled water before proceeding to the following stage. The mannose decorated cryogels were incubated in a solution that contains 0.05 mg/mL of FITC-ConA and rhodamine-PNA in

HEPES buffer (20mM, pH: 7.4) for 20 minutes before being completely washed with HEPES buffer. Cryogels incubated with DTT solution (10 mM, 3 mL) at room temperature for 3 hours to release FITC-ConA.

6.2.14. Cellular Attachment on Cryogel

L929 mouse fibroblast cells were used for cell attachment experiment and cells were grown under a 5% CO_2 containing atmosphere at 37 °C and cultured in Dulbecco's Modified Eagle's Medium (DMEM) supplemented with 10% fetal bovine serum (FBS). Before cell seeding, control cryogels, 20% PDS containing cryogels, mercaptoethanol-conjugated cryogels and linear RGD-conjugated cryogels (round disk around 2.5 cm^2) were incubated in DMEM for 2 hours to allow swelling. At the end of 2 hours, L929 cells (100 000 cells per 100 µL) were seeded onto cryogel samples and they were incubated at 37 ^oC under 5% CO_2 atmosphere for 1 h. After that, the cell medium (3 mL) was added to each well containing cryogels. At the end of 24 hours incubation, the cell medium was removed and cryogels were washed with 1 x PBS (1 mL, 3 times) and the cells were fixed by using 3.7 % formaldehyde solution at 37 ^oC for 10 min. After fixation, the cells were washed with 1 x PBS (1 mL x 2 times). For F-actins staining, the cells were treated with 0.1% Triton X-100 in PBS for 5 min. After washing with 1 x PBS (1 mL, 2 times), the cells were incubated with Alexa Fluor 488 phalloidin solution (5 units/mL) in 1 x PBS solution including 1% BSA for 20 min at 37 ^oC. After washing with PBS (1 mL, 3 times), cell nuclei were stained by DAPI for 15 min at 37 ^oC. After washing the cells, cell images were taken using Zeiss Observer Z1 fluorescence microscope and processed with Zeiss Zen Blue lite software.

6.3. Results and Discussion

6.3.1. Fabrication, Characterization, and Functionalization of Pyridyl Disulfide Containing Cryogels

Macroporous cryogels containing pyridyl disulfide reactive groups in different molar ratios were successfully fabricated using photo-polymerization in Figure 5.1a. Firstly, to

synthesize the pyridyl disulfide containing PEG-based methacrylate (PDS-PEG-MA) monomer, pyridyl disulfide ethylamine (PDS-NH_2) was obtained according to literature protocol.27 The PDS-amine was attached to a PEG-based 2-(acryloyloxy) ethyl methacrylate (PEG-AC-MA) in the presence of an organic base trimethylamine to yield PDS-PEG-MA monomer in good yield (82%). The purity of the PDS-PEG-MA monomer was confirmed evaluated ^{1}H NMR in Figure 6.1a and in addition to this ^{13}C NMR in Figure A.16. The characteristic peaks of pyridyl group were clearly observed in the ^{1}H NMR spectra of monomer at 8.47, 7.77 – 7.56 and 7.10 ppm, along with the peaks conforming to the vinyl protons on the methacrylate unit at 6.13 and 5.57 ppm in Figure 6.1b.

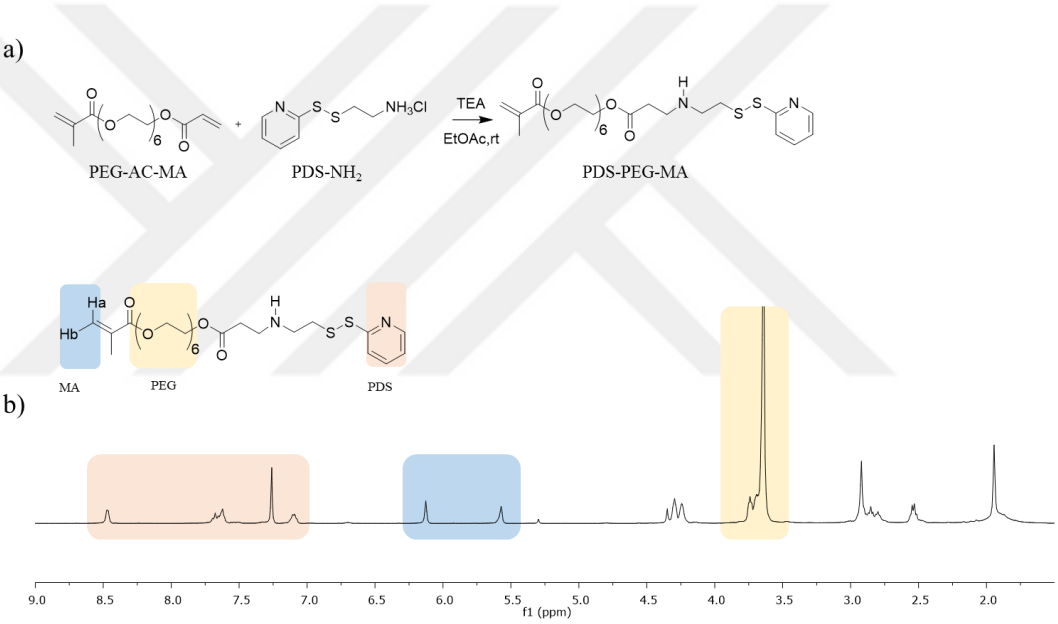

Figure 6.1. (a) Synthesis of PDS-containing monomer, and (b) ^{1}H NMR spectrum of PDS-PEG-MA.

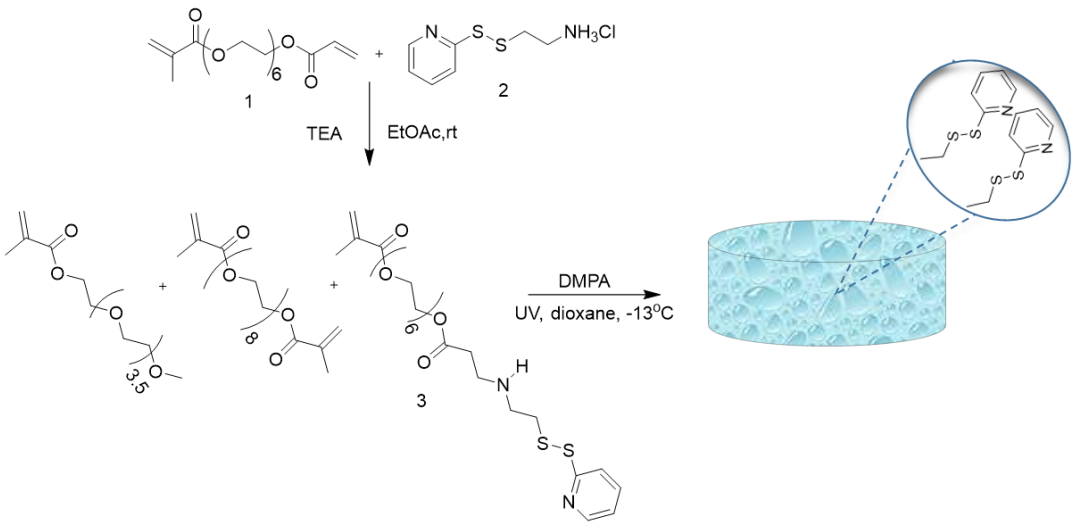

Figure 6.2. Synthesis PDS-PEG-MA monomer and fabrication of PDS-PEG-MA containing cryogels.

PEG-based pyridyl disulfide monomer PDS-PEG-MA and PEGMEMA (Mn = 300 g mol^{-1}) were utilized in the cross-linking process in the presence of the PEGDMA crosslinker and DMPA as a photoinitiator in Figure 6.2. Cryogels CG-CTRL, CG-PDS-PEGMA-10, CG-PDS-PEGMA-20, CG-PDS-PEGMA-30 containing 0, 10, 20, and 30 mol %, respectively were produced with high conversions (84-98%). After washing the cryogels with copious amounts of THF and water, samples were lyophilized to obtain them in dry form. To ascertain the quantity of the thiol-reactive PDS-disulfide groups, samples were treated with DTT (10 mM). Upon reaction with DTT, the disulfide group is cleaved to release a pyridothione fragment, which has a characteristic absorbance (343 nm in PBS).

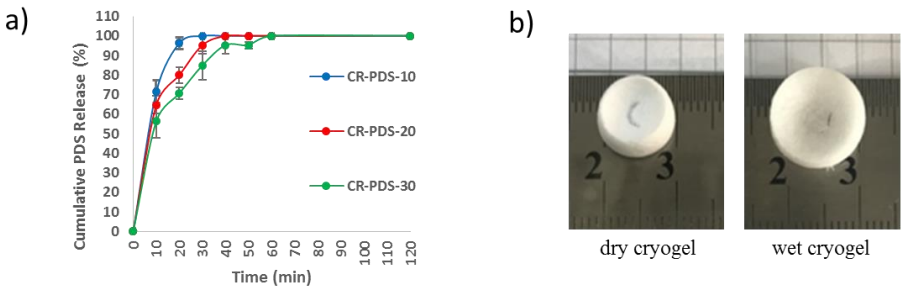

Figure 6.3. (a) Pyridothione release profiles from cryogels, and (b) photographs of the top views of dry, and wet cryogels.

The total amount of released pyridothione was calculated on the basis of the molar extinction coefficient of pyridothione (8080 $M^{-1}cm^{-1}$ in PBS) [128]. It was concluded that the incorporation of the PDS monomer in the cryogels was similar to the feed composition in Table 6.1. This indicated that the PDS groups did not undergo any decomposition during the cryogenic photo-polymerization. Additionally, the release of the pyridothione group was quite fast, with quantitative release observed with an hour, while the change in the amount of the PDS monomer within the gels had only a slight effect on their release profile in Figure 6.3a. The fast release observed for the cryogels are presumably due to their rapid and high swelling in aqueous media in Figure 6.3b, which allows the reducing agent to rapidly permeate through the gel scaffold.

Table 6.1. Conformation of cryogels with changing quantities of pyridyl disulfide monomer.

Cryogel	**[PDS-PEG-MA] :[PEGMEMA] Feed Ratio Mol %**	**[PDS-PEG-MA] :[PEGMEMA] Obtained Ratio Mol %**	**Gel Content %**	**Swelling %**
CG-C	0:100	0:100	95	916±30
CG-PDS-10	10:90	9:91	88	733±40
CG-PDS-20	20:80	22:88	84	640+29
CG-PDS-30	30:70	31:69	91	446±30

Morphology of obtained cryogels were analyzed using SEM analysis in Figure 6.4 and Figure A.17. Upon immersion in aqueous media, the cryogels underwent rapid swelling and reached equilibrium swelling capacity within a few minutes in Figure A.18. The final equilibrium swelling of the cryogels was found to be dependent on the amount of PDS-monomer incorporated into the matrix in Figure 6.4d. After 1 minute, the swelling ratio of CG-PDS-PEGMA-10 was 916 percent, whereas the swelling ratios of CG-PDS-PEGMA-20 and CG-PDS-PEGMA-30 were 733 percent and 446 percent, respectively. The macroporous morphology and high swelling capacity is quite different from what was observed for a conventional hydrogel with similar composition, where hydrogels were predominantly non-porous and had lower water uptake.

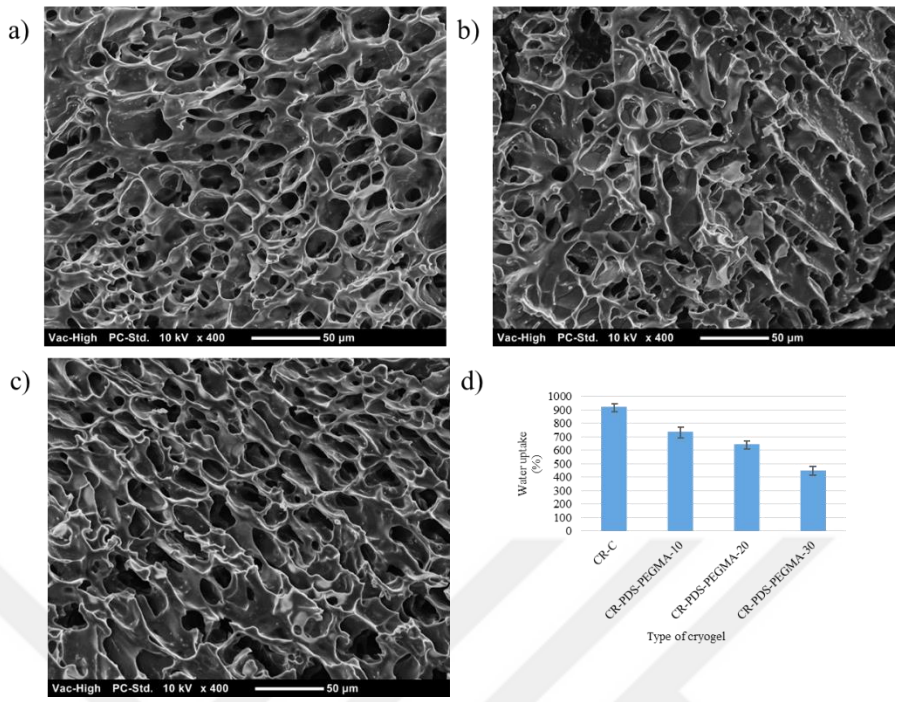

Figure 6.4. Scanning electron micrographs of cryogels synthesized using (a) 10% (b) 20% (c) 30% PDS (scale bar is 50 µm), and (d) graphical representation of the equilibrium swelling values of cryogels.

6.3.2. Direct immobilization of BODIPY-SH

Thiol-reactive cryogels were functionalized with a thiol-containing fluorescent dye, BODIPY-SH. All cryogels were treated with BODIPY-SH and the mole ratio of pyridyl disulfide to thiol was adjusted to 1:1.1. For the dye conjugation, a control gel (CG-CTRL) without reactive monomer and gels with a gradually increasing amount of the reactive monomer were used. As expected, fluorescence microscopy analysis revealed that gels devoid of the reactive PDS monomer did not show any noticeable fluorescence (Figure 6.5a). On the other hand, the gels containing the PDS group exhibited high fluorescence, which was consistent with the increase in the amount of the reactive monomer (Figure 6.5b, c, d). All samples were sonicated using fresh solvent to remove the dye was physically trapped in the gel network before the fluorescence image was taken. The amount of dye for the control gel was adjusted as in the sample containing the most reactive monomer. These results show

that we can adjust the amount of dye to be immobilized on the gels by changing the reactive monomer ratio in Figure 6.5d.

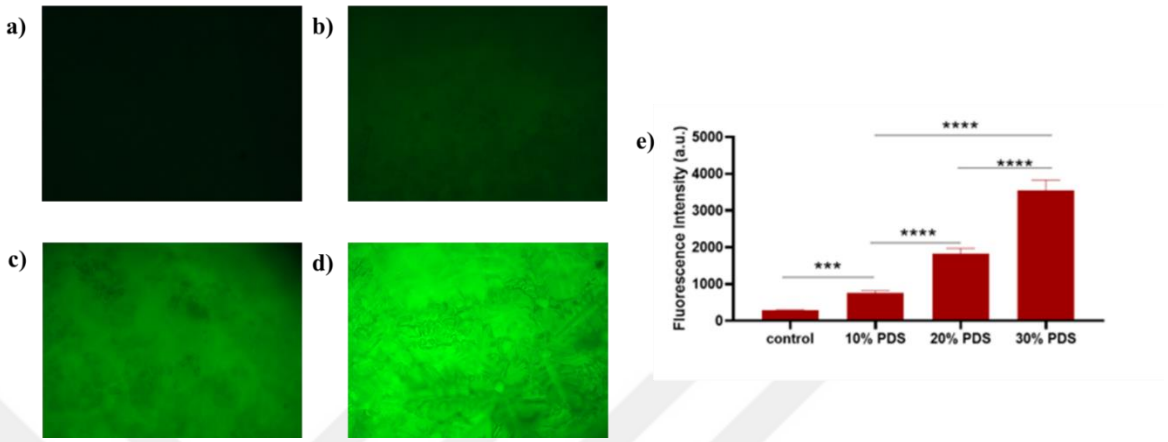

Figure 6.5. (a.b,c,d) Fluorescence microscopy images of the BODIPY-SH-immobilized cryogels and (e) the cryogels' relative fluorescence intensities after being functionalized with BODIPY-SH.

6.3.3. Catch and Release of Streptavidin onto the Biotinylated Cryogels

There is a well-known strong non-covalent interactions between biotin and streptavidin. Streptavidin is widely used in molecular biology because, apart from its exceptional affinity for biotin, extreme pH, temperature and organic solvents do not affect the binding of this protein to biotin [138]. In order to immobilize streptavidin on the gels, firstly, the gels were treated with Biotin-SH. Biotinylated cryogels were incubated in a PBS solution containing TRITC-streptavidin for 20 minutes, then extensively washed with PBS to remove unbound protein. Likewise, as a control experiment, cryogels devoid of any PDS groups were also treated with a dye-labeled protein solution, and washed to remove any unbound protein [139, 140]. As expected, fluorescence microscopy analysis revealed that while negligible protein attachment was observed in the gels that did not bind Biotin-SH, as the control did not contain reactive monomers in Figure 6.6a. On the other hand, the increase in the amount of PDS-based monomer significantly increased the fluorescence intensity in Figure 6.6b, c, d. The fluorescence results show that protein immobilization can be tuned during the construction of gels by using different amounts of reactive monomer.

Fluorescence microscopy analysis revealed that there was a significant reduction in the intensity of red fluorescence in cryogels treated with DTT, suggesting the release of streptavidin in Figure A.19.

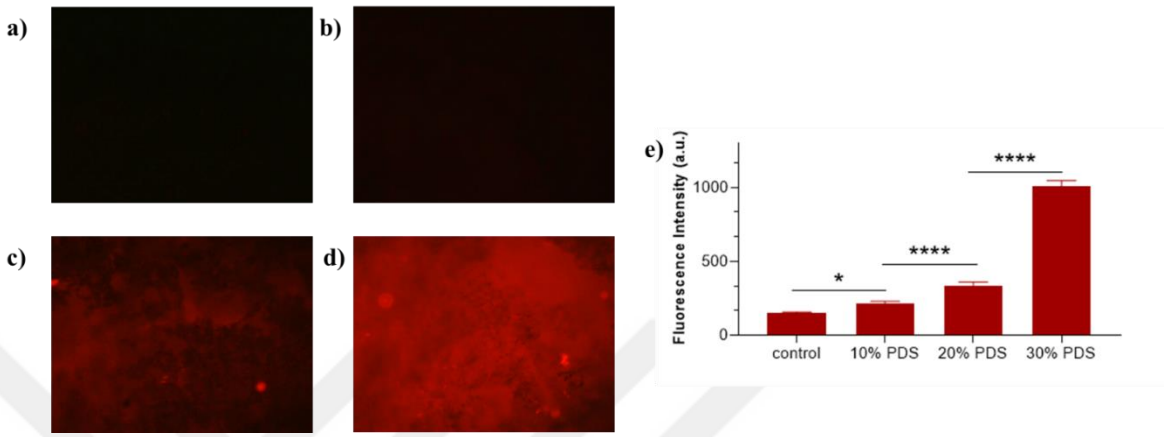

Figure 6.6. (a,b,c,d) TRITC-Streptavidin immobilized cryogels fluorescence microscopy pictures, and (e) Fluorescence intensity intensities of cryogels upon protein attachment

6.3.4. Immobilization ConA from Lectin mixture.

Lectins are glycoproteins that play an important role in biological recognition phenomena involving cells, carbohydrates , proteins and thus various strategies to detect as well as purify lectins have been developed [141]. Various sugar-based ligands are known to interact specifically with certain lectins, and thus have been widely conjugated to various interfaces. To evaluate the efficiency of the PDS-containing cryogels toward lectin immobilization, cryogels were decorated with mannose-SH, and exposed to a mixture of fluorescent dye-labeled proteins [142]. In particular, the mannose conjugated gels were immersed into a HEPES buffer solution containing a mixture of FITC-ConA and TRITC-PNA. Thereafter, protein attachment onto the cryogels was analyzed using fluorescence microscopy. After treatment with protein mixture containing solution and before any subsequent washing, presence of both green and fluorescence indicated that both FITC-ConA and TRITC-PNA were present in the gels in Figure 6.7a, but upon subsequent washing to remove unbound protein, gels exhibited only green fluorescence This suggests that

mannose conjugated cryogels were able to selectively retain the targeted protein ConA in Figure 6.7b.

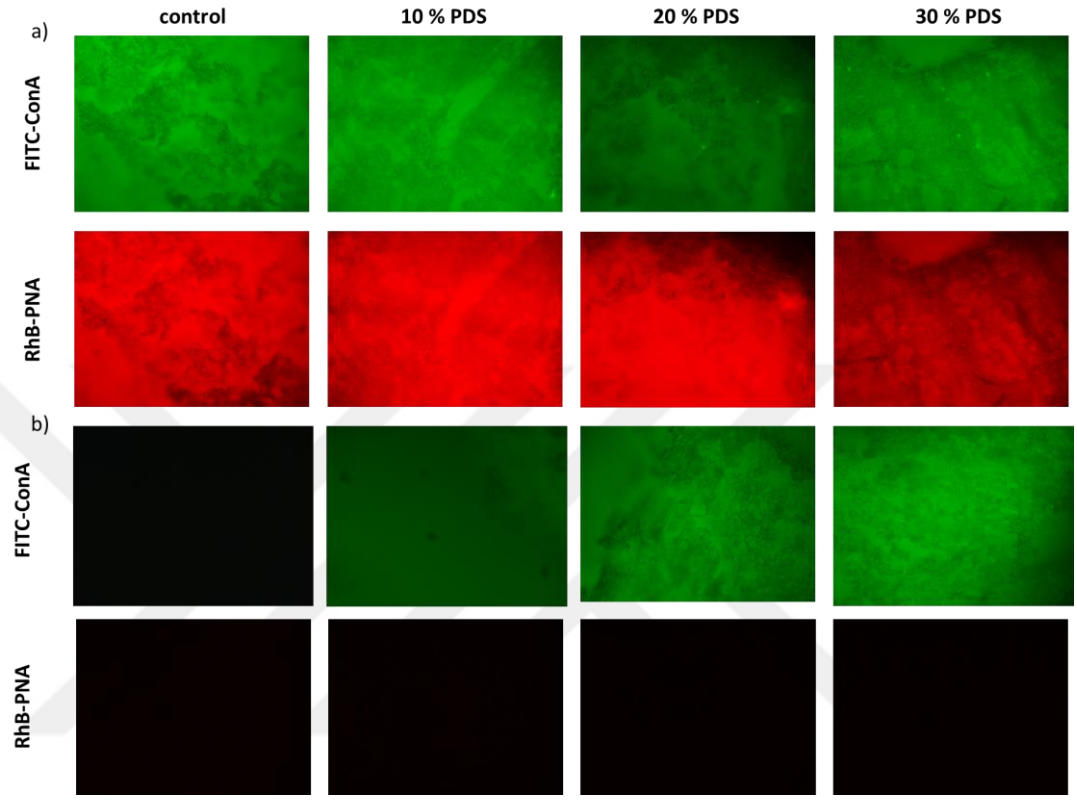

Figure 6.7. Fluorescence microscopy images of ConA and TRITC-PNA immobilized cryogels (a) before washing (b) after washing.

6.3.5. Cytotoxicity and RGD-based Cell Attachment

The survivability and proliferation of cells enclosed inside gel-based 3D scaffolds are critical measurements [143]. To increase the attachment of L929 fibroblast cells, the CG slides were treated with a thiol-containing ligand binding peptide (RGD-SH) in Figure 6.8. The actin cytoskeleton of these L929 fibroblast cells was detected with Alexa Fluor 488, and the nuclei was labeled with DAPI reagent. The first group is the control group without reactive monomer. When incubated with this group of cells, it was observed that no cells were attached. Cells did not adhere or spread on the normally bioinert surface without the addition of the cell-adhesive peptide to the cryogel. CGs containing active monomer and

mercaptoethanol-treated gels did not show significant cell attachment, as was the case with the control CGs. Through the non-cleavable disulfide bond, L929 fibroblast cells were grown on an RGD-SH connected cryogel and observed by fluorescence microscopy. Cells attached homogeneously and uniformly to the cryogel treated with RGD, growing across the full surface of the scaffold.

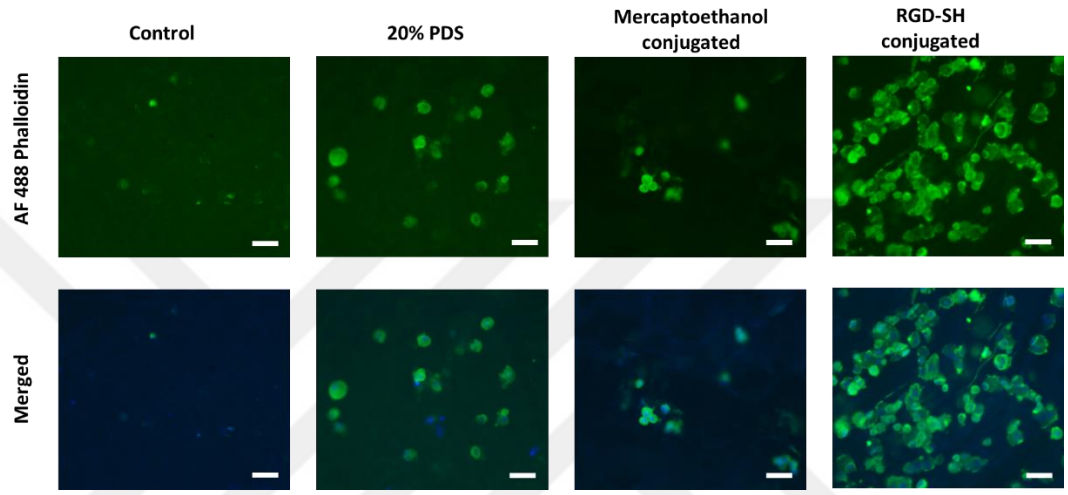

Figure 6.8. Images of cells trapped on the RGD-attached cryogel layer captured with fluorescence microscopy. After detachment, merged fluorescence microscopy pictures indicate viable (green) cells.

This is expected because the cell adhesion peptide is bound to the CG via a covalent disulfide bond in these CG. The ability of this platform to adapt to potential applications depends on cell survival following separation. The versatility of this platform to adapt to potential applications depends on cell survival following separation. Surface-detached cells were placed in a well plate and stained with an alexafluor488 to see if this was true. The majority of detached cells were alive following detachment from the surface, according to combined fluorescence microscopy images.

6.4. Conclusion

Fabrication of a new catch-and-release cryogel platform demonstrated based on the thiol-disulfide exchange reaction. Poly(ethylene glycol)-based cryogels containing thiol-reactive functional groups was synthesized using photo-polymerization method. The macroporous structure has given gels an incredible ability to swell water and also release profile. Equilibrium swelling in water, morphology, immobilization capacity and release profile adjusted changing reactive monomer.

Cryogels were also functionalized effectively with bodipy-thiol and mannose thiol, resulting in the immobilization of the proteins TRITC-Streptavidin and Concanavalin A, as well as the release of immobilized protein after DTT treatment. Mannose-thiol conjugated cryogels were assessed for selective binding toward ConA. Both separation and purification of ConA from a mixture of ConA and PNA, cryogels functionalized with mannose were utilized. Overall, novel thiol-reactive macroporous cryogel constructs will be used charming platform for various biomedical applications.

7. CONCLUSION

This thesis focused on the design, synthesis, and applications of stimuli-responsive biomaterials. The methods outlined here yield materials that can find possible applications in drug delivery, biosensing and tissue engineering.

In the first chapter, dendron-polymer conjugate-based self-assembled nano-sized aggregates are fabricated as drug-delivery systems to address diseases like cancer. In particular, an orthogonally reactive hydrophobic biodegradable polyester dendron was clicked together with an azide-terminated copolymer containing amine-reactive monomers to create a dendron-polymer conjugate. The targeting unit containing (cRGDfK) the amine group was successfully attached to the side chain of the polymer. A core-crosslinking strategy was applied to provide stability to the obtained micellar aggregates. For this purpose, a radical thiol-ene reaction was utilized. It was established that such a core crosslinking strategy increases the stability of aggregates against high dilution. It was also observed that apart from increasing the stability, crosslinking also enables a more controlled drug release by reducing the passive release in the absence of any stimuli. In addition to all these, it was observed that the micellar structures carrying the targeting group demonstrated higher internalization into the MDA-MB-231 breast cancer cells.

The second chapter is related to the construction of micellar structures based on redox-responsive dendron-polymer conjugates as controlled drug delivery vehicles. The construct consists of a hydrophobic biodegradable dendron conjugated to a linear PEG-based polymer through a disulfide linkage. In particular, a thiol-disulfide exchange reaction was utilized to synthesize these redox-responsive diblock copolymers. The same reaction was used to obtain a dendron-polymer conjugate that could be functionalized with a peptide-based targeting group. While the micellar aggregates obtained using the DPCs comprised of the third-generation dendrons were not stable against dilution, the aggregates prepared using the fourth-generation dendrons were resistant to dilution and possessed a higher drug loading capacity. In addition, it was observed that the structure carrying the targeting group showed faster and higher internalization than the structures devoid of targeting groups. When the

durability and drug release of the micellar aggregates were tested in neutral and GSH-containing environments, it was observed that both drug release and cytotoxicity were higher in a GSH-rich environment, which is in abundance in cancerous cells.

In the third chapter, a dendron-polymer conjugate with architecture different than the one utilized in the first two chapters was evaluated for obtaining micellar aggregates. In this study, 1st, 2nd and 3rd generation dendrons were connected to the side branches of the polymer chain through disulfide linkages. Attaching dendrons as side groups enabled the structure to be equipped with more dendrons than a linear polymer dendron conjugate. The self-assembly of thus synthesized structures was examined, and their degradation and drug release behavior was investigated in a reducing environment at various pH values for drug delivery investigations. While the nano-sized aggregates prepared with 3rd generation dendrons had a higher drug loading capacity, they were also more stable upon dilution. Encapsulation and efficient transport of hydrophobic agents using these micellar constructs into cells were achieved. Notably, a higher cytotoxic behavior was observed for drug-loaded aggregates upon internalization by GSH-enriched cells. This preliminary investigation using the utilization of a dendron-polymer conjugate with a different architecture offers an alternative platform for drug delivery.

Unlike the previous ones, the last chapter focuses on the design, synthesis, and application of a different biomaterial, namely cryogel. A photo-polymerization approach was used to make poly(ethylene glycol)-based cryogels containing a new disulfide-based thiol-reactive unit. Obtained gels possessed an exceptional ability to swell due to their macroporous structure. Changing the reactive monomer ratio is straightforward for adjusting equilibrium swelling in water, immobilization capability, and controlled release. Attachment and release of various thiol-containing dyes and bioactive ligands were demonstrated. These scaffolds were also amenable to facile functionalization with specific sugar molecules for immobilization and sensing of target lectins. Finally, it was demonstrated that cell-adhesive peptides could be conjugated to these other anti-biofouling polymeric gels to promote cellular attachment onto these scaffolds.

REFERENCES

1. Liu, D., F. Yang, F. Xiong, and N. Gu, "The Smart Drug Delivery System and Its Clinical Potential", *Theranostics*, Vol. 6, No. 9. pp. 1306–1323, 2016.

2. Plieva, F. M., M. Karlsson, M. R. Aguilar, D. Gomez, S. Mikhalovsky, and I. Y. Galaev', "Pore Structure in Supermacroporous Polyacrylamide Based Cryogels", *Soft Matter*, Vol. 1, No. 4, pp. 303–309, 2005.

3. Fathi, M., P. S. Zangabad, A. Aghanejad, J. Barar, H. Erfan-Niya, and Y. Omidi, "Folate-Conjugated Thermosensitive O-Maleoyl Modified Chitosan Micellar Nanoparticles for Targeted Delivery of Erlotinib", *Carbohydrate Polymers*, Vol. 172, pp. 130–141, 2017.

4. Turabee, M. H., T. H. Jeong, P. Ramalingam, J. H. Kang, and Y. T. Ko, "N,N,N-Trimethyl Chitosan Embedded in Situ Pluronic F127 Hydrogel for The Treatment of Brain Tumor", *Carbohydrate Polymers*, Vol. 203, pp. 302–309, 2019.

5. Altinbasak, I., M. Arslan, R. Sanyal, and A. Sanyal, "Pyridyl Disulfide-Based Thiol-Disulfide Exchange Reaction: Shaping The Design of Redox-Responsive Polymeric Materials", *Polymer Chemistry*, Vol. 11, No. 48, pp. 7603–7624, 2020.

6. Zhuang, J., B. Zhao, and S. Thayumanavan, "Cascaded Step-Growth Polymerization for Functional Polyamides with Diverse Architectures and Stimuli Responsive Characteristics", *ACS Macro Letters*, Vol. 8, No. 3, pp. 245–249, 2019.

7. Remya, R. R., A. Julius, T. Y. Suman, V. Mohanavel, A. Karthick, C. Pazhanimuthu, A. V. Samrot, and M. Muhibbullah, "Role of Nanoparticles in Biodegradation and Their Importance in Environmental and Biomedical Applications", *Journal of Nanomaterials*, Vol. 2022, No. 2, pp. 1–15, 2022.

8. Zhang, M. and J. P. Matinlinna, "E-Glass Fiber Reinforced Composites in Dental Applications", *Silicon*, Vol. 4, No. 1, pp. 73–78, 2012.

9. Samal, S. K., M. Dash, S. Van Vlierberghe, D. L. Kaplan, E. Chiellini, C. van Blitterswijk, L. Moroni, and P. Dubruel, "Cationic Polymers and Their Therapeutic Potential", *Chemical Society Reviews*, Vol. 41, No. 21, pp. 7147–94, 2012.

10. Chiara, G., F. Letizia, F. Lorenzo, S. Edoardo, S. Diego, S. Stefano, B. Eriberto, and Z. Barbara, "Nanostructured Biomaterials for Tissue Engineered Bone Tissue Reconstruction", *International Journal of Molecular Sciences*, Vol. 13, No. 1, pp. 737–757, 2012.

11. Gao, H., A. Miasnikova, and K. Matyjaszewski, "Effect Of Cross-Linker Reactivity on Experimental Gel Points During Atrcp of Monomer And Cross-Linker", *Macromolecules*, Vol. 41, No. 21, pp. 7843–7849, 2008.

12. Lin, C. C. and K. S. Anseth, "Controlling Affinity Binding with Peptide-Functionalized Poly(Ethylene Glycol) Hydrogels", *Advanced Functional Materials*, Vol. 19, No. 14, pp. 2325–2331, 2009.

13. Attia, M. F., N. Anton, J. Wallyn, Z. Omran, and T. F. Vandamme, "An Overview of Active and Passive Targeting Strategies to Improve The Nanocarriers Efficiency to Tumour Sites", *Journal of Pharmacy and Pharmacology*, Vol. 71, No. 8, pp. 1185–1198, 2019.

14. Mura, S. and P. Couvreur, "Nanotheranostics for Personalized Medicine", *Advanced Drug Delivery Reviews*, Vol. 64, No. 13, pp. 1394–1416, 2012.

15. Tang, Z., C. He, H. Tian, J. Ding, B. S. Hsiao, B. Chu, and X. Chen, "Progress in Polymer Science Polymeric Nanostructured Materials for Biomedical Applications", *Progress in Polymer Science*, Vol. 60, pp. 86–128, 2016.

16. Ingavle, G. C., L. W. J. Baillie, Y. Zheng, E. K. Lis, I. N. Savina, C. A. Howell, S. V. Mikhalovsky, and S. R. Sandeman, "Affinity Binding of Antibodies to Supermacroporous Cryogel Adsorbents with Immobilized Protein A for Removal of Anthrax Toxin Protective Antigen", *Biomaterials*, Vol. 50, No. 1, pp. 140–153, 2015.

17. Eggermont, L. J., Z. J. Rogers, T. Colombani, A. Memic, and S. A. Bencherif, "Injectable Cryogels for Biomedical Applications", *Trends in Biotechnology*, Vol. 38, No. 4, pp. 418–431, 2020.

18. Savina, I. N., V. Cnudde, S. D'Hollander, L. Van Hoorebeke, B. Mattiasson, I. Y. Galaev, and F. Du Prez, "Cryogels From Poly(2-Hydroxyethyl Methacrylate): Macroporous, Interconnected Materials with Potential As Cell Scaffolds", *Soft Matter*, Vol. 3, No. 9, pp. 1176–1184, 2007.

19. Perçin, I., R. Khalaf, B. Brand, M. Morbidelli, and O. Gezici, "Strong Cation-Exchange Chromatography of Proteins on A Sulfoalkylated Monolithic Cryogel", J*ournal of Chromatography A*, Vol. 1386, pp. 13–21, 2015.

20. Lu, S., J. Lam, J. E. Trachtenberg, E. J. Lee, H. Seyednejad, J. J. J. P. van den Beucken, Y. Tabata, M. E. Wong, J. A. Jansen, A. G. Mikos, and F. K. Kasper, "Dual Growth Factor Delivery from Bilayered, Biodegradable Hydrogel Composites for Spatially-Guided Osteochondral Tissue Repair", *Biomaterials*, Vol. 35, No. 31, pp. 8829–8839, 2014.

21. Zhang, J., Y. Lin, Z. Lin, Q. Wei, J. Qian, R. Ruan, X. Jiang, L. Hou, J. Song, J. Ding, and H. Yang, "Stimuli-Responsive Nanoparticles for Controlled Drug Delivery in Synergistic Cancer Immunotherapy", *Advanced Science*, Vol. 9, No. 5, pp. 1–27, 2022.

22. Xu, X.-D., Y.-J. Cheng, J. Wu, H. Cheng, S.-X. Cheng, R.-X. Zhuo, and X.-Z. Zhang, "Smart And Hyper-Fast Responsive Polyprodrug Nanoplatform for Targeted Cancer Therapy", *Biomaterials*, Vol. 76, pp. 238–249, 2016.

23. Gillies, E. R., T. B. Jonsson, and J. M. J. Fréchet, "Stimuli-Responsive Supramolecular Assemblies of Linear-Dendritic Copolymers", *Journal of the American Chemical Society*, Vol. 126, No. 38, pp. 11936–11943, 2004.

24. Gu, H., S. Mu, G. Qiu, X. Liu, L. Zhang, Y. Yuan, and D. Astruc, "Redox-Stimuli-Responsive Drug Delivery Systems with Supramolecular Ferrocenyl-Containing Polymers for Controlled Release", *Coordination Chemistry Reviews*, Vol. 364, No. 364, pp. 51–85, 2018.

25. Ferguson, J. E. and A. D. Redish, "Wireless Communication With Implanted Medical Devices Using the Conductive Properties of The Body", *Expert Review of Medical Devices*, Vol. 8, No. 4, pp. 427–433, 2011.

26. Hirabayashi, H. and J. Fujisaki, "Bone-Specific Drug Delivery Systems", *Clinical Pharmacokinetics*, Vol. 42, No. 15, pp. 1319–1330, 2003.

27. Wang, D., S. Miller, M. Sima, P. Kopečková, and J. Kopeček, "Synthesis and Evaluation of Water-Soluble Polymeric Bone-Targeted Drug Delivery Systems", *Bioconjugate Chemistry*, Vol. 14, No. 5, pp. 853–859, 2003.

28. Carter, T., P. Mulholland, and K. Chester, "Antibody-Targeted Nanoparticles for Cancer Treatment", *Immunotherapy*, Vol. 8, No. 8, pp. 941–958, 2016.

29. Kaushik, N., S. B. Borkar, S. K. Nandanwar, P. K. Panda, E. H. Choi, and N. K. Kaushik, "Nanocarrier Cancer Therapeutics with Functional Stimuli-Responsive Mechanisms", *Journal of Nanobiotechnology*, Vol. 20, No. 1, pp. 1–23, 2022.

30. Zhang, X., K. Achazi, and R. Haag, "Boronate Cross-linked ATP- and pH-Responsive Nanogels for Intracellular Delivery of Anticancer Drugs", *Advanced Healthcare Materials*, Vol. 4, No. 4, pp. 585–592, 2015.

31. Gan, Q., J. Zhu, Y. Yuan, H. Liu, J. Qian, Y. Li, and C. Liu, "A Dual-Delivery System of pH-Responsive Chitosan-Functionalized Mesoporous Silica Nanoparticles Bearing BMP-2 and Dexamethasone for Enhanced Bone Regeneration", *Journal of Materials Chemistry B*, Vol. 3, No. 10, pp. 2056–2066, 2015.

32. Bazban-Shotorbani, S., M. M. Hasani-Sadrabadi, A. Karkhaneh, V. Serpooshan, K. I. Jacob, A. Moshaverinia, and M. Mahmoudi, "Revisiting Structure-Property Relationship of pH-Responsive Polymers for Drug Delivery Applications", *Journal. of Controlled Release*, Vol. 253, pp. 46–63, 2017.

33. Ke, X., D. J. Coady, C. Yang, A. C. Engler, J. L. Hedrick, and Y. Y. Yang, "pH-Sensitive Polycarbonate Micelles for Enhanced Intracellular Release of Anticancer Drugs: A Strategy to Circumvent Multidrug Resistance", *Polymer Chemistry*, Vol. 5, No. 7, pp. 2621–2628, 2014.

34. Huang, H., J. Geng, J. Golzarian, J. Huang, and J. Yu, "Colloids and Surfaces B : Biointerfaces Fabrication of Doxorubicin-Loaded Ellipsoid Micelle Based on Diblock Copolymer With A Linkage of Enzyme-Cleavable Peptide", *Colloids Surfaces B Biointerfaces*, Vol. 133, pp. 362–369, 2015.

35. Ma, G., C. Zhang, L. Zhang, H. Sun, and C. Song, "Doxorubicin-Loaded Micelles Based on Multiarm Star-Shaped PLGA – PEG Block Copolymers : Influence of Arm Numbers On Drug Delivery", *Journal of Materials Science: Materials in Medicine*, Vol. 27, No. 1, pp. 1–15, 2016.

36. Gökçe, B. B., T. Boran, F. Emlik Çalık, G. Özhan, R. Sanyal, and S. Güngör, "Dermal Delivery and Follicular Targeting of Adapalene Using PAMAM Dendrimers", *Drug Delivery and Translational Research*, Vol. 11, No. 2, pp. 626–646, 2021.

37. Kesharwani, P., R. K. Tekade, and N. K. Jain, "Generation Dependent Cancer Targeting Potential of Poly(Propyleneimine) Dendrimer", *Biomaterials*, Vol. 35, No. 21, pp. 5539–48, 2014.

38. Shiba, H., M. Nishio, M. Sawada, M. Tamaki, M. Michigami, S. Nakai, I. Nakase, I. Fujii, A. Matsumoto, and C. Kojima, "Carboxy-Terminal Dendrimers with Phenylalanine For A pH-Sensitive Delivery System Into Immune Cells Including T Cells", *Journal of Materials Chemistry B*, Vol. 10, No. 14, pp. 2463–2470, 2022.

39. Li, Z., J. Huang, and J. Wu, "pH-Sensitive Nanogels for Drug Delivery in Cancer Therapy", *Biomaterials Science*, Vol. 9, No. 3, pp. 574–589, 2021.

40. Niroumandi, S., M. Shojaeifard, and M. Baghani, "On Single and Multiple pH-Sensitive Hydrogel Micro-valves: A 3D Transient Fully Coupled Fluid–Solid Interaction Study", *Transport in Porous Media*, Vol. 142, No. 1, pp. 295–316, 2021.

41. Liu, J., D. Obando, V. Liao, T. Lifa, and R. Codd, "The Many Faces of the Adamantyl Group in Drug Design", *European Journal of Medicinal Chemistry*, Vol. 46, No. 6, pp. 1949–1963, 2011.

42. Nagaiah, G. and S. C. Remick, "Combretastatin A4 phosphate: A Novel Vascular Disrupting Agent", *Future Oncology*, Vol. 6, No. 8, pp. 1219–1228, 2010.

43. De Gaetano Donati, K., R. Rabagliati, L. Iacoviello, and R. Cauda, "HIV Infection, HAART, and Endothelial Adhesion Molecules: Current Perspectives", *Lancet Infectious Diseases*, Vol. 4, No. 4, pp. 213–222, 2004.

44. Viola, H. M., A. A. Shah, J. A. Kretzmann, C. W. Evans, M. Norret, K. S. Iyer, and L. C. Hool, "A Dendronized Polymer Variant That Facilitates Safe Delivery of A Calcium Channel Antagonist to the Heart", *Nanomedicine: Nanotechnology, Biology and Medicine*, Vol. 29, p. 102264, 2020.

45. Maeda, H., H. Nakamura, and J. Fang, "The EPR Effect For Macromolecular Drug Delivery to Solid Tumors: Improvement of Tumor Uptake, Lowering Of Systemic Toxicity, And Distinct Tumor Imaging *in vivo*", *Advanced Drug Delivery Reviews*, Vol. 65, No. 1, pp. 71–79, 2013.

46. Hrubý, M., Č. Koňák, and K. Ulbrich, "Polymeric Micellar pH-Sensitive Drug Delivery System for Doxorubicin", *Journal of Controlled Release*, Vol. 103, No. 1, pp. 137–148, 2005.

47. Xia, J., Y. Du, L. Huang, B. Chaurasiya, J. Tu, T. J. Webster, and C. Sun, "Redox-Responsive Micelles from Disulfide Bond-Bridged Hyaluronic Acid-Tocopherol Succinate for The Treatment of Melanoma", *Nanomedicine: Nanotechnology, Biology, and Medicine*, Vol. 14, No. 3, pp. 713–723, 2018.

48. Wang, Y., F. Wang, T. Sun, and J. Wang, "Redox-Responsive Nanoparticles from the Single Disulfide Bond-Bridged Block Copolymer as Drug Carriers for Overcoming Multidrug Resistance in Cancer Cells", *Bioconjugate Chemistry*, Vol. 22, No. 10, pp. 1939–1945, 2011.

49. Egorov, T. A., A. Svenson, L. Ryden, and J. Carlsson, "A Rapid and Specific Method for Isolation of Thiol Containing Peptides From Large Proteins by Thiol Disulfide Exchange on A Solid Support", *Proceedings of the National Academy of Sciences of the United States of America*, Vol. 72, No. 8, pp. 3029–3033, 1975.

50. Zhong, Y., J. Zhang, R. Cheng, C. Deng, F. Meng, F. Xie, and Z. Zhong, "Reversibly Crosslinked Hyaluronic Acid Nanoparticles for Active Targeting and Intelligent Delivery of Doxorubicin to Drug Resistant CD44+ Human Breast Tumor Xenografts", *Journal of Controlled Release*, Vol. 205, pp. 144–154, 2015.

51. Zhuang, Y., Y. Su, Y. Peng, D. Wang, H. Deng, X. Xi, X. Zhu, and Y. Lu, "Facile Fabrication of Redox-Responsive Thiol-Containing Drug Delivery System via RAFT Polymerization", *Biomacromolecules*, Vol. 15, No. 4, pp. 1408–1418, 2014.

52. Bej, R., P. Dey, and S. Ghosh, "Disulfide Chemistry in Responsive Aggregation of Amphiphilic Systems", *Soft Matter*, Vol. 16, No. 1, pp. 11–26, 2019.

53. Chang, S., Y. Wang, T. Zhang, X. Pu, L. Zong, H. Zhu, L. Zhao, and B. Feng, "Redox-Responsive Disulfide Bond-Bridged Mpeg-PBLA Prodrug Micelles for Enhanced Paclitaxel Biosafety and Antitumor Efficacy", *Frontiers in Oncology*, Vol. 9, No. AUG, pp. 1–11, 2019.

54. Wang, Y. C., F. Wang, T. M. Sun, and J. Wang, "Redox-Responsive Nanoparticles from the Single Disulfide Bond-Bridged Block Copolymer As Drug Carriers for Overcoming Multidrug Resistance in Cancer Cells", *Bioconjugate Chemistry*, Vol. 22, No. 10, pp. 1939–1945, 2011.

55. Arslan, M., R. Sanyal, and A. Sanyal, "Thiol-Reactive Thiosulfonate Group Containing Copolymers: Facile Entry to Disulfide-Mediated Polymer Conjugation and Redox-Responsive Functionalizable Networks", *Polymer Chemistry*, Vol. 11, No. 10, pp. 1763–1773, 2020.

56. Chacko, R. T., J. Ventura, J. Zhuang, and S. Thayumanavan, "Polymer Nanogels: A Versatile Nanoscopic Drug Delivery Platform", *Advanced Drug Delivery Reviews*, Vol. 64, No. 9, pp. 836–851, 2012.

57. Gevrek, T. N., M. Cosar, D. Aydin, E. Kaga, M. Arslan, R. Sanyal, and A. Sanyal, "Facile Fabrication Of A Modular "Catch and Release" Hydrogel Interface: Harnessing Thiol-Disulfide Exchange for Reversible Protein Capture and Cell Attachment", *ACS Applied Materials and Interfaces*, Vol. 10, No. 17, pp. 14399–14409, 2018.

58. Siegel, R., J. Ma, Z. Zou, and A. Jemal, "Cancer Statistics", *CA: A Cancer Journal for Clinicians*, Vol. 64, No. 1, pp. 9–29, 2014.

59. Seyfried, T. N., R. E. Flores, A. M. Poff, and D. P. D'Agostino, "Cancer as A Metabolic Disease: Implications for Novel Therapeutics", *Carcinogenesis*, Vol. 35, No. 3, pp. 515–527, 2014.

60. Hanahan, D. and R. A. Weinberg, "Hallmarks of Cancer: The next generation", *Cell*, Vol. 144, No. 5, pp. 646–674, 2011.

61. Mitra, A., A. Nan, J. C. Papadimitriou, H. Ghandehari, and B. R. Line, "Polymer-Peptide Conjugates for Angiogenesis Targeted Tumor Radiotherapy", *Nuclear Medicine and Biology*, Vol. 33, No. 1, pp. 43–52, 2006.

62. Yasuhiro, M. and H. Maeda, "A New Concept for Macromolecular Therapeutics in Cancer Chemotherapy : Mechanism of Tumoritropic Accumulation of Proteins and the Antitumor Agent Smancs A New Concept for Macromolecular Therapeutics in Cancer Chemotherapy : Mechanism of Tumoritropic Accum", *Cancer Research*, Vol. 46, pp. 6387–6392, 1986.

63. Sumer Bolu, B., B. Golba, A. Sanyal, and R. Sanyal, "Trastuzumab Targeted Micellar Delivery of Docetaxel Using Dendron-Polymer Conjugates", *Biomaterials Science*, Vol. 8, No. 9, pp. 2600–2610, 2020.

64. Peer, D., "Harnessing RNAi Nanomedicine for Precision Therapy", *Molecular and Cellular Therapies*, Vol. 2, No. 1, p. 5, 2014.

65. Djokovic, D. and C. Calhaz-Jorge, "Angiogenesis As A Therapeutic Target in Endometriosis", *Acta Medica Portuguesa*, Vol. 27, No. 4, pp. 489–497, 2014.

66. Brooks, P. C., S. Strömblad, R. Klemke, D. Visscher, F. H. Sarkar, and D. A. Cheresh, "Antiintegrin αvβ3 Blocks Human Breast Cancer Growth and Angiogenesis in Human Skin", *Journal of Clinical Investigation*, Vol. 96, No. 4, pp. 1815–1822, 1995.

67. Liang, L., S.-W. Lin, W. Dai, J.-K. Lu, T.-Y. Yang, Y. Xiang, Y. Zhang, R.-T. Li, and Q. Zhang, "Novel Cathepsin B-Sensitive Paclitaxel Conjugate: Higher Water Solubility, Better Efficacy and Lower Toxicity", *Journal of Controlled Release*, Vol. 160, No. 3, pp. 618–629, 2012.

68. Boonpavanitchakul, K., L. K. Bast, N. Bruns, and R. Magaraphan, "Silk Sericin-Polylactide Protein-Polymer Conjugates as Biodegradable Amphiphilic Materials and Their Application in Drug Release Systems", *Bioconjugate Chemistry*, Vol. 31, No. 10, pp. 2312–2324, 2020.

69. Guo, C., R. H. Khengar, M. Sun, Z. Wang, A. Fan, and Y. Zhao, "Acid-Responsive Polymeric Nanocarriers for Topical Adapalene Delivery", *Pharmaceutical Research*, Vol. 31, No. 11, pp. 3051–3059, 2014.

70. Cabral, H., Y. Matsumoto, K. Mizuno, Q. Chen, M. Murakami, M. Kimura, Y. Terada, M. R. Kano, K. Miyazono, M. Uesaka, N. Nishiyama, and K. Kataoka, "Accumulation of Sub-100 nm Polymeric Micelles in Poorly Permeable Tumours Depends on Size", *Nature Nanotechnology*, Vol. 6, No. 12, pp. 815–823, 2011.

71. Ling, Y., K. Wei, Y. Luo, X. Gao, and S. Zhong, "Dual Docetaxel/Superparamagnetic Iron Oxide Loaded Nanoparticles for Both Targeting Magnetic Resonance Imaging And Cancer Therapy", *Biomaterials*, Vol. 32, No. 29, pp. 7139–7150, 2011.

72. Hood, J. D., M. Bednarski, R. Frausto, S. Guccione, R. a Reisfeld, R. Xiang, and D. A. Cheresh, "Tumor Regression by Targeted Gene Delivery to the Neovasculature", *Science*, Vol. 296, No. 5577, pp. 2404–7, 2002.

73. Hynes, R. O., "Integrins : Bidirectional , Allosteric Signaling Machines in Their Roles as Major Adhesion Receptors , Integrins", *Myelin Biology and Disorders*, Vol. 110, No.1, pp. 673–687, 2002.

74. Goodman, S. L. and M. Picard, "Integrins as Therapeutic Targets", *Trends in Pharmacological Sciences*, Vol. 33, No. 7, pp. 405–12, 2012.

75. Attia, M. F., N. Anton, J. Wallyn, Z. Omran, and T. F. Vandamme, "An Overview of Active and Passive Targeting Strategies to Improve The Nanocarriers Efficiency to Tumour Sites", *Journal of Pharmacy and Pharmacology*, Vol. 71, No. 8, pp. 1185–1198, 2019.

76. Miura, Y., T. Takenaka, K. Toh, S. Wu, H. Nishihara, M. R. Kano, Y. Ino, T. Nomoto, Y. Matsumoto, H. Koyama, H. Cabral, N. Nishiyama, and K. Kataoka, "Cyclic RGD-Linked Polymeric Micelles for Targeted Delivery of Platinum Anticancer Drugs to Glioblastoma Through the Blood-Brain Tumor Barrier", *ACS Nano*, Vol. 7, No. 10, pp. 8583–8592, 2013.

77. Holford, N. and D. S. Yim, "Volume of Distribution", *Translational and Clinical Pharmacology*, Vol. 24, No. 2, pp. 74–77, 2016.

78. Danhier, F., O. Feron, and V. Préat, "To Exploit the Tumor Microenvironment: Passive and Active Tumor Targeting of Nanocarriers for Anti-Cancer Drug Delivery", *Journal of Controlled Release*, Vol. 148, No. 2, pp. 135–46, Dec. 2010.

79. Bae, K. H., H. J. Chung, and T. G. Park, "Nanomaterials for Cancer Therapy and Imaging", *Molecules Cells*, Vol. 31, No. 4, pp. 295–302, 2011.

80. Gavas, S., S. Quazi, and T. M. Karpiński, "Nanoparticles for Cancer Therapy: Current Progress and Challenges", *Nanoscale Research Letters*, Vol. 16, No. 1, 2021.

81. Chenthamara, D., S. Subramaniam, S. G. Ramakrishnan, S. Krishnaswamy, M. M. Essa, F. H. Lin, and M. W. Qoronfleh, "Therapeutic Efficacy of Nanoparticles and Routes of Administration", *Biomaterials Research.*, Vol. 23, No. 1, pp. 1–29, 2019.

82. De Jong, W. H. and P. J. A. Borm, "Drug Delivery and Nanoparticles: Applications and Hazards", *International Journal of Nanomedicine*, Vol. 3, No. 2, pp. 133–149, 2008.

83. Batty, C. J., E. M. Bachelder, and K. M. Ainslie, "Historical Perspective of Clinical Nano and Microparticle Formulations for Delivery of Therapeutics", *Trends in Molecular Medicine*, Vol. 27, No. 6, pp. 516–519, 2021.

84. Leiro, V., J. P. Garcia, H. Tomás, and A. P. Pêgo, "The Present and the Future of Degradable Dendrimers and Derivatives in Theranostics", *Bioconjugate Chemistry*, Vol. 26, No. 7, pp. 1185–1197, 2015.

85. Altin, H., I. Kosif, and R. Sanyal, "Fabrication of “Clickable” Hydrogels via Dendron−Polymer Conjugates", *Macromolecules*, Vol. 43, No. 8, pp. 3801–3808, 2010.

86. Kempe, K., S. Onbulak, U. S. Schubert, A. Sanyal, and R. Hoogenboom, "pH Degradable Dendron-Functionalized Poly(2-Ethyl-2-Oxazoline) Prepared by A Cascade “Double-Click” Reaction", *Polymer Chemistry*, Vol. 4, No. 11, pp. 3236–3244, 2013.

87. Kose, M. M., S. Onbulak, I. I. Yilmaz, and A. Sanyal, "Orthogonally “Clickable” Biodegradable Dendrons", *Macromolecules*, Vol. 44, No. 8, pp. 2707–2714, 2011.

88. Sumer Bolu, B., E. Manavoglu Gecici, and R. Sanyal, "Combretastatin A-4 Conjugated Antiangiogenic Micellar Drug Delivery Systems Using Dendron-Polymer Conjugates", *Molecular Pharmaceutics*, Vol. 13, No. 5, pp. 1482–1490, 2016.

89. Zhao, F. and W. Li, "Dendrimer/Inorganic Nanomaterial Composites: Tailoring Preparation, Properties, Functions, and Applications of Inorganic Nanomaterials with Dendritic Architectures", *Science China Chemistry*, Vol. 54, No. 2, pp. 286–301, 2011.

90. Bolu, B. S., R. Sanyal, and A. Sanyal, "Drug Delivery Systems from Self-Assembly of Dendron-Polymer Conjugates", *Molecules*, Vol. 23, No. 7, pp. 1–26, 2018.

91. Unsal, H., S. Onbulak, F. Calik, M. Er-Rafik, M. Schmutz, A. Sanyal, and J. Rzayev, "Interplay between Molecular Packing, Drug Loading, and Core Cross-Linking in Bottlebrush Copolymer Micelles", *Macromolecules*, Vol. 50, No. 4, pp. 1342–1352, 2017.

92. Calik, F., A. Degirmenci, M. Eceoglu, A. Sanyal, and R. Sanyal, "Dendron-Polymer Conjugate Based Cross-Linked Micelles: A Robust and Versatile Nanosystem for Targeted Delivery", *Bioconjugate Chemistry*, Vol. 30, No. 4, pp. 1087–1097, 2019.

93. Gok, O., P. Erturk, B. Sumer Bolu, T. N. Gevrek, R. Sanyal, and A. Sanyal, "Dendrons and Multiarm Polymers with Thiol-Exchangeable Cores: A Reversible Conjugation Platform for Delivery", *Biomacromolecules*, Vol. 18, No. 8, pp. 2463–2477, 2017.

94. Li, X., Y. Qian, T. Liu, X. Hu, G. Zhang, Y. You, and S. Liu, "Amphiphilic Multiarm Star Block Copolymer-Based Multifunctional Unimolecular Micelles for Cancer Targeted Drug Delivery and MR Imaging", *Biomaterials*, Vol. 32, No. 27, pp. 6595–6605, 2011.

95. Liu, X. Q., C. Y. Sun, X. Z. Yang, and J. Wang, "Polymeric Micelle Based Nanomedicine for siRNA Delivery", *Particle and Particle Systems Characterization*, Vol. 30. pp. 211–228, 2013.

96. Pan, D., X. Zheng, M. Chen, Q. Zhang, Z. Li, Z. Duan, Q. Gong, Z. Gu, H. Zhang, and K. Luo, "Dendron-Polymer Hybrid Mediated Anticancer Drug Delivery for Suppression of Mammary Cancer", *Journal of Materials Science and Technology*, Vol. 63, pp. 115–123, 2021.

97. Bolu, B. S., B. Golba, N. Boke, A. Sanyal, and R. Sanyal, "Designing Dendron−Polymer Conjugate Based Targeted Drug Delivery Platforms with A “Mix-and-Match” Modularity", *Bioconjugate Chemistry*, Vol. 28, No. 12, pp. 2962-2975, 2017.

98. Kumari, M., S. Gupta, K. Achazi, C. Böttcher, J. Khandare, S. K. Sharma, and R. Haag, "Dendronized Multifunctional Amphiphilic Polymers as Efficient Nanocarriers for Biomedical Applications", *Macromolecular Rapid Communications*, Vol. 36, No. 2, pp. 254–261, 2015.

99. Kumar, A., A. Rodríguez-Caballero, F. M. Plieva, I. Y. Galaev, K. S. Nandakumar, M. Kamihira, R. Holmdahl, A. Orfao, and B. Mattiasson, "Affinity Binding of Cells to Cryogel Adsorbents with Immobilized Specific Ligands: Effect of Ligand Coupling and Matrix Architecture", *Journal of Molecular Recognition*, Vol. 18, No. 1, pp. 84–93, 2005.

100. Wegst, U. G. K., M. Schecter, A. E. Donius, and P. M. Hunger, "Biomaterials by Freeze Casting", *Philosophical Transactions of the Royal Society A*, Vol. 368, No. 1917, pp. 2099–2121, 2010.

101. Lozinsky, V. I., N. G. Faleev, A. L. Zubov, S. B. Ruvinov, T. V. Antonova, E. S. Vainerman, V. M. Belikov, and S. V. Rogozhin, "Use of PVA-Cryogel Entrapped Citrobacter Intermedius Cells for Continuous Production of 3-Fluoro-L-Tyrosine", *Biotechnology Letters*, Vol. 11, No. 1, pp. 43–48, 1989.

102. Aydin, D., M. Arslan, A. Sanyal, and R. Sanyal, "Hooked on Cryogels: A Carbamate Linker Based Depot for Slow Drug Release", *Bioconjugate Chemistry*, Vol. 28, No. 5, pp. 1443–1451, 2017.

103. Chambre, L., H. Maouati, Y. Oz, R. Sanyal, and A. Sanyal, "Thiol-Reactive Clickable Cryogels: Importance of Macroporosity and Linkers on Biomolecular Immobilization", *Bioconjugate Chemistry*, Vol. 31, No. 9, pp. 2116–2124, 2020.

104. Kim, S., Y. Shi, J. Y. Kim, K. Park, and J.-X. Cheng, "Overcoming the Barriers in Micellar Drug Delivery: Loading Efficiency, *in vivo* Stability, and Micelle-Cell Interaction", *Expert Opinion on Drug Delivery*, Vol. 7, pp. 49–62, 2010.

105. Talelli, M., M. Barz, C. J. F. Rijcken, F. Kiessling, W. E. Hennink, and T. Lammers, "Core-Crosslinked Polymeric Micelles: Principles, Preparation, Biomedical Applications and Clinical Translation", *Nano Today*, Vol. 10, No. 1, pp. 93–117, 2015.

106. McCusker, C. F., P. J. Kocienski, F. T. Boyle, and A. G. Schätzlein, "Solid-Phase Synthesis of c(Rgdfk) Derivatives: On-Resin Cyclisation and Lysine Functionalisation", *Bioorganic & Medicinal Chemistry Letters*, Vol. 12, No. 4, pp. 547–549, 2002.

107. Mantovani, G., V. Ladmiral, L. Tao, and D. M. Haddleton, "One-Pot Tandem Living Radical Polymerisation – Huisgens Cycloaddition Process (“‘ Click ’”) Catalysed By N -Alkyl-2-Pyridylmethanimine / Cu (I) Br Complexes", *Chemical Communications*, Vol. 47, No. 16, pp. 2089–2091, 2005.

108. Nelson, D. M., Z. Ma, C. E. Leeson, and W. R. Wagner, "Extended and Sequential Delivery of Protein from Injectable Thermoresponsive Hydrogels", *Journal of Biomedical Materials Research*, Vol. 100, No. 3, pp. 776–785, 2013.

109. Wu, P., M. Malkoch, J. N. Hunt, R. Vestberg, E. Kaltgrad, M. G. Finn, V. V Fokin, K. B. Sharpless, and C. J. Hawker, "Multivalent, Bifunctional Dendrimers Prepared by Click Chemistry.", *Chemical communications*, Vol. 127, No. 46, pp. 5775–5777, 2005.

110. Çalık, F., *"Targeted Micellar Structures for Anticancer Drug Delivery"*, M.S. Thesis, Boğaziçi University, 2014.

111. Cengiz, N., T. N. Gevrek, R. Sanyal, and A. Sanyal, "Orthogonal Thiol-Ene "Click" Reactions: A Powerful Combination for Fabrication and Functionalization of Patterned Hydrogels", *Chemical Communications*, Vol. 53, No. 63, pp. 8894–8897, 2017.

112. Lotocki, V., H. Yazdani, Q. Zhang, E. R. Gran, A. Nyrko, D. Maysinger, and A. Kakkar, "Miktoarm Star Polymers with Environment-Selective ROS/GSH Responsive Locations: from Modular Synthesis to Tuned Drug Release through Micellar Partial Corona Shedding and/or Core Disassembly", *Macromolecular Bioscience*, Vol. 21, No. 2, pp. 1–13, 2021.

113. Baird, R. D., D. S. P. Tan, and S. B. Kaye, "Weekly Paclitaxel in the Treatment of Recurrent Ovarian Cancer", *Nature Reviews Clinical Oncology*, Vol. 7, No. 46, p. 575, 2010.

114. Ke, X., V. Wee, L. Ng, S. Gao, Y. Wah, and J. L. Hedrick, "Biomaterials Co-Delivery of Thioridazine and Doxorubicin Using Polymeric Micelles for Targeting Both Cancer Cells and Cancer Stem Cells", *Biomaterials*, Vol. 35, No.3, pp. 1096–1108, 2014.

115. Ding, J., J. Chen, D. Li, C. Xiao, J. Zhang, C. He, X. Zhuang, and X. Chen, "Biocompatible Reduction-Responsive Polypeptide Micelles as Nanocarriers for Enhanced Chemotherapy Efficacy *in vitro*", *Journal of Materials Chemistry B*, Vol. 1, No. 1, pp. 69–81, 2013.

116. Harnoy, A. J., I. Rosenbaum, E. Tirosh, Y. Ebenstein, R. Shaharabani, R. Beck, and R. J. Amir, "Enzyme-Responsive Amphiphilic PEG-Dendron Hybrids and Their Assembly into Smart Micellar Nanocarriers", *Journal of the American Chemical Society.*, Vol. 136, No. 21, pp. 7531–7534, 2014.

117. Zhang, H., X. Liu, T. Xu, K. Xu, B. Du, and Y. Li, "Biodegradable Reduction and pH Dual-Sensitive Polymer Micelles Based on Poly(2-Ethyl-2-Oxazoline) for Efficient Delivery of Curcumin", *RSC Advance*, Vol. 10, No. 43, pp. 25435–25445, 2020.

118. Xu, P., H. Yu, Z. Zhang, Q. Meng, H. Sun, X. Chen, Q. Yin, and Y. Li, "Hydrogen-Bonded and Reduction-Responsive Micelles Loading Atorvastatin for Therapy of Breast Cancer Metastasis", *Biomaterials*, Vol. 35, No. 26, pp. 7574–7587, 2014.

119. Gok, O., P. Erturk, B. Sumer Bolu, T. N. Gevrek, R. Sanyal, and A. Sanyal, "Dendrons and Multiarm Polymers with Thiol-Exchangeable Cores: A Reversible Conjugation Platform for Delivery", *Biomacromolecules*, Vol. 18, No. 8, pp. 2463–2477, 2017.

120. Walter, M. V., P. Lundberg, A. Hult, and M. Malkoch, "Novel Macrothiols for The Synthesis of A Structurally Comprehensive Dendritic Library Using Thiol-Ene Click Chemistry", *Journal of Polymer Science, Part A: Polymer Chemistry*, Vol. 49, No. 13, pp. 2990–2995, 2011.

121. Hong, R., G. Han, J. M. Fernández, B. J. Kim, N. S. Forbes, and V. M. Rotello, "Glutathione-Mediated Delivery and Release Using Monolayer Protected Nanoparticle Carriers", *Journal of the American Chemical Society*, Vol. 128, No. 4, pp. 1078–1079, 2006.

122. Berenson James R., M. D. and M. D. Lipton Allan, "Bisphosphonates in the Treatment of Malignant Bone Disease", *Annual Review of Medicine*, Vol. 50, No. 1, pp. 237–248, 1999.

123. Wartenberg, A., J. Weisser, and M. Schnabelrauch, "Glycosaminoglycan-Based Cryogels as Scaffolds for Cell Cultivation and Tissue Regeneration", *Molecules*, Vol. 26, No. 18, pp. 1–21, 2021.

124. Fassina, L., E. Saino, L. Visai, M. A. Avanzini, M. G. Cusella De Angelis, F. Benazzo, S. Van Vlierberghe, P. Dubruel, and G. Magenes, "Use of A Gelatin Cryogel as Biomaterial Scaffold in The Differentiation Process of Human Bone Marrow Stromal Cells", *Annual International Conference of the IEEE Engineering in Medicine and Biology Society*, Buenos Aires, Argentina, No. 30, pp. 247–250, 2010.

125. Wang, M., J. Hu, Y. Ou, X. He, Y. Wang, C. Zou, Y. Jiang, F. Luo, D. Lu, Z. Li, J. Li, and H. Tan, "Shape-Recoverable Hyaluronic Acid–Waterborne Polyurethane Hybrid Cryogel Accelerates Hemostasis and Wound Healing", *ACS Applied Materials & Interfaces Interfaces*, Vol. 14, No. 15, pp. 17093–17108, 2022.

126. Yamamoto, K., "Intracellular Lectins Are Involved in Quality Control of Glycoproteins", *Proceedings of the Japan Academy Series B: Physical and Biological Sciences*, Vol. 90, No. 2, pp. 67–82, 2014.

127. Maynard, H. D., S. Y. Okada, and R. H. Grubbs, "Synthesis of Norbornenyl Polymers with Bioactive Oligopeptides by Ring-Opening Metathesis Polymerization", *Macromolecules,* Vol. 33, No. 17, pp. 6239–6248, 2000.

128. Carlsson, J., H. Drevin, and R. Axen, "Protein Thiolation and Reversible Protein-Protein Conjugation. N-Succinimidyl 3-(2-Pyridyldithio)Propionate, A New Heterobifunctional Reagent", *Biochemical Journal*, Vol. 173, No. 3, pp. 723–737, 1978.

129. Stayton, P. S., S. Freitag, L. A. Klumb, A. Chilkoti, V. Chu, J. E. Penzotti, R. To, D. Hyre, I. Le Trong, T. P. Lybrand, and R. E. Stenkamp, "Streptavidin-Biotin Binding Energetics", *Biomolecular Engineering*, Vol. 16, No. 1–4, pp. 39–44, 1999.

130. Zhu, H., H. Luo, M. Lin, Y. Li, A. Chen, H. He, F. Sheng, and J. Wu, "Methacrylated Gelatin Shape-Memorable Cryogel Subcutaneously Delivers Epcs and Afgf for Improved Pressure Ulcer Repair in Diabetic Rat Model", *International Journal of Biological Macromolecules,* Vol. 199, pp. 69–76, 2022.

131. Henderson, T. M. A., K. Ladewig, D. N. Haylock, K. M. McLean, and A. J. O'Connor, "Cryogels for Biomedical Applications", *Journal of Materials Chemistry B*, Vol. 1, No. 21, pp. 2682–2695, 2013.

132. Wang, S., Z. Fan, B. Zhou, Y. Wang, P. Du, W. Tan, M. J. Lammi, and X. Guo, "Roles of Glycoproteins in the Diagnosis and Differential Diagnosis of Chronic and Latent Keshan Disease", *Molecules*, Vol. 22, No. 5, pp.746-759, 2017.

133. Chen, Z., L. Xu, Y. Liang, J. Wang, M. Zhao, and Y. Li, "Polyethylene Glycol Diacrylate-Based Supermacroporous Monolithic Cryogel as High-Performance Liquid Chromatography Stationary Phase for Protein and Polymeric Nanoparticle Separation", *Journal of Chromatography A*, Vol. 1182, No. 1, pp. 128–131, 2008.

134. Hajizadeh, S., C. Xu, H. Kirsebom, L. Ye, and B. Mattiasson, "Cryogelation of Molecularly Imprinted Nanoparticles: A Macroporous Structure as Affinity Chromatography Column for Removal of B-Blockers from Complex Samples", J*ournal of Chromatography A*, Vol. 1274, No.2, pp. 6–12, 2013.

135. Firer, M. A. and G. Gellerman, "Targeted Drug Delivery for Cancer Therapy : The Other Side of Antibodies" , *Journal of Hematology and Oncology*, Vol. 5, No.70, pp. 1–16, 2012.

136. Annis, I., L. Chen, and G. Barany, "Novel Solid-Phase Reagents for Facile Formation of Intramolecular Disulfide Bridges In Peptides Under Mild Conditions", *Journal of the American Chemical Society*, Vol. 120, No. 29, pp. 7226–7238, 1998.

137. Oz, Y. and A. Sanyal, "The Taming of the Maleimide : Fabrication of Maleimide-Containing " Clickable " Polymeric Materials", *Chemical Record*, Vol. 18, No.6, pp. 570–586, 2018.

138. Gevrek, T. N., I. Kosif, and A. Sanyal, "Surface-Anchored Thiol-Reactive Soft Interfaces: Engineering Effective Platforms for Biomolecular Immobilization and Sensing", *ACS Applied Materials & Interfaces*, Vol. 9, No. 33, pp. 27946–27954, 2017.

139. Park, E. J., T. N. Gevrek, R. Sanyal, and A. Sanyal, "Indispensable Platforms for Bioimmobilization: Maleimide-Based Thiol Reactive Hydrogels", *Bioconjugate Chemistry*, Vol. 25, No. 11, pp. 2004–2011, 2014.

140. Gevrek, T. N., T. Bilgic, H. A. Klok, and A. Sanyal, "Maleimide-Functionalized Thiol Reactive Copolymer Brushes: Fabrication and Post-Polymerization Modification", *Macromolecules*, Vol. 47, No. 22, pp. 7842–7851, 2014.

141. Clark, R. A. C., J. W. Gurd, N. Bissoon, N. Tricaud, E. Molnar, S. E. Zamze, R. A. Dwek, R. A. J. McIlhinney, and D. R. Wing, "Identification Of Lectin-Purified Neural Glycoproteins, Gps 180, 116, and 110, with NMDA and AMPA Receptor Subunits: Conservation of Glycosylation at The Synapse", *Journal of Neurochemistry*, Vol. 70, No. 6, pp. 2594–2605, 1998.

142. Arslan, M., T. N. Gevrek, J. Lyskawa, S. Szunerits, R. Boukherroub, R. Sanyal, P. Woisel, and A. Sanyal, "Bioinspired Anchorable Thiol-Reactive Polymers: Synthesis and Applications Toward Surface Functionalization of Magnetic Nanoparticles", *Macromolecules*, Vol. 47, No. 15, pp. 5124–5134, 2014.

143. Oz, Y., M. Arslan, T. N. Gevrek, R. Sanyal, and A. Sanyal, "Modular Fabrication of Polymer Brush Coated Magnetic Nanoparticles: Engineering the Interface for Targeted Cellular Imaging", *ACS Applied Materials & Interfaces*, Vol. 8, No. 30, pp. 19813–19826, 2016.

APPENDIX A: ADDITIONAL DATA

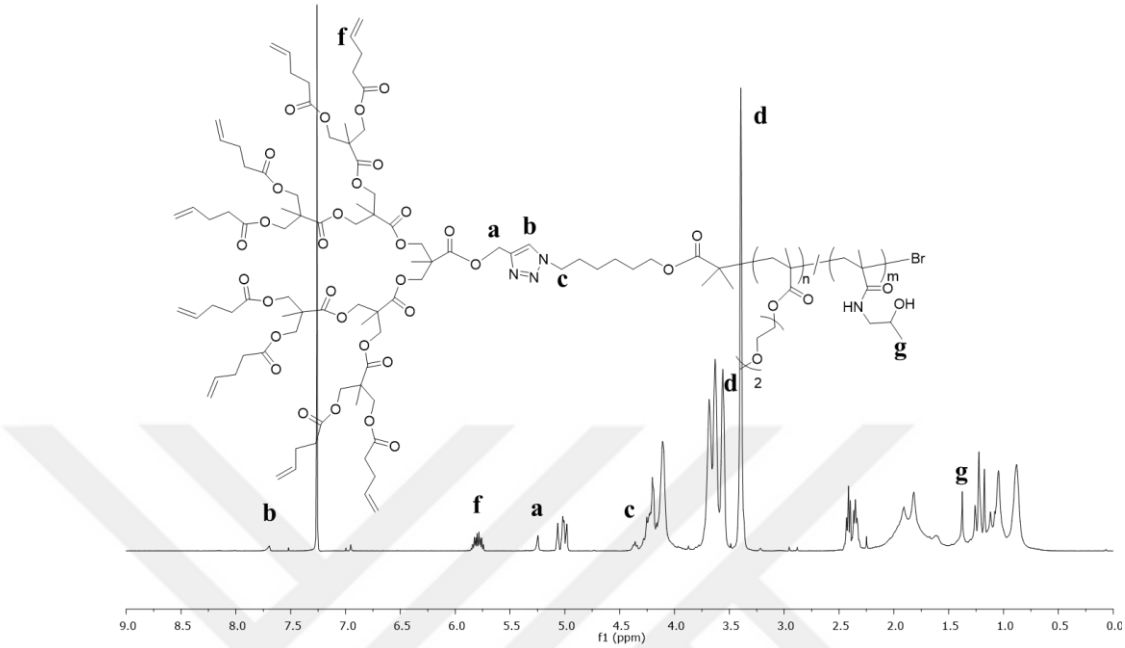

Figure A.1. ^{1}H NMR spectrum (in $CDCl_3$) of polymer-dendron conjugate (PDC-C).

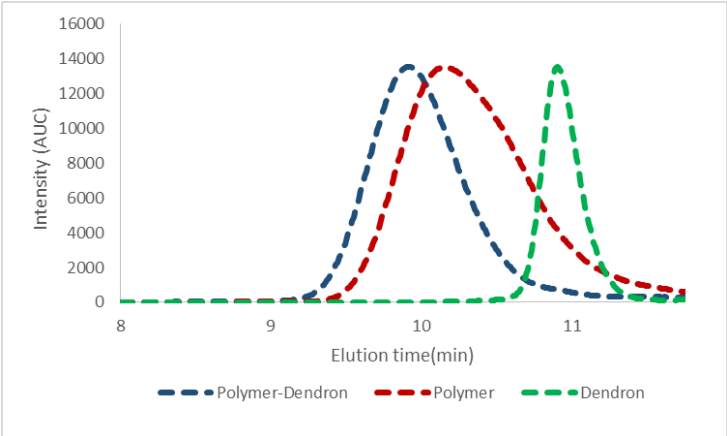

Figure A.2. SEC traces of polymer-dendron conjugate (PDC), copolymer and dendron .

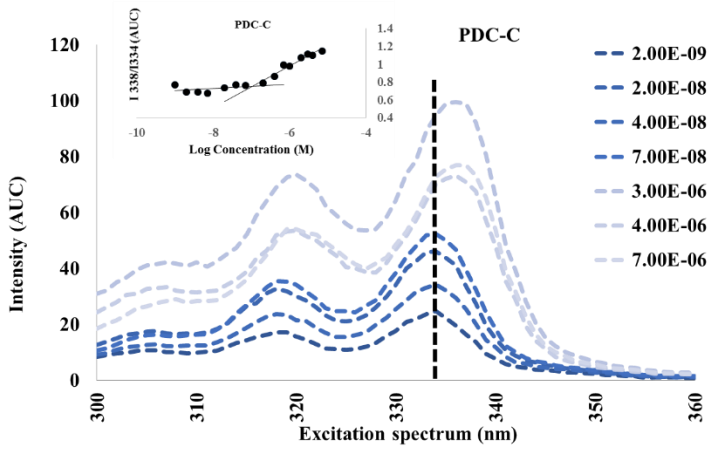

Figure A.3. Pyrene excitation spectrum of PDC-C micelles. Left inset: I_{338}/I_{334} vs log concentration graph to calculate CMC value.

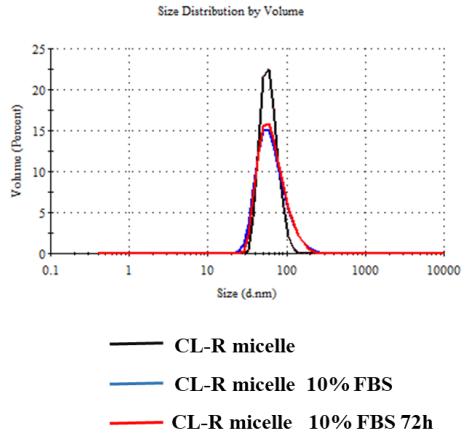

Figure A.4. Size stability of crosslinked (CL-R) micelles from PDC-R in 10% FBS.

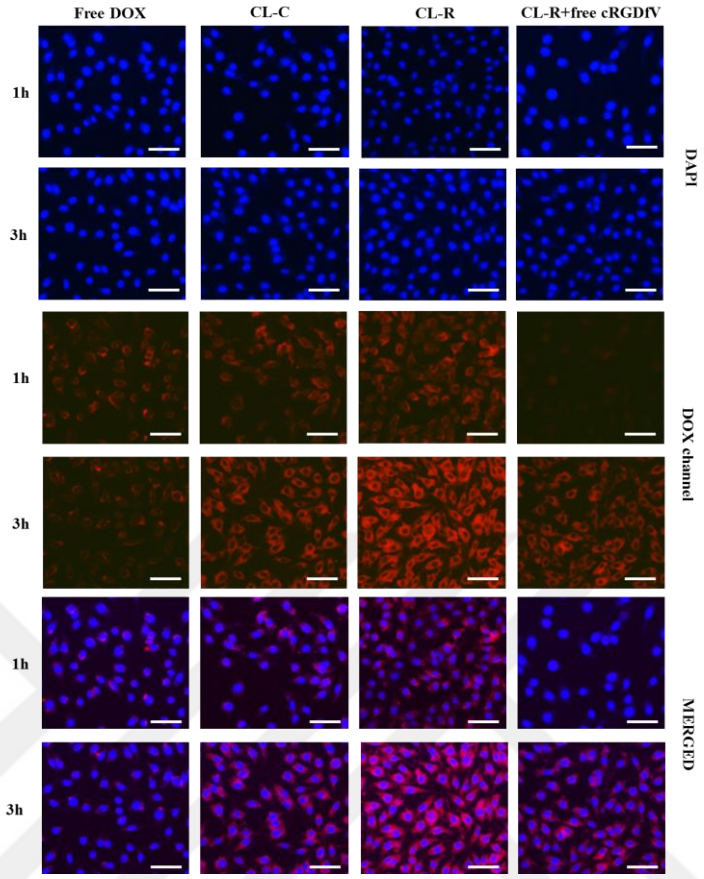

Figure A.5. Fluorescence microscopy images of MDA-MB-231 cells treated with free DOX and DOX loaded micelles. Cell nuclei were stained with DAPI (blue). Merged images were generated by overlapping DAPI channel (blue) with DOX channel (red) (Scale bar 50 μm).

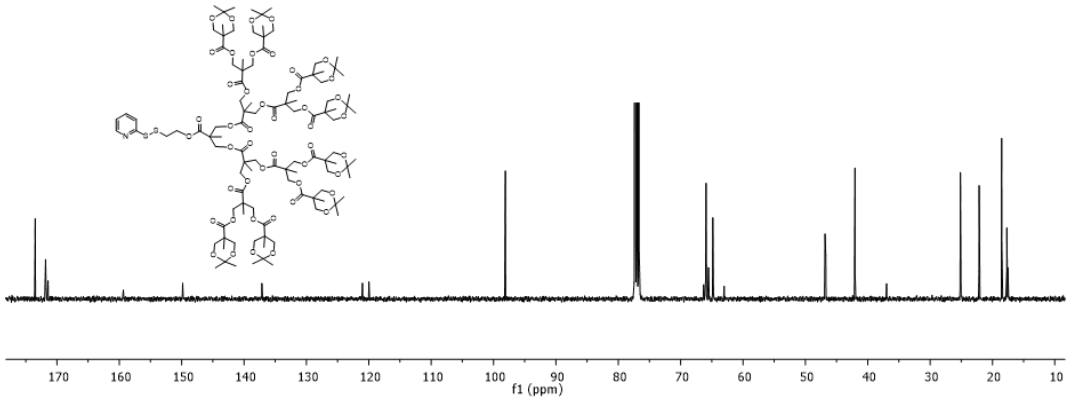

Figure A.6. ^{13}C NMR spectrum of 4th generation polyester dendron.

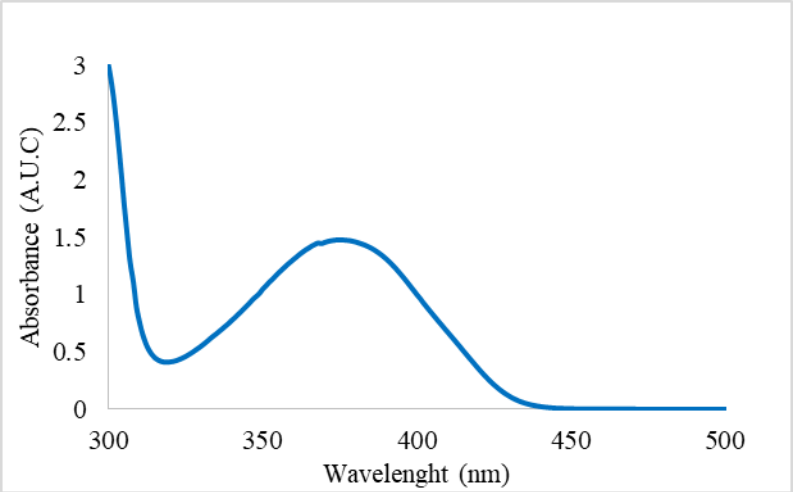

Figure A.7.UV-Vis spectrum of pyridine-2-thione released from pyridyl sulfide-thiol exchange reaction during PEG-SS-DEN4 conjugation.

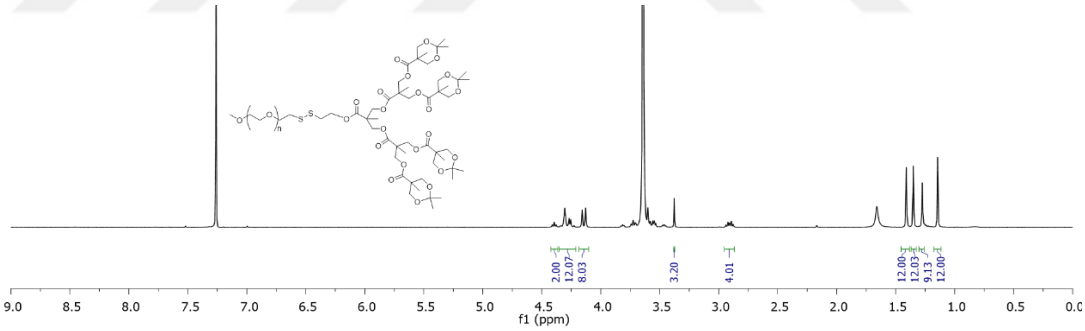

Figure A.8. ^{13}C NMR spectrum of 4th generation polyester dendron.

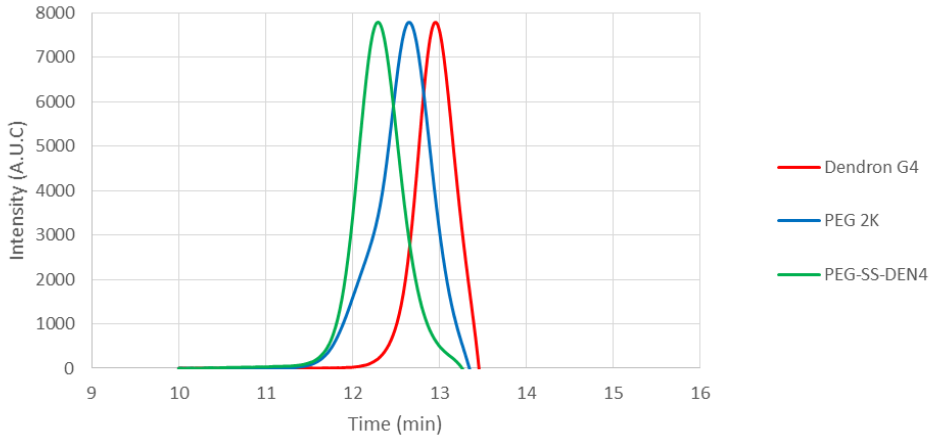

Figure A.9. GPC traces of dendron G4, PEG and PEG-SS-DEN4.

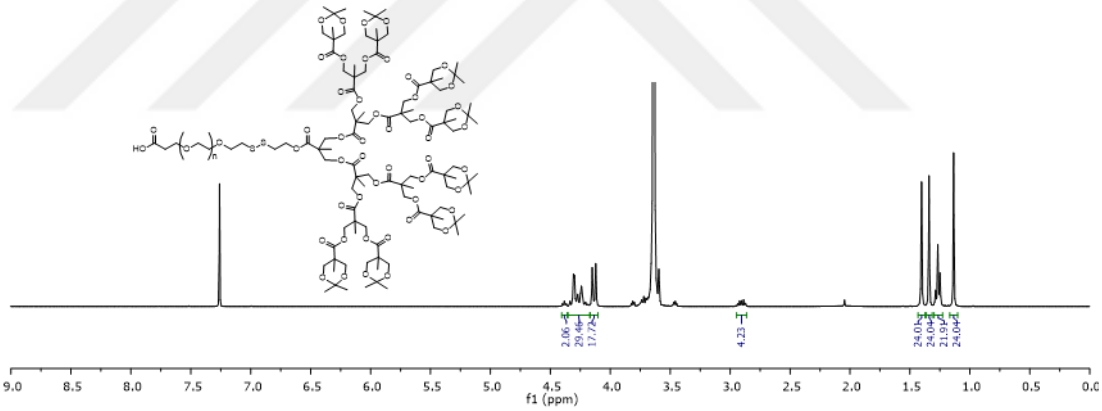

Figure A.10. ^{1}H NMR spectrum of redox-responsive (HOOC-PEGDG4).

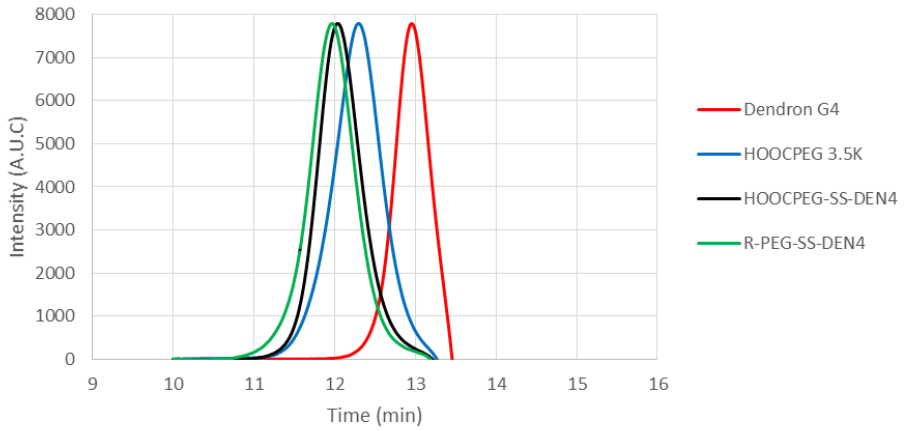

Figure A.11. GPC traces of Dendron G4, PEG and R-PEG-SS-DEN4.

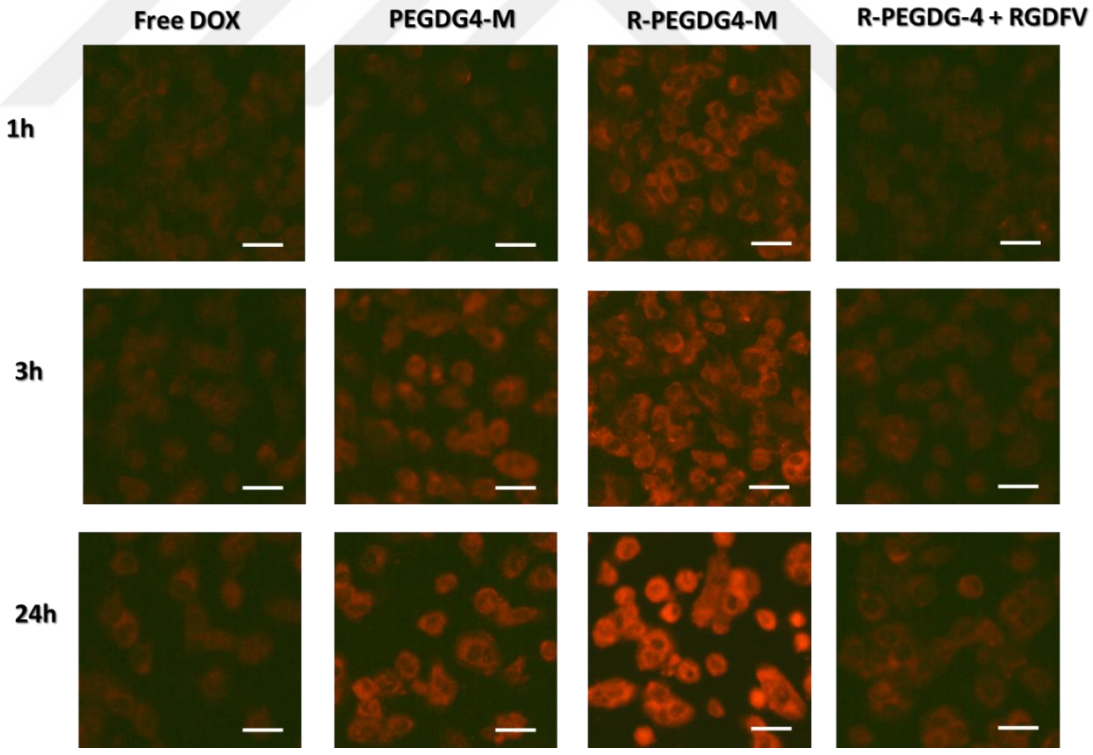

Figure A.12**.** Fluorescence microscopy images of MDA-MB-231 cells treated with free DOX and DOX loaded micelles.

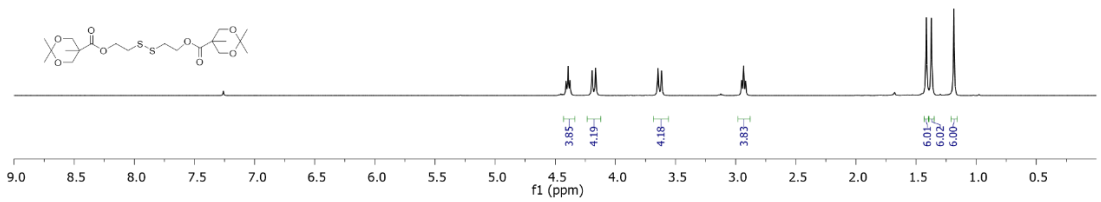

Figure A.13. ^{1}H NMR spectrum of redox-responsive dendrimer SS(G1X)$_2$.

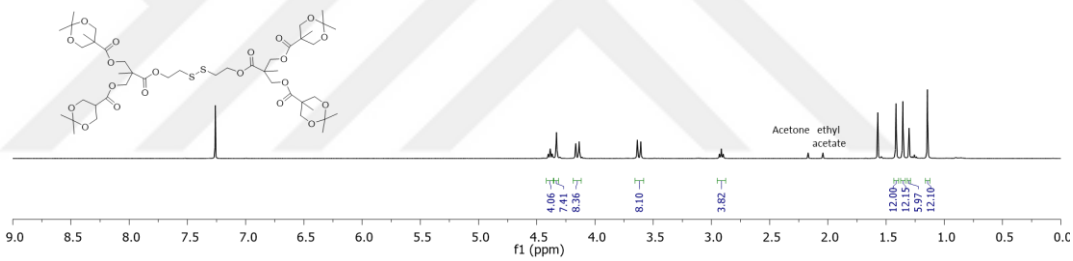

Figure A.14**.** ^{1}H NMR spectrum of redox-responsive dendrimer SS(G2X)$_2$.

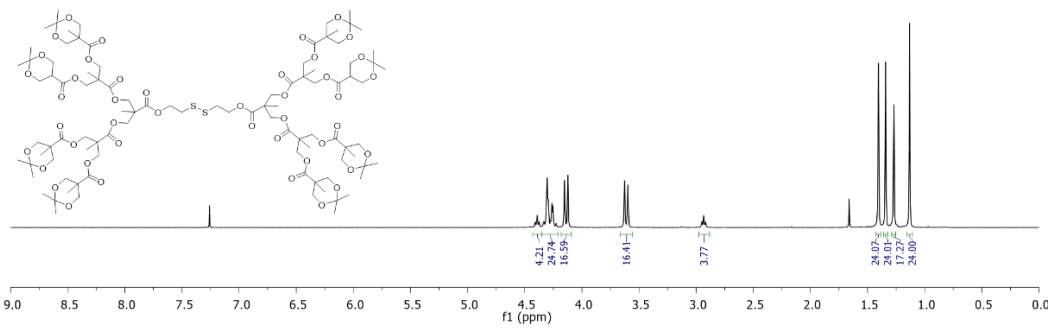

Figure A.15**.** ^{1}H NMR spectrum of redox-responsive dendrimer SS(G3X)$_2$.

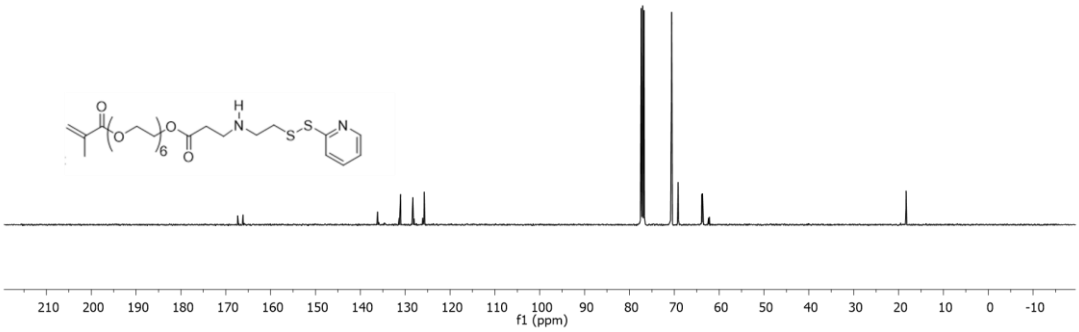

Figure A.16. ^{13}C NMR spectrum of PEG-based pyridyl-disulfide group containing methacrylate (PDS-PEG-MA).

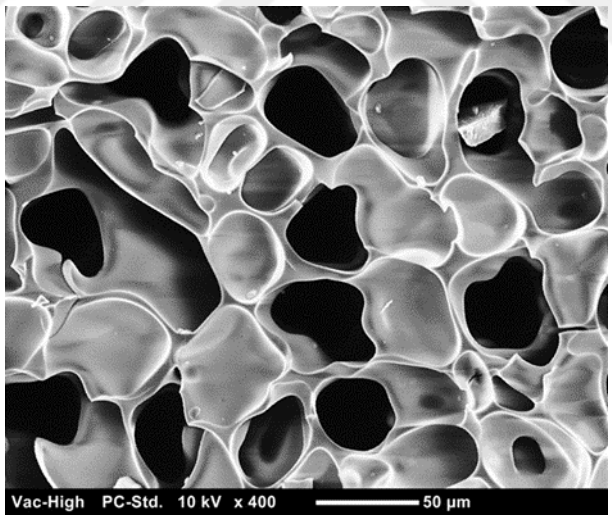

Figure A.17. Scanning electron micrograph of control cryogel synthesized without reactive monomer.

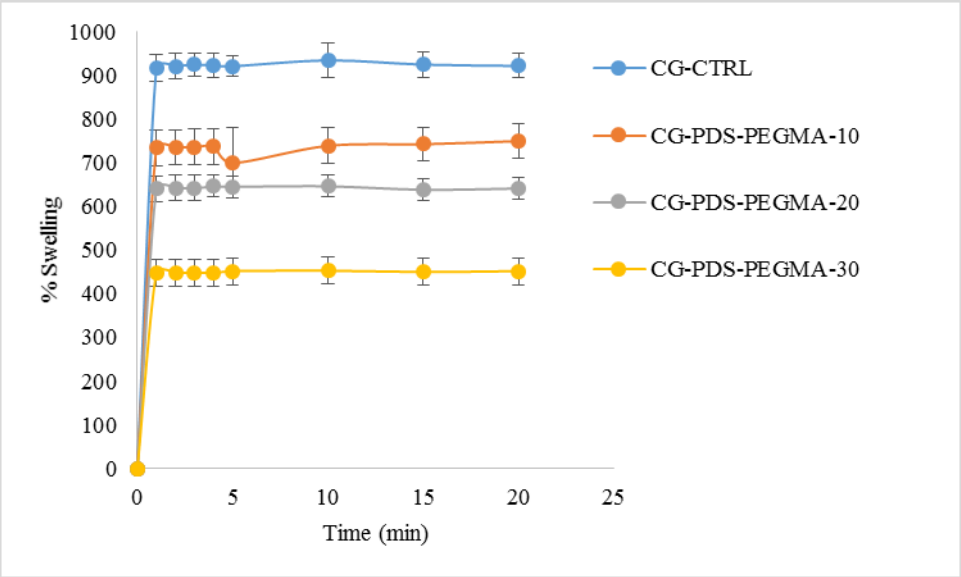

Figure A.18. Water uptake profile of cryogels.

.

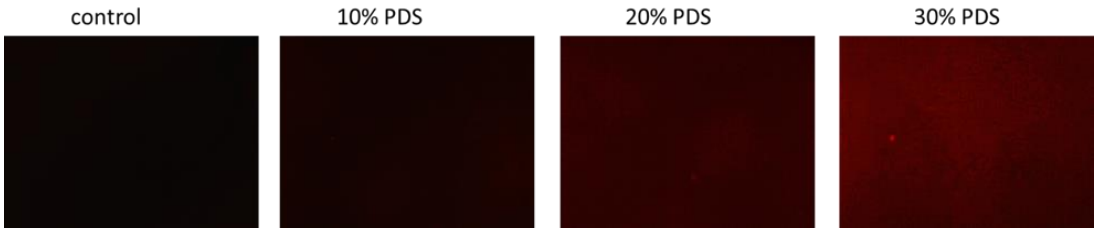

Figure A.19. Fluorescence micrographs of TRITC−streptavidin immobilized cryogels after DTT treatment.

APPENDIX B: PERMISSIONS FOR FIGURES

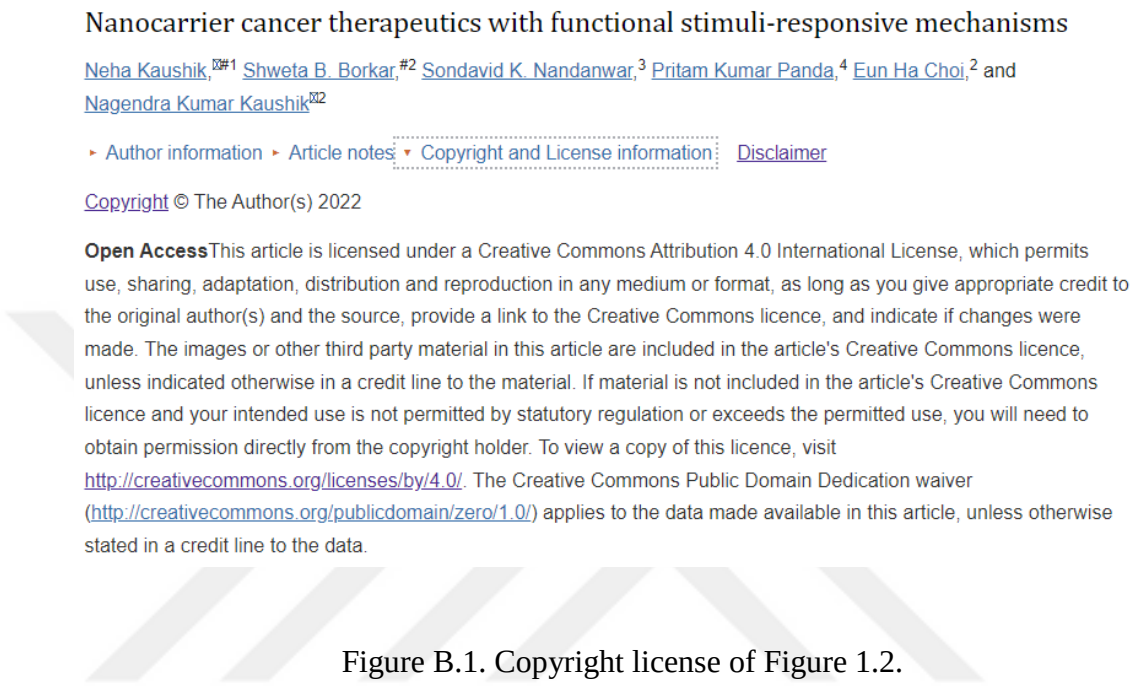

Nanocarrier cancer therapeutics with functional stimuli-responsive mechanisms

Neha Kaushik,[#1] Shweta B. Borkar,[#2] Sondavid K. Nandanwar,[3] Pritam Kumar Panda,[4] Eun Ha Choi,[2] and Nagendra Kumar Kaushik[2]

▸ Author information ▸ Article notes ▾ Copyright and License information Disclaimer

Copyright © The Author(s) 2022

Open Access This article is licensed under a Creative Commons Attribution 4.0 International License, which permits use, sharing, adaptation, distribution and reproduction in any medium or format, as long as you give appropriate credit to the original author(s) and the source, provide a link to the Creative Commons licence, and indicate if changes were made. The images or other third party material in this article are included in the article's Creative Commons licence, unless indicated otherwise in a credit line to the material. If material is not included in the article's Creative Commons licence and your intended use is not permitted by statutory regulation or exceeds the permitted use, you will need to obtain permission directly from the copyright holder. To view a copy of this licence, visit http://creativecommons.org/licenses/by/4.0/. The Creative Commons Public Domain Dedication waiver (http://creativecommons.org/publicdomain/zero/1.0/) applies to the data made available in this article, unless otherwise stated in a credit line to the data.

Figure B.1. Copyright license of Figure 1.2.

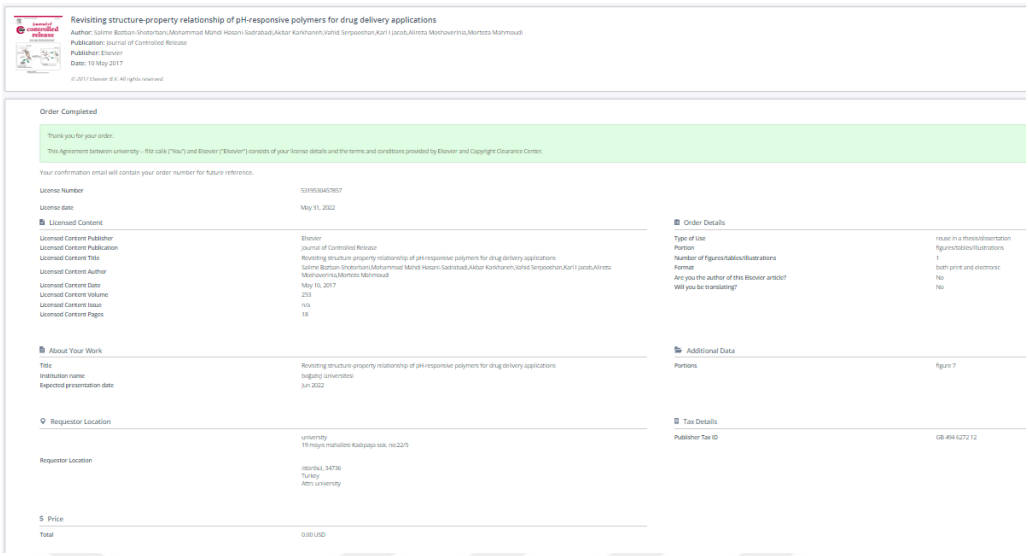

Revisiting structure-property relationship of pH-responsive polymers for drug delivery applications

Author: Salime Bozkır Shotorbani,Mohammad Mahdi Hasani-Sadrabadi,Akbar Karkhaneh,Vahid Serpooshan,Karl I Jacob,Alireza Moshaverinia,Morteza Mahmoudi

Publication: Journal of Controlled Release

Publisher: Elsevier

Date: 10 May 2017

© 2017 Elsevier B.V. All rights reserved.

Order Completed

Thank you for your order.

This Agreement between university -- filiz calik ("You") and Elsevier ("Elsevier") consists of your license details and the terms and conditions provided by Elsevier and Copyright Clearance Center.

Your confirmation email will contain your order number for future reference.

License Number	5319530457857
License date	May 31, 2022

Licensed Content

Licensed Content Publisher	Elsevier
Licensed Content Publication	Journal of Controlled Release
Licensed Content Title	Revisiting structure-property relationship of pH-responsive polymers for drug delivery applications
Licensed Content Author	Salime Bozkır Shotorbani,Mohammad Mahdi Hasani-Sadrabadi,Akbar Karkhaneh,Vahid Serpooshan,Karl I Jacob,Alireza Moshaverinia,Morteza Mahmoudi
Licensed Content Date	May 10, 2017
Licensed Content Volume	253
Licensed Content Issue	n/a
Licensed Content Pages	18

Order Details

Type of Use	reuse in a thesis/dissertation
Portion	figures/tables/illustrations
Number of figures/tables/illustrations	1
Format	both print and electronic
Are you the author of this Elsevier article?	No
Will you be translating?	No

About Your Work

Title	Revisiting structure-property relationship of pH-responsive polymers for drug delivery applications
Institution name	boğaziçi üniversitesi
Expected presentation date	Jun 2022

Additional Data

Portions	figure 7

Requestor Location

	university 19 mayıs mahallesi Kadıpaşa sok. no:22/5
Requestor Location	istanbul, 34736 Turkey Attn: university

Tax Details

Publisher Tax ID	GB 494 6272 12

$ Price

Total	0.00 USD

Figure B.2. Copyright license of Figure 1.3.

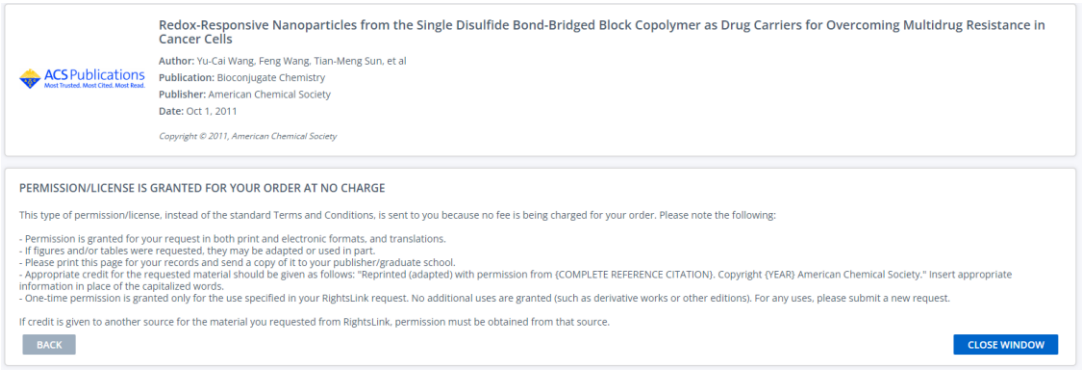

Figure B.3. Copyright license of Figure 1.4.



Figure B.4. Copyright license of Figure 1.5.

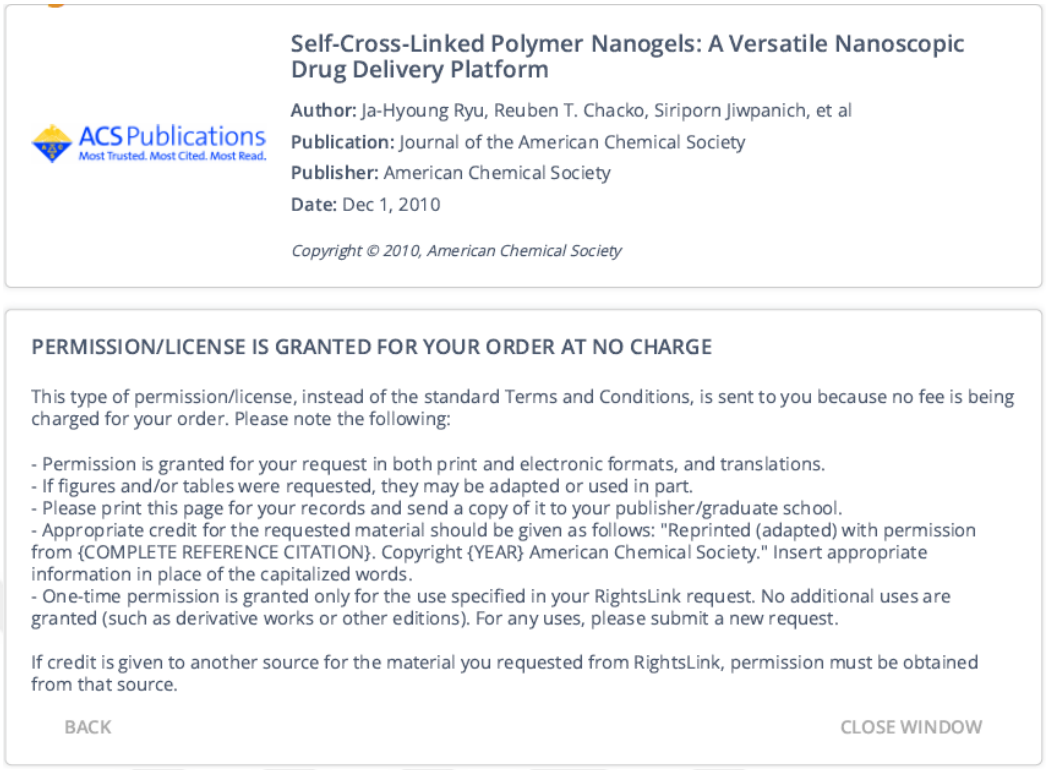

Self-Cross-Linked Polymer Nanogels: A Versatile Nanoscopic Drug Delivery Platform

Author: Ja-Hyoung Ryu, Reuben T. Chacko, Siriporn Jiwpanich, et al
Publication: Journal of the American Chemical Society
Publisher: American Chemical Society
Date: Dec 1, 2010

Copyright © 2010, American Chemical Society

PERMISSION/LICENSE IS GRANTED FOR YOUR ORDER AT NO CHARGE

This type of permission/license, instead of the standard Terms and Conditions, is sent to you because no fee is being charged for your order. Please note the following:

- Permission is granted for your request in both print and electronic formats, and translations.
- If figures and/or tables were requested, they may be adapted or used in part.
- Please print this page for your records and send a copy of it to your publisher/graduate school.
- Appropriate credit for the requested material should be given as follows: "Reprinted (adapted) with permission from {COMPLETE REFERENCE CITATION}. Copyright {YEAR} American Chemical Society." Insert appropriate information in place of the capitalized words.
- One-time permission is granted only for the use specified in your RightsLink request. No additional uses are granted (such as derivative works or other editions). For any uses, please submit a new request.

If credit is given to another source for the material you requested from RightsLink, permission must be obtained from that source.

BACK CLOSE WINDOW

Figure B.5. Copyright license of Figure 1.6.

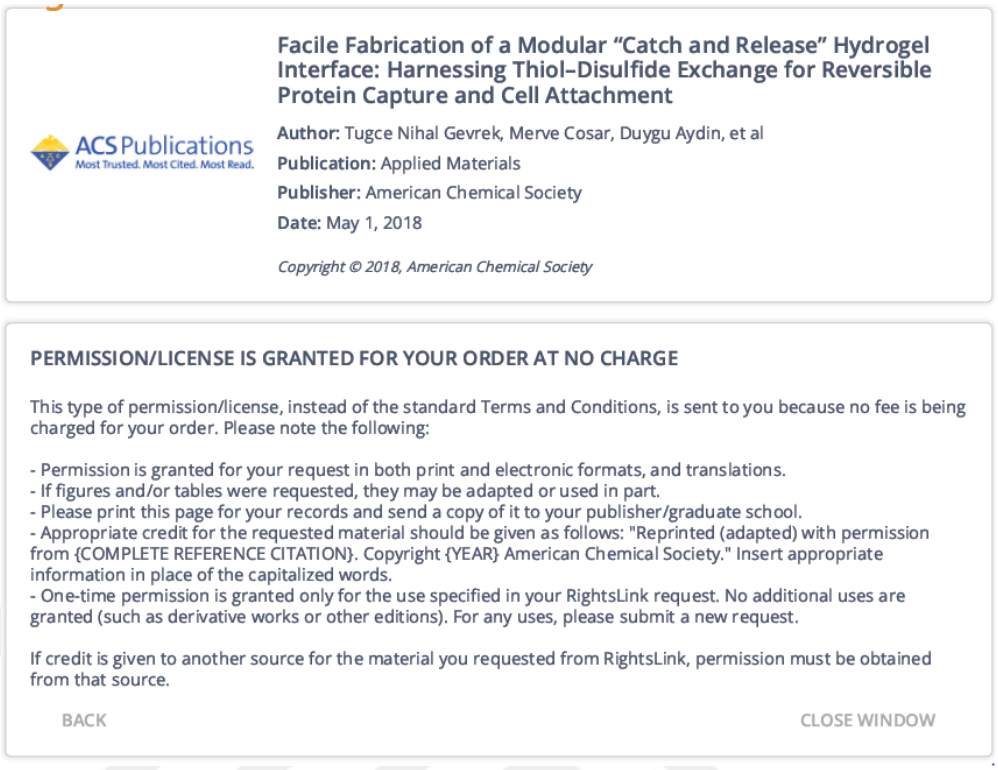

Facile Fabrication of a Modular "Catch and Release" Hydrogel Interface: Harnessing Thiol–Disulfide Exchange for Reversible Protein Capture and Cell Attachment

ACS Publications
Most Trusted. Most Cited. Most Read.

Author: Tugce Nihal Gevrek, Merve Cosar, Duygu Aydin, et al
Publication: Applied Materials
Publisher: American Chemical Society
Date: May 1, 2018

Copyright © 2018, American Chemical Society

PERMISSION/LICENSE IS GRANTED FOR YOUR ORDER AT NO CHARGE

This type of permission/license, instead of the standard Terms and Conditions, is sent to you because no fee is being charged for your order. Please note the following:

- Permission is granted for your request in both print and electronic formats, and translations.
- If figures and/or tables were requested, they may be adapted or used in part.
- Please print this page for your records and send a copy of it to your publisher/graduate school.
- Appropriate credit for the requested material should be given as follows: "Reprinted (adapted) with permission from {COMPLETE REFERENCE CITATION}. Copyright {YEAR} American Chemical Society." Insert appropriate information in place of the capitalized words.
- One-time permission is granted only for the use specified in your RightsLink request. No additional uses are granted (such as derivative works or other editions). For any uses, please submit a new request.

If credit is given to another source for the material you requested from RightsLink, permission must be obtained from that source.

BACK CLOSE WINDOW

Figure B.6. Copyright license of Figure 1.7.

Mol Cell Ther. 2014; 2: 5.
Published online 2014 Feb 5. doi: 10.1186/2052-8426-2-5
PMCID: PMC4452054
PMID: 26056574

Harnessing RNAi nanomedicine for precision therapy

Dan Peer✉

▸ Author information ▸ Article notes ▾ Copyright and License information Disclaimer

Copyright © Peer; licensee BioMed Central Ltd. 2014

This article is published under license to BioMed Central Ltd. This is an Open Access article distributed under the terms of the Creative Commons Attribution License (http://creativecommons.org/licenses/by/2.0), which permits unrestricted use, distribution, and reproduction in any medium, provided the original work is properly credited. The Creative Commons Public Domain Dedication waiver (http://creativecommons.org/publicdomain/zero/1.0/) applies to the data made available in this article, unless otherwise stated.

Figure B.7. Copyright license of Figure 1.8.

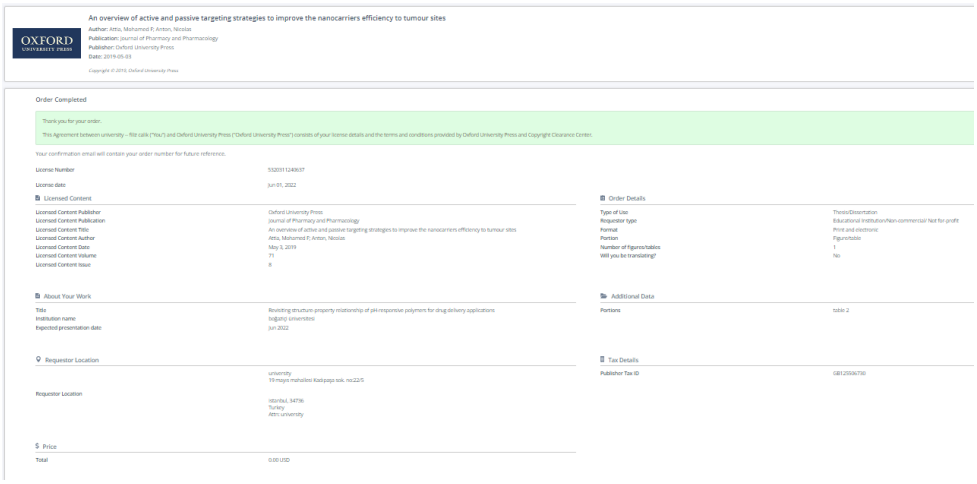

An overview of active and passive targeting strategies to improve the nanocarriers efficiency to tumour sites

Author: Attia, Mohamed F. Anton, Nicolas
Publication: Journal of Pharmacy and Pharmacology
Publisher: Oxford University Press
Date: 2019-05-03

Order Completed

Thank you for your order.

This Agreement between university -- fitir calik ("You") and Oxford University Press ("Oxford University Press") consists of your license details and the terms and conditions provided by Oxford University Press and Copyright Clearance Center.

Your confirmation email will contain your order number for future reference.

License Number	5320311240637
License date	Jun 01, 2022

Licensed Content

Licensed Content Publisher	Oxford University Press
Licensed Content Publication	Journal of Pharmacy and Pharmacology
Licensed Content Title	An overview of active and passive targeting strategies to improve the nanocarriers efficiency to tumour sites
Licensed Content Author	Attia, Mohamed F. Anton, Nicolas
Licensed Content Date	May 3, 2019
Licensed Content Volume	71
Licensed Content Issue	8

Order Details

Type of Use	Thesis/Dissertation
Requestor type	Educational Institution/Non-commercial/ Not for profit
Format	Print and electronic
Portion	Figure/table
Number of figures/tables	1
Will you be translating?	No

About Your Work

Title	Revisiting structure-property relationship of pH-responsive polymers for drug delivery applications
Institution name	bağatiş üniversitesi
Expected presentation date	Jun 2022

Additional Data

Portions	table 2

Requestor Location

	university 19 mayis mahallesi Kadıpaşa sok. no:22/5
Requestor Location	Istanbul, 34736 Turkey Attn: university

Tax Details

Publisher Tax ID	GB125506730

Price

Total	0.00 USD

Order Summary

Licensee:	university
Order Date:	Jun 1, 2022
Order Number:	5320311240637
Publication:	Journal of Pharmacy and Pharmacology
Title:	An overview of active and passive targeting strategies to improve the nanocarriers efficiency to tumour sites
Type of Use:	Thesis/Dissertation
Order Total:	0.00 USD

Figure B.8. Copyright license of Table 1.1.

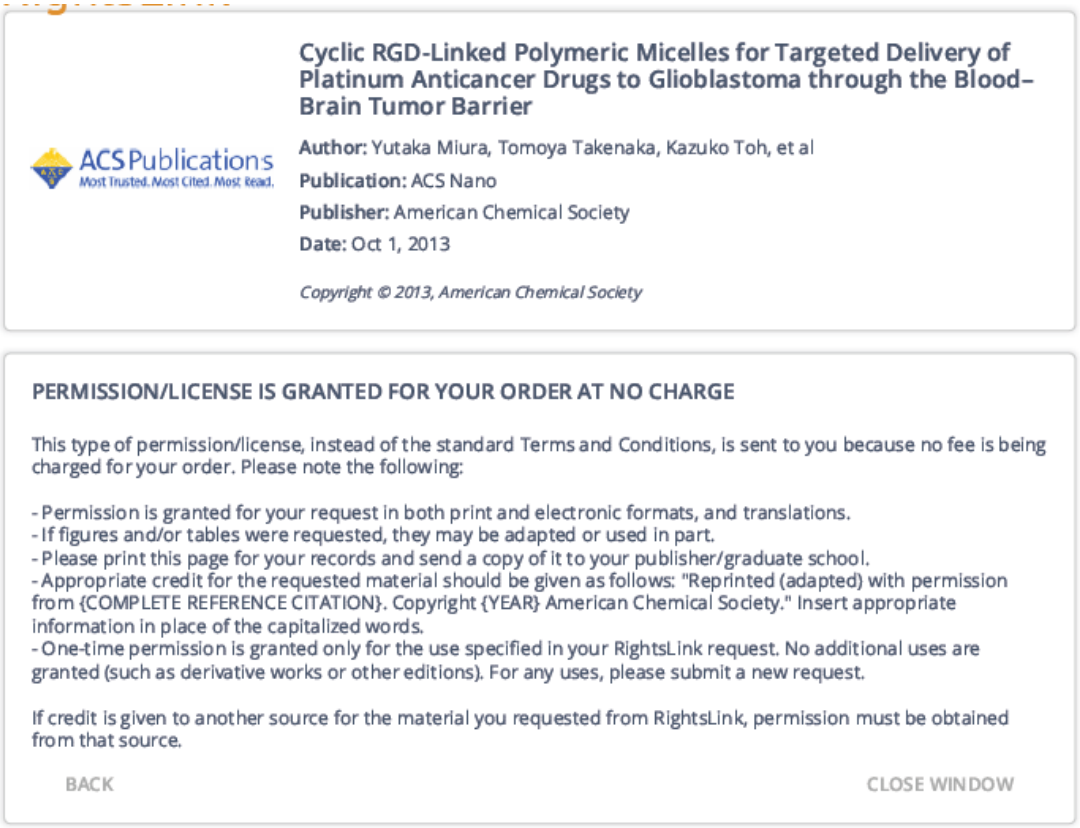

Cyclic RGD-Linked Polymeric Micelles for Targeted Delivery of Platinum Anticancer Drugs to Glioblastoma through the Blood–Brain Tumor Barrier

ACS Publications
Most Trusted. Most Cited. Most Read.

Author: Yutaka Miura, Tomoya Takenaka, Kazuko Toh, et al
Publication: ACS Nano
Publisher: American Chemical Society
Date: Oct 1, 2013

Copyright © 2013, American Chemical Society

PERMISSION/LICENSE IS GRANTED FOR YOUR ORDER AT NO CHARGE

This type of permission/license, instead of the standard Terms and Conditions, is sent to you because no fee is being charged for your order. Please note the following:

- Permission is granted for your request in both print and electronic formats, and translations.
- If figures and/or tables were requested, they may be adapted or used in part.
- Please print this page for your records and send a copy of it to your publisher/graduate school.
- Appropriate credit for the requested material should be given as follows: "Reprinted (adapted) with permission from {COMPLETE REFERENCE CITATION}. Copyright {YEAR} American Chemical Society." Insert appropriate information in place of the capitalized words.
- One-time permission is granted only for the use specified in your RightsLink request. No additional uses are granted (such as derivative works or other editions). For any uses, please submit a new request.

If credit is given to another source for the material you requested from RightsLink, permission must be obtained from that source.

BACK CLOSE WINDOW

Figure B.9. Copyright license of Figure 1.9.

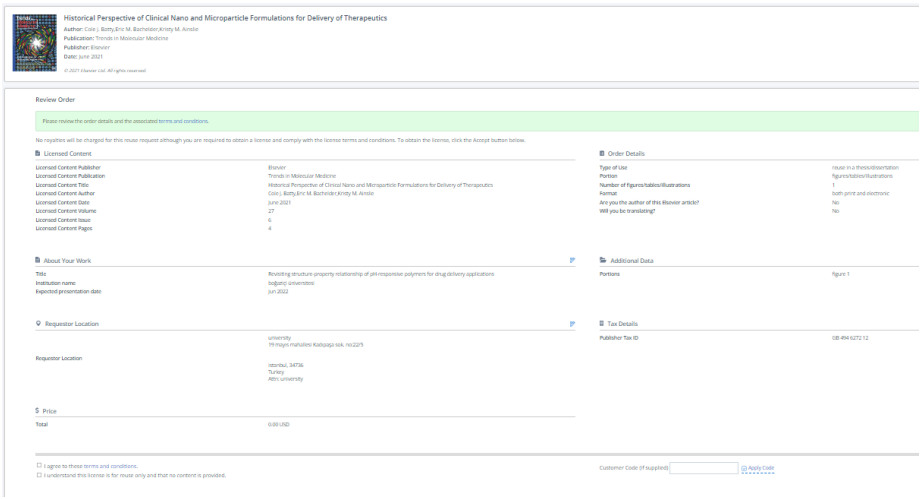

Figure B.10. Copyright license of Figure 1.10.

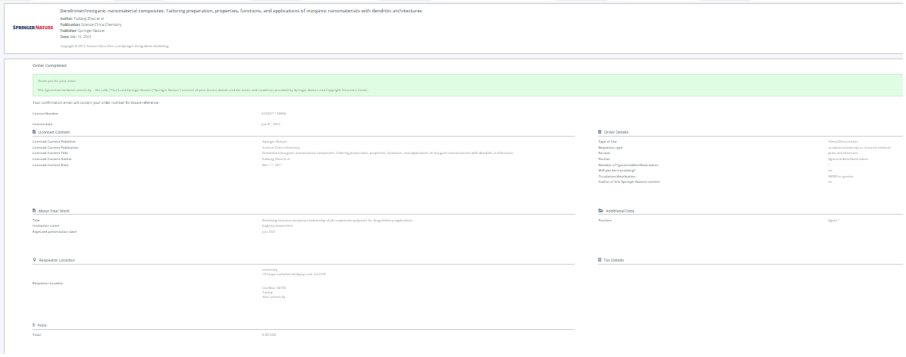

Figure B.11. Copyright license of Figure 1.11.

Molecules. 2018 Jul; 23(7): 1570.
Published online 2018 Jun 28. doi: 10.3390/molecules23071570
PMCID: PMC6099537
PMID: 29958437

Drug Delivery Systems from Self-Assembly of Dendron-Polymer Conjugates †

Burcu Sumer Bolu,[1] Rana Sanyal,[1,2,*] and Amitav Sanyal[1,2,*]

Ashok Kakkar, Academic Editor

▸ Author information ▸ Article notes ▾ Copyright and License information Disclaimer

Copyright © 2018 by the authors.

Licensee MDPI, Basel, Switzerland. This article is an open access article distributed under the terms and conditions of the Creative Commons Attribution (CC BY) license (http://creativecommons.org/licenses/by/4.0/).

Figure B.12. Copyright license of Figure 1.12.

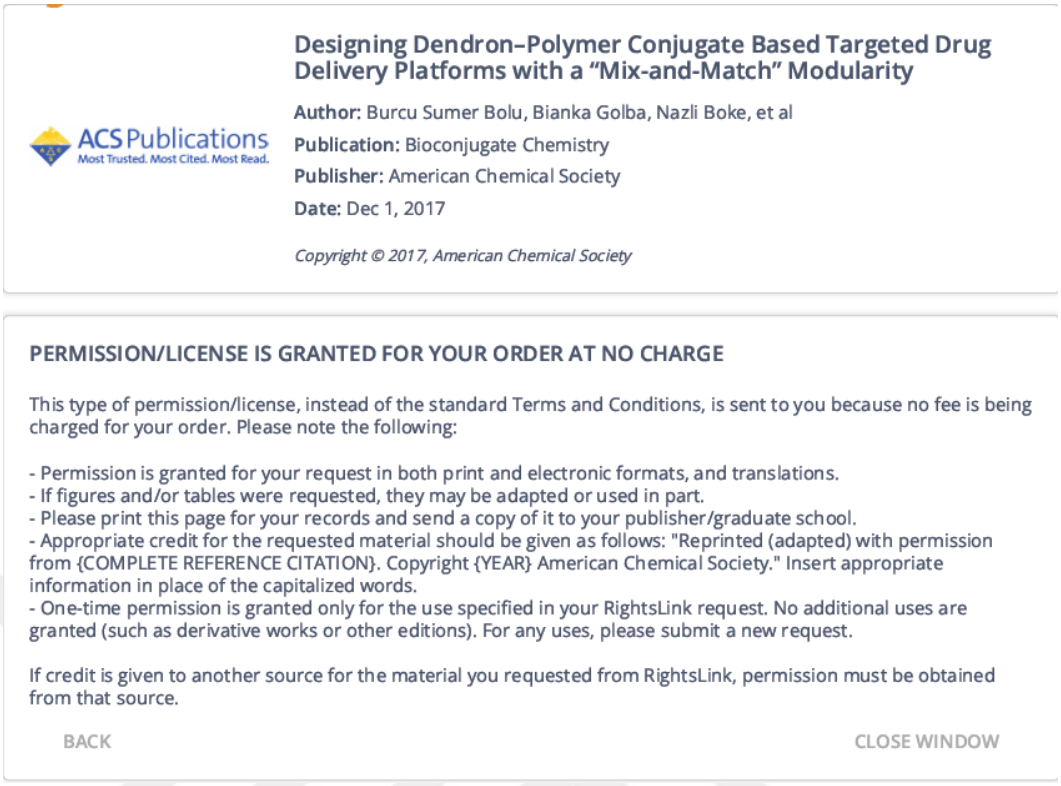

Designing Dendron–Polymer Conjugate Based Targeted Drug Delivery Platforms with a "Mix-and-Match" Modularity

Author: Burcu Sumer Bolu, Bianka Golba, Nazli Boke, et al

Publication: Bioconjugate Chemistry

Publisher: American Chemical Society

Date: Dec 1, 2017

Copyright © 2017, American Chemical Society

PERMISSION/LICENSE IS GRANTED FOR YOUR ORDER AT NO CHARGE

This type of permission/license, instead of the standard Terms and Conditions, is sent to you because no fee is being charged for your order. Please note the following:

- Permission is granted for your request in both print and electronic formats, and translations.
- If figures and/or tables were requested, they may be adapted or used in part.
- Please print this page for your records and send a copy of it to your publisher/graduate school.
- Appropriate credit for the requested material should be given as follows: "Reprinted (adapted) with permission from {COMPLETE REFERENCE CITATION}. Copyright {YEAR} American Chemical Society." Insert appropriate information in place of the capitalized words.
- One-time permission is granted only for the use specified in your RightsLink request. No additional uses are granted (such as derivative works or other editions). For any uses, please submit a new request.

If credit is given to another source for the material you requested from RightsLink, permission must be obtained from that source.

BACK CLOSE WINDOW

Figure B.13. Copyright license of Figure 1.13.

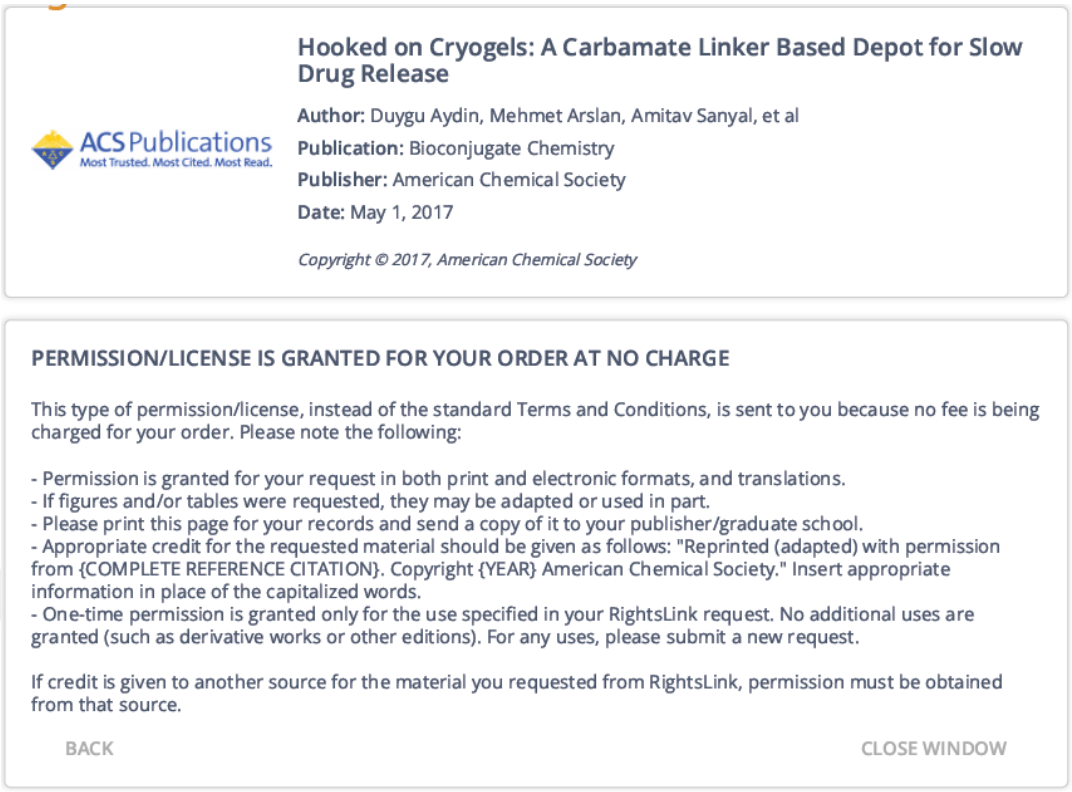

Figure B.14. Copyright license of Figure 1.15.



Figure B.15. Copyright license of Figure 1.16.



Dendron–Polymer Conjugate Based Cross-Linked Micelles: A Robust and Versatile Nanosystem for Targeted Delivery

Author: Filiz Calik, Aysun Degirmenci, Melike Eceoglu, et al

Publication: Bioconjugate Chemistry

Publisher: American Chemical Society

Date: Apr 1, 2019

Copyright © 2019, American Chemical Society

PERMISSION/LICENSE IS GRANTED FOR YOUR ORDER AT NO CHARGE

This type of permission/license, instead of the standard Terms and Conditions, is sent to you because no fee is being charged for your order. Please note the following:

- Permission is granted for your request in both print and electronic formats, and translations.
- If figures and/or tables were requested, they may be adapted or used in part.
- Please print this page for your records and send a copy of it to your publisher/graduate school.
- Appropriate credit for the requested material should be given as follows: "Reprinted (adapted) with permission from {COMPLETE REFERENCE CITATION}. Copyright {YEAR} American Chemical Society." Insert appropriate information in place of the capitalized words.
- One-time permission is granted only for the use specified in your RightsLink request. No additional uses are granted (such as derivative works or other editions). For any uses, please submit a new request.

If credit is given to another source for the material you requested from RightsLink, permission must be obtained from that source.

BACK CLOSE WINDOW

Figure B.16. Copyright license of Chapter 3.